Comparative biochemical and pharmacological investigations of various newly developed opioid receptor ligands

Ph.D. thesis

Edina Szűcs

Supervisor:

Sándor Benyhe, PhD, DSc

Institute of Biochemistry,
Biological Research Centre, Szeged

Doctoral School of Theoretical Medicine,
Faculty of Medicine, University of Szeged

Szeged, Hungary
2020

TABLE OF CONTENTS

LIST OF PUBLICATIONS

This thesis is based on the following publications:

I. **Edina Szűcs**, János Marton, Zoltán Szabó, Sándor Hosztafi, Gabriella Kékesi, Gábor Tuboly, László Bánki, Gyöngyi Horváth, Pál T. Szabó, Csaba Tömböly, Zsuzsanna Varga, Sándor Benyhe, Ferenc Ötvös (2020) **Synthesis, biochemical, pharmacological characterization and in silico profile modelling of highly potent opioid orvinol and thevinol derivatives.** EUR. J. MED. CHEM., 191:1121-45.

(5.572 impact factor, Q1)

II. **Edina Szűcs**, Azzurra Stefanucci, Marilisa Pia Dimmito, Ferenc Zádor, Stefano Pieretti, Gokhan Zengin, László Vécsei, Sándor Benyhe, Adriano Mollica (2020) **Discovery of Kynurenines containing oligopeptides as potent opioid receptor agonists.** BIOMOLECULES, 10:1-18.

(4.082 impact factor, Q1)

Sum of the impact factors related to the thesis: 9.654

Other thematic publications not directly connected to this thesis:

1. **Szűcs, E.**, Büki, A., Kékesi, G., Horváth, G., Benyhe, S. (2016) **Mu-Opioid (MOP) receptor mediated G-protein signaling is impaired in specific brain regions in a rat model of schizophrenia.** NEUROSCI. LETTERS, 619: 29-33.

(2.180 impact factor, Q3)

2. Monti, L., Stefanucci, A., Pieretti, S., Marzoli, F., Fidanza, L., Mollica, A., Mirzaie, S., Carradori, S., De Petrocellis, L., Schiano Moriello, A., Benyhe, S., Zádor, F., **Szűcs, E.**, Ötvös, F., Erdei, A.I., Samavati, R., Dvorácskó, S., Tömböly, C., Novellino, E. (2016) **Evaluation of the analgesic effect of 4-anilidopiperidine scaffold containing ureas and carbamates.** J. ENZYME INHIB. MED. CHEM., 31: 1638-47.

(4.293 impact factor, Q2)

3. **Szűcs, E.**, Dvorácskó, S., Tömböly, C., Büki, A., Kékesi, G., Horváth, G., Benyhe, S. (2016) **Decreased CB receptor binding and cannabinoid signaling in three brain regions of a rat model of schizophrenia.** NEUROSCI. LETTERS, 633: 87-93.

(2.180 impact factor, Q3)

4. Mollica, A., Pelliccia, S., Famiglini, V., Stefanucci, A., Macedonio, G., Chiavaroli, A., Orlando, G., Brunetti, L., Ferrante, C., Pieretti, S., Novellino, E., Benyhe, S., Zador, F., Erdei, I.A., **Szűcs, E.**, Samavati, R., Dvorácskó, S., Tömböly, C., Ragno, R., Patsilinakos, A., Silvestri, R. (2017) **Exploring the first Rimonabant analog-opioid peptide hybrid compound, as bivalent ligand for CB1 and opioid receptors.** J. ENZYME INHIB. MED. CHEM., 32: 444-451.

(3.638 impact factor, Q2)

5. Zádor F, Balogh M, Váradi A, Zádori S Z, Király K, **Szűcs E**, Varga B, Lázár B, Hosztafi S, Riba P, Benyhe, S, Fürst S, Al-Khrasani M. (2017) **14-O-Methylmorphine: A Novel selective mu-opioid receptor agonist with high efficacy and affinity.** EUR. J. PHARMACOL., 814: 264-273.

(3.040 impact factor, Q1)

6. Samavati, R., Zádor, F., **Szűcs, E.**, Tuka, B., Martos, D., Veres, G., Gáspár, R., Mándity, I.M., Fülöp, F., Vécsei, L., Benyhe, S., Borsodi, A. (2017) **Kynurenic acid and its analogue can alter the opioid receptor G-protein signaling after acute treatment via NMDA receptor in rat cortex and striatum.** J. NEUROL. SCI., 376: 63-70.

(2.448 impact factor, Q2)

7. Stefanucci, A., Novellino, E., Mirzaie, S., Macedonio, G., Pieretti, S., Minosi, P., **Szűcs, E.**, Erdei, A.I., Zádor, F., Benyhe, S., Mollica, A. (2017) **Opioid receptor activity and analgesic potency of DPDPE peptide analogues containing a xylene bridge.** AMER. CHEM. SOC. MED. CHEM. LETTERS, 8: 449-454.

(3.794 impact factor, Q1)

8. Stefanucci A, Carotenuto A, Macedonio G, Novellino E, Pieretti S, Marzoli F, **Szűcs E**, Erdei AI, Zádor F, Benyhe, S., Mollica A. (2017) **Cyclic biphalin analogues incorporating a xylene bridge: Synthesis, characterization, and biological profile.** AMER. CHEM. SOC. MED. CHEM. LETTERS, 8: 858-863.

(3.794 impact factor, Q1)

9. Erdei, A.I., Borbély, A., Magyar, A., Taricska, N., Perczel, A., Zsíros, O., Garab, G., **Szűcs, E.**, Ötvös, F., Zádor, F., Balogh, M., Al-Khrasani, M., Benyhe, S. (2018) **Biochemical and pharmacological characterization of three opioid-nociceptin hybrid peptide ligands reveals substantially differing modes of their actions.** PEPTIDES, 99: 205-216.

(2.659 impact factor, Q2)

10. Dadam F, Zádor F, Caeiro X, **Szűcs E**, Erdei AI, Samavati R, Gáspár R, Borsodi A, Vivas L. (2018) **The effect of increased NaCl intake on rat brain endogenous μ-opioid receptor signalling.** J. NEUROENDOCRINOL., 30: e12585

(3.040 impact factor, Q2)

11. Ewelina Rojewska, Agnieszka Wawrzczak-Bargiela, **Edina Szűcs**, Sándor Benyhe, Joanna Starnowska, Joanna Mika, Ryszard Przewlocki, Barbara Przewlocka (2018) **Alterations in the Activity of Spinal and Thalamic Opioid Systems in a Mice Neuropathic Pain Model.** NEUROSCIENCE, 390: 293-302.

(3.244 impact factor, Q2)

12. Anna I Erdei, Adina Borbély, Anna Magyar, **Edina Szűcs**, Ferenc Ötvös, Dávid Gombos, Mahmoud Al-Khrasani, Azzurra Stefanucci, Marilisa Pia Dimmito, Grazia Luisi, Adriano Mollica, Sándor Benyhe (2019) **Biochemical and pharmacological investigation of novel nociceptin/OFQ analogues and N/OFQ-RYYRIK hybrid peptides.** PEPTIDES, 112: 106-113.

(2.843 impact factor, Q2)

13. Piotr F. J. Lipiński, **Edina Szűcs**, Małgorzata Jarończyk, Piotr Kosson, Sándor Benyhe, Aleksandra Misicka, Ján Cz. Dobrowolski, Joanna Sadlej (2019) **Affinity of fentanyl and its derivatives for the σ1 receptor.** MED. CHEM. COMM., 10: 1187 –1191.

(2.807 impact factor, Q1)

14. Ferenc Zádor, Gábor Nagy-Grócz, Gabriella Kékesi, Szabolcs Dvorácskó, **Edina Szűcs**, Csaba Tömböly, Gyöngyi Horváth, Sándor Benyhe, László Vécsei (2019) **Kynurenines and the Endocannabinoid System in Schizophrenia: Common Points and Potential Interactions.** MOLECULES, 24: 3709.

(3.267 impact factor, Q1)

15. Ferenc Zádor, Gábor Nagy-Grócz, Szabolcs Dvorácskó, Zsuzsanna Bohár, Edina Katalin Cseh, Dénes Zádori, Árpád Párdutz, **Edina Szűcs**, Csaba Tömböly, Anna Borsodi, Sándor Benyhe, László Vécsei (2020) **Long-term systemic administration of kynurenic acid brain region specifically elevates the abundance of functional CB1 receptors in rats.** NEUROCHEM. INT., 138:1047-52.

(3.881 impact factor, Q1)

16. **Edina Szűcs**, Eszter Ducza, Alexandra Büki, Gabriella Kékesi, Sándor Benyhe, Gyöngyi Horváth (2020) **Characterization of dopamine D2 receptor binding, expression and signaling in different brain regions of control and schizophrenia-model Wisket rats.** BRAIN RESEARCH, 1748:147-74.

(2.929 impact factor, Q2)

Cumulative impact factor (∑IF): 50.037

ACKNOWLEDGEMENTS

The work on orvinol and thevinol derivatives was carried out in cooperation with the former staff of the research laboratory of the discontinued Alkaloida Tiszavasvári Pharmaceutical Company. The research and development on opioid peptides containing kynurenines is a result of an ongoing Italian-Hungarian scientific cooperation between the Biological Research Centre of the Hungarian Academy of Sciences in Szeged, and the Department of Pharmacy, University of Chieti-Pescara "G. d'Annunzio" in Italy. The leaders of the joint project were Dr. Adriano Mollica, and Dr. Sándor Benyhe (OTKA-108518, supported by the National Research, Development and Innovation Office (NKFIH), Budapest, Hungary) scientific advisor on the Hungarian side. The kynurenine topic is also part of a running GINOP project led by Prof. László Vécsei (GINOP 2.3.2-15-2016-00034, provided by NKFIH, Budapest, Hungary and the Ministry of Human Capacities, Hungary grant 20391-3/2018/FEKUSTRAT) at the Department of Neurology, Faculty of Medicine, University of Szeged and MTA-SZTE Neuroscience Research Group, Szeged, Hungary.

Our contribution in this research was financially granted by the National Research, Development and Innovation Office (NKFIH, Budapest) which is the leading governmental agency for basic and applied scientific research.

My study is dedicated to the memory of our wonderful colleague, the late professor Maria Wollemann, MD, PhD, DSc (1923-2019), former institute director and founder and leader of the Opioid Receptor Group at the Institute of Biochemistry, Biological Research Centre of the Hungarian Academy of Sciences, Szeged, Hungary.

I am very grateful to Prof. Anna Borsodi who gave me the opportunity to start my work in this group.

I am sincerely thankful to my supervisor Dr. Sándor Benyhe for his support and advice throughout my PhD studies.

I am deeply thankful to Dr. Ferenc Ötvös for supporting and supervising me and for performing docking calculations.

I am very grateful to Dr. Ferenc Zádor for his advice and for giving me help performing experiments.

I am grateful to Dr. Csaba Tömböly and Dr. Szabolcs Dvorácskó for synthesizing and providing the radioactive and unlabelled opioid ligands.

I would like to thank Dr. János Marton, Dr. Sándor Hosztafi and their laboratories for synthesizing the Bentley analogues.

I would like to thank Prof. Gyöngyi Horváth and her group members for the *in vivo* characterization of the Bentley analogues.

I thank my beloved son Viktor and my family for their patience and support.

LIST OF ABBREVIATIONS

1a:	diprenorphine
1b:	buprenorphine
1e:	dihydroetorphine
1f:	20-methyl-dihydroorvinol
2a:	6-*O*-desmethyl-diprenorphine
2b:	6-*O*-desmethyl-buprenorphine
2c:	6-*O*-desmethyl-dihydroetorphine
2d:	6-*O*-desmethyl-phenethyl-orvinol
4:	20*R*-phenethyl-thevinol
5:	6-*O*-desmethyl-phenethyl-thevinol
7:	6-*O*-ethyl-6-*O*-desmethyl-phenethyl-thevinol
8:	3-methoxyetorphine
9:	etorphine
AC:	adenylyl cyclase
βPh:	beta-phenylethyl group, beta-phenethyl group, CH_2CH_2Ph
cAMP:	adenosine 3',5'-cyclic mono-phosphate
CNS:	central nervous system
CPM:	cyclopropylmethyl group
CSF:	cerebrospinal fluid
Cyp:	cyprodime, selective MOR antagonist
DAMGO:	[D-Ala^2, N-Me-Phe^4, Gly^5-ol]-enkephalin, selective MOR agonist
DMSO:	dimethyl sulfoxide
DOR:	δ-opioid receptor
DRG:	dorsal root ganglion
EC_{50}:	"ligand potency": the agonist concentration that produces 50% of the maximal possible effect of ligand
ED_{30}:	30% of the dose or concentration of a drug that produces a biological response

EGTA:	ethyleneglycol-tetraacetate
EM-2:	endomorphin-2
E_{max}:	"G-protein efficacy": the maximal effect of a G-protein after ligand modulated activation in a given tissue preparation
GDP:	guanosine diphosphate
GTP:	guanosine-5'-triphosphate
GTPγS:	guanosine-5'-O-(3-thiotriphosphate)
[^{35}S]GTPγS:	guanosine-5'-[^{35}S]thiophosphate
IC_{50}:	"ligand's affinity": the concentration of a drug that inhibits 50% of the specific binding of a competitor ligand
KA1:	NH_2-Tyr-D-Ala-Gly-N-Me-Phe-ethanolamine-KYNA
K2:	NH_2-Tyr-Pro-kyn-Phe-NH_2
K3:	NH_2-Tyr-Pro-Phe-kyn-NH_2
K4:	NH_2-Tyr-D-Ala-Gly-Phe-kyn-OCH_3
K5:	NH_2-Tyr-D-Ala-Gly-Phe-kyn-OH
K6:	NH_2-Tyr-D-Ala-Gly-Phe-kyn-NH_2
K_i:	"ligand affinity": equilibrium inhibition constant
KOR:	κ-opioid receptor
kyn:	L-kynurenine
KYNA:	kynurenic acid
MIA:	monosodium iodoacetate
MK-801:	(+)-MK-801 maleate
MOR:	μ-opioid receptor
NMDA:	N-methyl-D-aspartate
Nor-BNI:	norbinaltorphimine, selective KOR antagonist
NTI:	naltrindole, selective DOR antagonist
S.E.M.:	standard error of means
Tris-HCl:	tris-(hydroxymethyl)-aminomethane hydrochloride
U-69,593:	(+)-(5α,7α,8β)-N-Methyl-N-[7-(1-pyrrolidinyl)-1-oxaspiro[4.5]dec-8-yl]-benzeneacetamide, selective KOR agonist

1 INTRODUCTION

1.1 G-protein coupled receptors (GPCRs)

1.1.1 About GPCRs in general

The G-protein coupled receptor (GPCR), also known as seven-transmembrane domain receptor (7TM receptor), is a protein located in the cell membrane, which binds extracellular signalling substances (ligand) and transmits the binding signal to the intracellular environment. These substances can be light sensitive compounds, amines, hormones, small molecules, neurotransmitters, peptides, etc. GPCRs only exist in eukaryotes [1–3] and more than 800 genes of GPCRs are encoded by the human genome [4]. There are many classification schemes for the GPCR superfamily, one of witch called GRAFS divides the superfamily into five classes: Glutamate-, Rhodopsin-, Adhesion-, Frizzled/Taste2- and Secretin-like receptor family [4]. GPCRs play important roles in several physiological processes, for example: the visual sense, the gustatory sense (taste), the sense of smell, behavioural and mood regulation, regulation of the immune system [5,6], autonomic nervous system transmission, cell density sensing, homeostasis modulation [7], or the regulation of growth and metastasis of some types of tumours [8]. Robert J. Lefkowitz and Brian K. Kobilka won the 2012 Nobel Prize in Chemistry for their research of GPCR structure and function.

1.1.2 The structure of GPCRs

Several crystallography methods have been developed to solve GPCR crystal structures. The first crystal structure of a mammalian GPCR, the bovine rhodopsin (PDB: 1F88) was determined in 2000 [9]. In 2007, the first structure of human β_2-adrenergic receptor was solved, which GPCR structure showed similarity with the bovine rhodopsin receptor [10–12]. The structure of the GPCRs consist of three parts: (1) the extracellular amino-terminal (N terminus) segment and three extracellular loops (EL1-EL3); (2) the TM segment consisting of seven α-helices (TM1-TM7) and (3) the intracellular segment containing three intracellular loops (ICL1-ICL3), an intracellular amphiatic helix, and the carboxy-terminal tail (C terminus) (**Figure 1**).

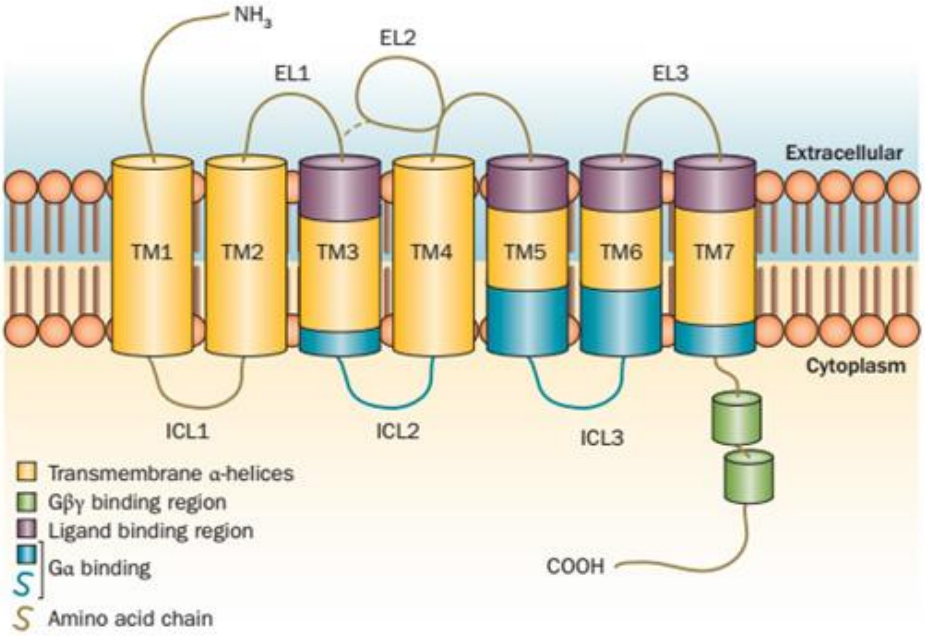

Figure 1. Schematic diagram of the GPCR structure. Adopted from [13].

1.1.3 GPCR signalling

The signalling cascades of GPCRs initiate from the binding of an external signal, which causes conformational changes in the receptor leading to the activation of the G-protein [14]. The G-protein consists of G_{α}, G_{β} and G_{γ} subunits, the beta and gamma subunits form a stable dimeric complex, thus they are also called the beta-gamma complex ($G_{\beta\gamma}$) [15]. The four main classes of G_{α} subunits are $G_{\alpha s}$ (stimulatory), $G_{\alpha i}$ (inhibitory), $G_{\alpha q}$, and $G_{\alpha 12/13}$. In inactive state, the GPCR is bound to a heterotrimeric G-protein complex, the G_{α} subunit is bound to GDP and is attached to the $G_{\beta\gamma}$ subunit. The activation of a G-protein causes the transmission of bound G_{α} subunit to active status, along with the exchange of GDP to GTP as well as the dissociation of G_{α} subunit (which bounds GTP) from the $G_{\beta\gamma}$ dimer and from the receptor. Both GTP-bound G_{α} [16] in the active form and the released $G_{\beta\gamma}$ dimer can stimulate a numerous signalling cascades (second messenger pathways) and effector proteins. When the GTP on G_{α} is hydrolysed to GDP, the original form of the receptor is restored [17–19].

Ligands could be separated based on the nature of their functional interaction with the target receptor. Due to the functional effects governed by efficacy and potency, the ligands can be distinguished to full agonists, partial agonists, neutral antagonists or inverse agonists depending on the alteration of GPCRs G-protein basal activity. The ligands with agonist

properties induce the receptor to alter its G-protein conformation to the active state, increasing the basal activity. While the inverse agonists induce the inactive state of the receptor, decreasing the basal activity [20,21]. The neutral antagonists bind equally to both receptor states, usually with a high affinity, therefore possessing a physiological role by competitively inhibiting agonist and inverse agonist binding [22]. Neutral antagonists do not alter the basal activity (**Figure 2**). Partial agonists exhibit intermediate levels of G-protein activity and are able to decrease the efficacy of the full agonists to their own stimulation level as previously reported by Szűcs et al. [23].

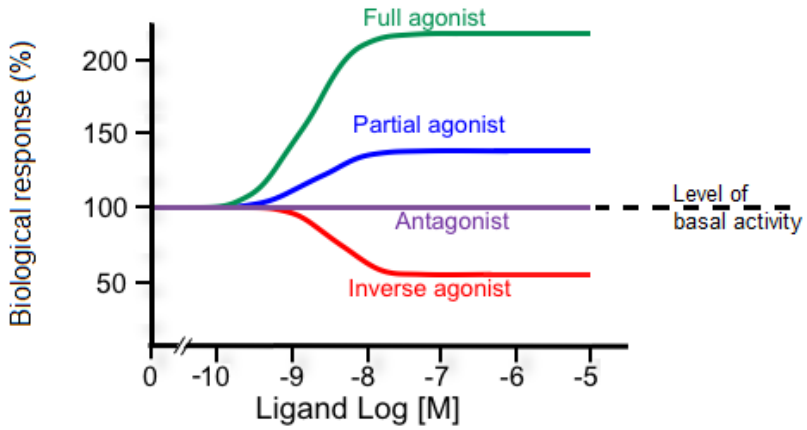

Figure 2. The spectrum of GPCR ligand efficacy.

1.1.3.1 G_α signalling

The adenylate cyclase (AC) enzyme is the effector protein of the $G_{\alpha s}$ and $G_{\alpha i}$ pathways, which catalyse the transformation of cytosolic adenosine triphosphate (ATP) to cAMP. The $G_{\alpha s}$ stimulates the production of cAMP from ATP. The level of cAMP can affect the activity of various ion channels and Ser/Thr-specific protein kinase A (PKA), thus cAMP acts as a second messenger. The $G_{\alpha i}$ subunit inhibits AC from generating cAMP (e.g. somatostatin, prostaglandin receptor).

The $G_{\alpha q}$ pathway stimulates the membrane–bound phospholipase C-β (PLCβ) effector, which catalyses the cleavage of phosphatidylinositol 4,5-bisphosphate (PIP_2) into the second messengers inositol (1,4,5) trisphosphate (IP3) and diacylglycerol (DAG).

In the $G_{\alpha 12/13}$ pathway the elevated intracellular Ca^{2+} also binds and activates calmodulin proteins related to small GTPase, Rho. When Rho binds to GTP, it activates Rho-kinase (ROCK) responsible for regulating the actin cytoskeleton.

1.1.3.2 $G_{\beta\gamma}$ signalling

The effects of $G_{\beta\gamma}$ signalling is also important. The primary effectors of $G_{\beta\gamma}$ pathway are various ion channels, *e.g.* G-protein coupled inwardly rectifying potassium channels (GIRKs), P/Q- and N-type voltage-gated Ca^{2+} channels, as well as some isoforms of AC and PLC, along with some phosphoinositide-3-kinase (PI3K) isoforms.

1.2 The opioid system

1.2.1 Poppy plant

The narcotic drug opium is derived from the opium poppy plant (*Papaver somniferum*), which is a dried latex extract from the seed capsules. The opium poppy is a widely cultivated plant domesticated by Sumerians around 3000 BC [24]. Ancient Egyptian medicine used opium for their anasthetic and narcotic effects. Opium contains opiates, natural alkaloid compounds, such as morphine and codein [25]. Morphine can be processed chemically to produce heroin and other semi-synthetic opioids.

1.2.2 Opioid receptors

Pain modulation is mainly regulated through the activation of the three classical types of opioid receptors, *i.e.* the μ-, δ- and κ-opioid receptors (MOR, DOR and KOR, respectively). [26–30]. The clone of MOR has been isolated from a rat brain cDNA containing 398 amino acid residues [31]. The cDNAs of DOR and KOR were isolated from mouse, containing 372 and 380 amino acids, respectively [32,33].

At the same time, cloning studies revealed the fourth receptor named “opioid receptor-like” (ORL) sequence from numerous labs [34–38]. ORL was renamed to nociception/orphanin FQ receptor (NOP) after the endogenous ligand of the receptor, nociceptin was identified by the lab of Meunier et al. [39]. Although it shows 48-49% homology with the opioid receptor family, it is classified separate as the semi-synthetic

neutral opioid antagonist, naloxone is not able to inhibit nociceptin receptor specific binding, in contrast to the three classical opioid receptors [40].

Opioid receptors are members of the Rhodopsin-like inhibitory GPCRs, their activation leads to the inhibition of AC [41], which results in hyperpolarisation [42,43] and inhibits certain presynaptic neurotransmitter (GABA, acetylcholine, norepinephrine, serotonin) release [44–47]. The main target of the antinociceptive drugs in the treatment of pain is MOR. Opioid receptors are expressed in the neurons of the central (CNS) and peripheral nervous system (PNS) (**Table 1**).

Table 1. The distribution and physiological functions of opioid receptors [48–50]**.**

Opioid receptors	Receptor distribution in CNS	Physiological function
MOR	periaqueductal gray, spinal cord (substantia gelatinosa of Rolando), olfactory bulb, nucleus accumbens, cerebral cortex, amygdala	analgesia, respiratory depression, cardiovascular functions, reduced gastrointestinal motility, miosis, euphoria, thermoregulation, hormone secretion, immune function
DOR	amygdala, olfactory bulb, cortex, pontine nuclei	analgesia, antidepressant effects, olfaction, cardiovascular regulation, respiration, gastrointestinal motility
KOR	hypothalamus, periaqueductal gray, claustrum	nociception, diuresis, thermoregulation, miosis, sedation, stress, depression

1.2.3 Opioid ligands

Endogenous opioid peptides such as Met- and Leu-enkephalin [51], β-endorphin [52] and dynorphin-A [53] are mainly released by neurons in the CNS. Enkephalins are also produced by adrenal medulla, spinal cord and other peripheral tissues [54], β-endorphin is primarly synthesized in the pituitary gland [55] and immune cells [56], while dynorphin-A can be found in hypothalamus, medulla and spinal cord [57]. Two endomorphin tetrapeptides, endomorphin-1 and endomorphin-2 (EM-2) [58] were found to be highly selective endogenous agonists for MOR.

Natural alkaloids called “opiates” are derived from the resin of the opium poppy, including morphine, codeine, thebaine, oripavine and many semi-synthetic congeners derived from them. The term opiates are also used for the semi-synthetic drugs derived from morphine. The esthers of morphine are diacetylmorphine (morphine diacetate; heroin), nicomorphine (morphine dinicotinate), dipropanoylmorphine (morphine dipropionate), diacetyldihydromorphine, acetylpropionylmorphine, desomorphine, methyldesorphine, dibenzoylmorphine, dihydrocodeine, ethylmorphine and heterocodeine. Semi-synthetic alkaloid derivatives are the oripavine derivatives (buprenorphine, etorphine), hydrocodone, hydromorphone, oxycodone and oxymorphone.

Numerous synthetic opioid ligands were discovered, the main chemical groups are the anilidopiperidines (fentanyl, carfentanil), the phenylpiperidines (pethidine), the diphenylpropylamine derivatives (diphenoxylate, propoxyphene, methadone), the benzomorphan derivatives (pentazocine, dezocine).

1.3 Kynurenines

1.3.1 The kynurenine pathway

Tryptophan is an essential amino acid that is a precursor in synthesis for modulatory biomolecules including serotonin, melatonin, tryptamine, and kynurenine. Tryptophan can be found in proteins and it also has an important structural or functional role. For example, tryptophan residues play special roles in anchoring membrane proteins within the cell membrane. The majority (~90%) of tryptophan is metabolized through the kynurenine pathway by three crucial enzymes: the two isoforms of indoleamine 2-3-dioxygenase (IDO1 and IDO2) and tryptophan 2,3-dioxygenase (TDO). The enzymes initiate the oxidation of tryptophan, this transformation results in L-kynurenine (kyn) through the N-formylkynurenine, the final product is the nicotinamide adenine dinucleotide (NAD^+) (**Figure 3**).

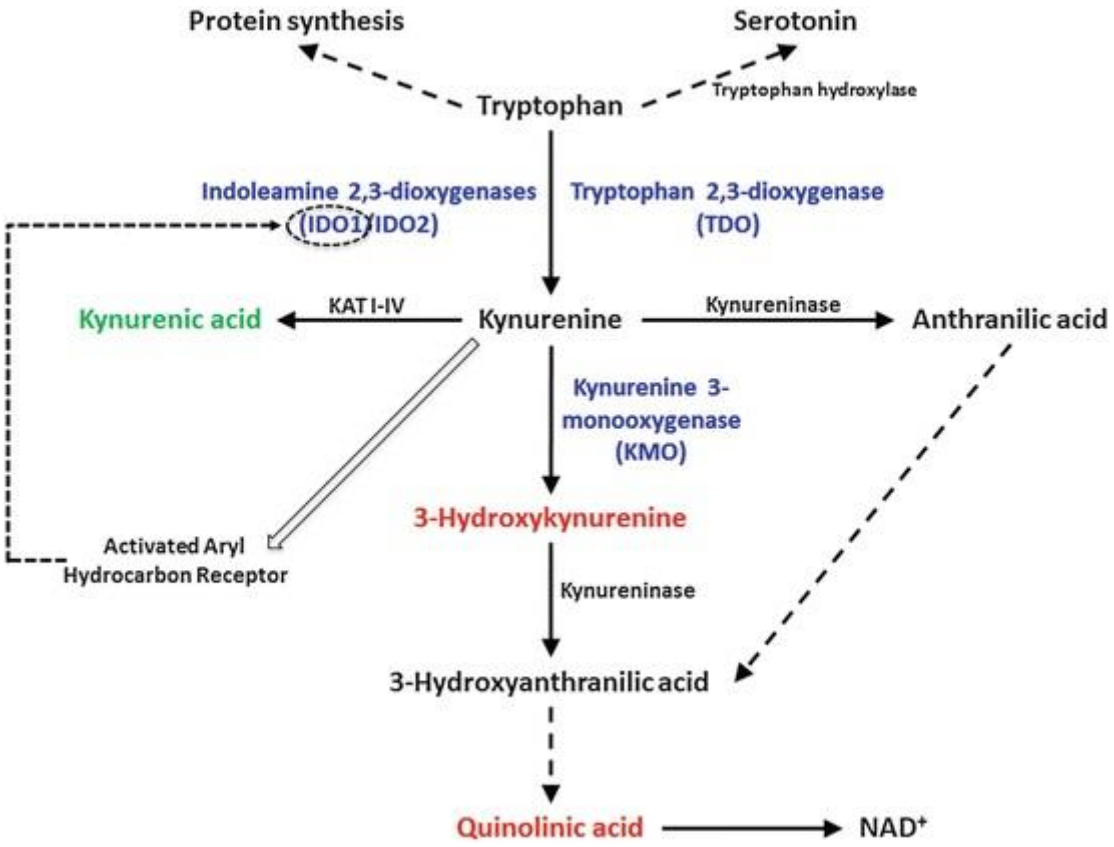

Figure 3. Pathways of tryptophan metabolism. Adopted from [59]**.**

The dysregulation of the kynurenine pathway is associated with aging and neurodegenerative diseases [60,61]. Changes in the kynurenine/tryptophan ratio may be responsible for many diseases, *e.g.* arthritis, HIV/AIDS, neuropsychiatric disorders, cancer and inflammations [62–64]. The ratio of kynurenine and tryptophan is also an indicator for the activity of indoleamine 2,3-dioxygenase (IDO) [65,66].

Kyn is synthesized in the brain, and depending on the quantity produced, it can be neurotoxic or neuroprotective. Quinolinic acid has a neurotoxic effect, it is produced from kyn, *via* the additional toxic metabolites (3-hydroxykynurenine and 3-hydroxyanthranillic acid). It acts as an N-methyl-D-aspartate (NMDA) receptor agonist [67]. Within the brain, quinolinic acid is only produced by activated microglia and macrophages [68]. In contrast, kynurenic acid (KYNA) is neuroprotective, which is formed directly from kyn catalysed by kynurenine aminotransferase (KAT).

1.3.2 KYNA receptors

The neuroprotective and antinociceptive effects of KYNA are due to the inhibition of the excitatory amino acid (EAA) receptors [69]. KYNA possesses an antagonistic effect on the NMDA receptor and other glutamate receptors such as AMPA and kainate receptors [69,70]. NMDA receptors are essential for the control of the glutamatergic work at the CNS; in contrast to the kainate and AMPA receptors, the NMDA receptor mediates the influx of Ca^{2+} ions into neurons, playing an important role in synaptic plasticity, memory, and learning [69,70]. Over activation of NMDA receptors can lead to excitotoxicity, severe cell damage, and apoptosis of neurons, which are strongly related to neurodegenerative and CNS disorders such as depression, stroke, ischemia, and neuropathic pain [71–73].

KYNA is also found to have an agonistic effect on the orphan GPCR GPR35 [71,74], which can be found in various tissues and organs such as gastrointestinal tract, liver, immune system, CNS, and cardiovascular system [72]. GPR35 protein is mainly expressed in both neurons and glial cells in the brain, but also in the neurons of the dorsal root ganglion (DRG).

KYNA acts as an agonist for the orphan GPCR hydroxyl-carboxylic acid receptor 3 (HCAR3), which is also a target for the 3-hydroxyoctanoic acid and for niacin (nicotinic acid) [75,76]. The HCAR3 is present only in higher primates, it is expressed in adipocytes and it mediats antilipolytic effects in fat cells. HCAR3 is also expressed in a variety of immune cells and it plays a role in the regulation of gene transcription, in the embryonic development and in the maturation of cells in the immune and nervous system.

1.3.3 Kyn and KYNA

The two most studied metabolites of the kynurenine pathway are kyn and KYNA. They are present in lens crystalline, human $Cu^{2+/}Zn^{2+}$ dismutase, milk proteins and several bioactive compounds produced by bacteria and marine organisms [77]. Daptomycin is a cyclic kyn-containing lipodepsipeptide approved by the Food and Drug Administration (FDA), isolated from *Streptomyces roseoporus* used in the treatment of Gram-positive pathogen skin infections [78]. Cyclomontanin B isolated from *Annona montana* exhibits a promising anti-inflammatory activity [79]. The kyn-containing peptide FP-kyn-LNH_2 is the minor component of the Australian red tree frog (*Litoria rubella*) skin collected in central Australia, endowed with opioid activity at 10^{-7} M (**Figure 4**) [80].

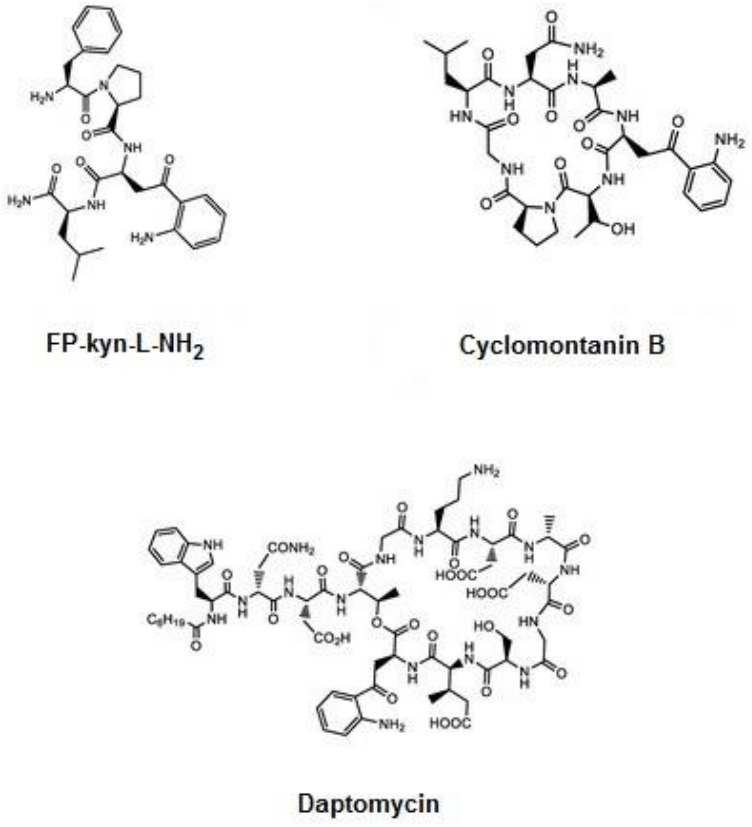

Figure 4. Natural bioactive compounds containing kyn residue.

The occurrence of kyn in natural products suggests a possible specificity towards their biological targets. The enzymes of the human kynurenine pathway are expressed in different tissues and cell types throughout the body [77]. In humans, the majority of kyn is excreted by urine; thus, its bioavailability increases according to the tryptophan flux downstream of the kynurenic pathway [81]. Kyn is able to penetrate the CNS by transport across the blood–brain barrier (BBB), but it is also produced locally [61].

KYNA was originally discovered in canine urine, but a huge amount has been measured in the gut, bile, human saliva, synovial and amniotic fluid; it has also been detected in food products such as broccoli, some potatoes, and honeybee products [77]. KYNA itself, the only known endogenous NMDA receptor antagonist, hardly crosses the BBB at all [82,83]. Different therapeutic approaches based on the kynurenine pathway have been postulated to circumvent this problem, such as the use of KYNA prodrugs or analogues able to penetrate more readily than the parent compounds or the involvement of ascorbate

conjugation to promote the interaction of KYNA with SVCT2 transporter (sodium-dependent vitamin C transporter 2) protein [84–86].

Changes in levels of KYNA int he brain have been identified in several neurological disorders. Elevated KYNA levels in the striatum and hippocampus [87], and decreased KYNA levels in the blood [88] and cerebrospinal fluid (CSF) [89] have been observed in Alzheimer's disease. The levels of KYNA were decreased in the substantia nigra pars compacta (SNpc), frontal cortex and putamen [90] in Parkinson's disease. Decreased KYNA levels were characteristic in the cortex [91], striatum [92,93] and CSF in Huntington's disease. In multiple sclerosis in the CSF elevated KYNA levels were measured during acute relapse [94], while the amount of KYNA was definitely lower during chronic remission [95]. In epilepsy decreased KYNA [96] and kyn [97,98] levels can be detected in the CSF of patients with infantile spasms, while the KYNA levels were smaller in the CSF of patients with West syndrome [99].

1.4 Pain

1.4.1 Pain in general

The International Association for the Study of Pain's (IASP) definition of pain is: "an unpleasant sensory and emotional experience associated with, or resembling that associated with, actual or potential tissue damage" [100]. Pain can be characterized by its neurobiological component, nociception (perception of a noxious stimulus), the affective component (emotion of pain) can only be studied in humans. In animal experiments the activation of nociceptors and the behavioural response given to painful stimuli can be observed.

Nociceptors, which are sensory nerve endings that specifically respond to tissue-damaging stimuli, can be distinguished in several ways. Based on sensitivity, there are unimodal (stimulated only by thermal or mechanical stimuli) and polymodal (activated by thermal, mechanical and chemical stimuli) receptors.

Based on the duration of pain, it can be divided into acute and chronic pain [101]. Pain is designated acute if it lasts only until the noxious stimulus is removed or the pathology has healed. Pain lasting more than 6 months is called chronic pain, such as rheumatoid arthritis,

peripheral neuropathy, cancer and idiopathic pain. Based on the myelination of their axons, there are myelinated, fast-conducting (12–30 m/s) Aδ-fibers and myelinated, fast-conducting (0.5–2 m/s) C-fibers.

Increased pain induced by mild painful stimuli is termed hyperalgesia, while pathological pain induced by non-painful stimuli is termed allodynia [102]. Both mechanical and thermal allodynia and hyperalgesia can occur as a result of inflammation and central or peripheral nerve injury of various origins (traumatic, toxic), which can occur at any level of the somatosensory or spinothalamic-cortical system [103].

1.4.2 Opioid system and pain

Morphine is a prototype opioid agonist binding to MOR and is still the most frequently used drug in pain medication (**Table 2**). Beside pain relief and analgesia, it has serious side effects including decreased respiratory effort, tolerance development, low blood pressure and it also has a high potential for addiction and abuse [104–106]. Therefore, it is very important to find new ligands with higher affinity, selectivity and stability with decreased side effects.

An opioid epidemic is the overuse or misuse of addictive opioid drugs. It has significant medical-, social- and economic consequences, including overdose deaths. The proclamation of “The Opioid Crisis” by the U.S. Surgeon General began with the over-prescription of opioids in the 1990s, which are the most prescribed class of medications in the United States. Opioids administrated postoperatively or for pain management are one of the leading causes of opioid misuse, where approximately 6% of people continued opioid use after surgery or trauma [107]. In 2017 fentanyl was the most commonly used synthetic opioid, it was also listed by the World Health Organization as an essential drug in the form of fentanyl patches for cancer pain [107]. Yet in 2016, the illegal fentanyl and its analogues were the cause of most common overdose deaths in the United States, accounting for more than 20,000, around half of opioid-related deaths [108].

Table 2. List of the most common opioids used as medication.

	Chemical name	Drug name	Use for medication
Short-acting opioids	morphine sulfate	Avinza	for both acute pain and chronic pain and it is frequently used for pain from myocardial infarction [109]
	fentanyl	Fentora	was developed for pain management treatment of cancer patients [110]
	oxycodone	OxyContin	used for treatment of moderate to severe pain [111]
	hydrocodone	Hysingla	used to treat severe pain and also used as a cough suppressant in adults [112]
	codeine	Fiorinal or Prometh	used to treat pain, coughing, and diarrhea [113]
	heroin	-	used for management of breakthrough pain in children with cancer [114]
Long-acting opioids	methadone	Dolophine	used for opioid maintenance therapy in opioid dependence and for chronic pain management [115,116]
	etorphine (animal)	Immobilon or M99	used as a sedative in veterinary practice [117]
	carfentanil (animal)	-	used in ungulates due to its immobilizing properties [118]
	oxymorphone	Numorphan or Opana	used for the relief of moderate to severe pain and for treatment of acute post surgical pain [119]
	tramadol	Ultram	used primarily to treat mild to severe pain, both acute and chronic [120]
Mixed agonist/antagonist	butorphanol	Stadol	used for management of migraine using the intranasal spray formulation [121] also used as a supplement for balanced general anesthesia used in domestic and nondomestic veterinary species for analgesia, sedation, or improved quality of anesthesia [122]
	nalbuphine	Nubain	used as a supplement to balanced anesthesia, for preoperative and postoperative analgesia [123]
	dezozine	Dalgan	administered intravenously to relieve post-operative pain [124]
Partial agonist	buprenorphine	Subutex	used for detoxification and opioid replacement therapy, acute pain, and chronic pain [125]
	meptazinol	Meptid	used to treat moderate to severe pain, most commonly used to treat pain in obstetrics [126]

Antagonist	diprenorphine	Revivon	used to reverse the effects of super-potent opioid analgesics such as etorphine and carfentanil, the drug is not approved for use in humans [127,128]
	naloxone	Narcantin	used to counter decreased breathing in opioid overdose [129] used as an antidote for acute alcohol intoxication [130]
	naltrexone	ReVia or Vivitrol	used to manage alcohol or opioid dependence [129] also used to treat obesity [131]
	nalmefene	Selincro	used primarily in the management of alcohol dependence [132]

The three primary symptoms (which may not always be present together) for opioid toxicity are: respiratory depression, generally accompanied by depressed consciousness and miosis. Naloxone therapy is the standard treatment for opioid toxicity [133]. Naloxone can precipitate withdrawal symptoms including anxiety, irritability, and restlessness; gooseflesh; hot and cold sweats; muscle-, bone- and joint aches; tremor; nausea, vomitting and diarrhea; increased resting pulse rate [134].

Opioids combined with non-opioid drugs are another way to treat moderate to severe pain decreasing the risk of tolerance and dependence (*e.g.* Percodan: oxycodone/aspirin, Percocet: oxycodone/paracetamol, Vicodin: hydrocodone/paracetamol, Vicoprofen: hydrocodone/ibuprofen) [135].

1.4.3 KYNA and pain

Different NMDA receptor sites were examined in the rat model of formalin-induced facial pain. The results showed that the nociceptive behavioural responses were effectively reduced by the NR2 subunits, which means that these subunits have importance in inflammatory pain diseases [136,137]. Intracisternal KYNA attenuates formalin-induced nociception in animals together with antagonist activity at the glycine binding site of NMDA receptor, which is associated with analgesic properties in rats [138]. At the peripheral sites, KYNA decreases the nociceptive behaviour in the tail flick- and hot plate tests [139]. Administration of kyn and probenecid together with KYNA analogues inhibits NMDA receptors in animal models of trigeminal activation and sensitization [139]. Noteworthy,

KYNA and its analogues are able to act on second-order neurons, decreasing mechanical allodynia and pain sensitivity in different animal pain models [140].

The activation of GPR35 by KYNA, leads to hyperpolarization in the cell, which decreases glutamate and pro-inflammatory substance release from the glial and immune cells, another way of the analgesic effect of KYNA in inflammatory models. The agonist KYNA and zaprinast could inhibit the AC of DRG in an inflammatory pain model through GPR35 [141]. Probenecid injection amplified the effects of the two agonists, zaprinast was more effective in lower concentration compared to KYNA. These results suggest that the GPR35 could be a promising and novel pharmacological target for the inflammatory pain reduction [142].

Both kynurenine and KYNA binds to HACR3, which is then able to promote the generation of immune-suppressive T cells that support cancer development [143]. The question is whether the KYNA-induced activation of HCAR3 and the effects, such as elevated kynurenine/KYNA levels can increase the risk of developing malignancies. Or the anti-inflammatory actions of kynurenines due to a controlled activation of HACR3 may be used for the treatment of different immune disorders [144,145]. This can be another approach for the management of cancer related pain.

1.5 Approaches to overcome opioid side-effects

1.5.1 Bentley analogues

Natural morphine alkaloids (*e.g.* morphine, codeine, thebaine, neopine, oripavine) [146] can be converted into a variety of pharmacologically more advantageous compounds, such as the so called nal-compounds (naloxone, naltrexone, nalbuphine) and the ring-C bridged derivatives (6,14-ethenomorphinans or Bentley-compounds, *e.g.* etorphine (**9**), buprenorphine, diprenorphine). In this study nine previously synthesized orvinol and thevinol-type MOR-selective ligands [147–156] were examined (compounds **1e**, **1f**, **2a**, **2b**, **2d**, **4**, **5**, **7**, **8** (3-methoxyetorphine)). 6-*O*-desmethyl-dihydroethorphine (**2c**) is a new compound synthesized for this study (**Figure 5**, **6**, **7**).

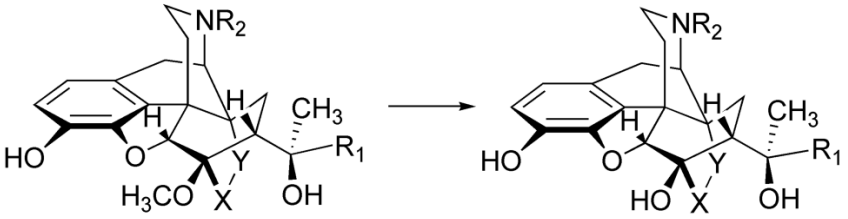

a: $R_1 = CH_3$, R_2 = CPM, X-Y = CH_2CH_2
b: R_1 = *tert*-Bu, R_2 = CPM, X-Y = CH_2CH_2
c: R_1 = *n*-Pr, $R_2 = CH_3$, X-Y = CH_2CH_2
d: $R_1 = CH_2CH_2Ph$, $R_2 = CH_3$, X-Y = CH=CH
e: $R_1 = CH_3$, $R_2 = CH_3$, X-Y = CH=CH
f: $R_1 = CH_3$, $R_2 = CH_3$, X-Y = CH_2CH_2

Figure 5. Structures of 6-*O*-desmethyl-orvinol analogues.

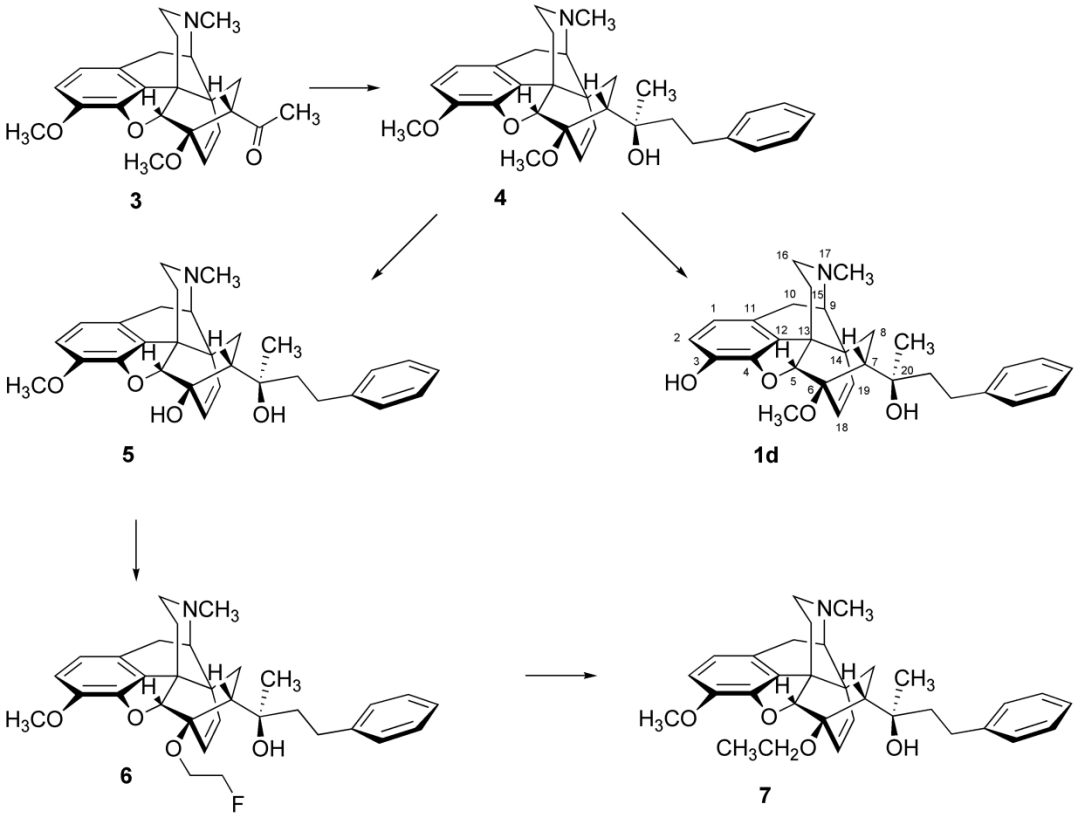

Figure 6. Structures of phenethyl-thevinol- and -orvinol derivatives.

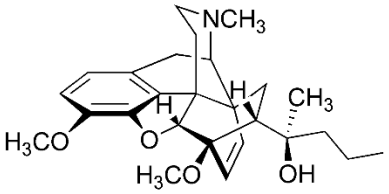

8

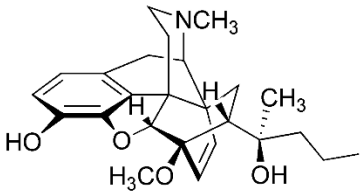

9

Figure 7. The structure of compound 8 and 9.

A number of structure-activity relationship studies dealing with thevinol and orvinol derivatives are available [157,158], but the biochemical and pharmacological properties of our target compounds have not been reported except for **8** [156].

The presence or absence of specific functional groups in the orvinol and thevinol derivatives can not be straightforwardly related to their pharmacological profiles. As an example, the 17-*N*-substituent serves as an acknowledged pharmacological switch between agonists and antagonists being methyl or cyclopropymethyl (CPM), respectively. However, it is highly ambiguous within this class of opioids, regarding that 17-*N*-CPM derivative can be full agonist as well [159,160] which may be a consequence of the bigger size of these opiates resulting in a more complex interaction pattern with the receptor. According to this, it seems plausible to investigate the interacting residues or atoms of the receptor leading to the specific response, *i.e.* pharmacological feature.

1.5.2 Oligopeptides

Considering the presence of kyn residue in natural peptide sequences and the important role exerted by both kynurenines in the CNS [161–163], the aim was to investigate the biological consequences of the insertion of these residues in opioid pharmacophore sequences. Kyn could be used in place of phenylalanine (Phe), considering its aromatic side chain, whereas KYNA could be used as a C-terminus to mimic an additional aromatic residue. The synthesis and biological screening of six novel kynurenines containing peptides were performed (**Figure 8**), aiming to investigate the modifications imposed by the presence of kyn and KYNA on the biological properties of known endogenous and synthetic opioid peptides *in vivo* and *in vitro*. Peptide **KA1** retains the [D-Ala^2, N-Me-Phe^4, Gly^5-ol]-enkephalin (DAMGO, synthetic opioid peptid) primary sequence, but the OH terminal group is esterified

by KYNA. Peptides **K2** and **K3** are EM-2 analogues in which the Phe residues in positions 3 and 4 have been replaced with kyn and kyn C-terminal amides, respectively. Peptides **K4**–**K6** are enkephalin-like peptides containing kyn in position 5, bearing as C-terminal the methyl ester, acid, and amide group, respectively.

KA1

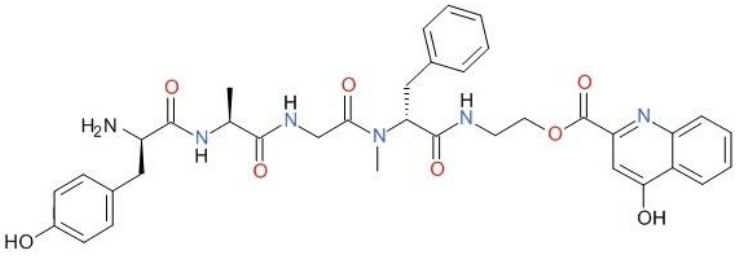

K2

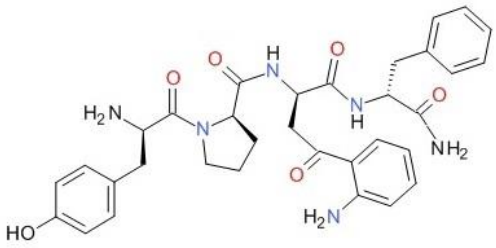

K3

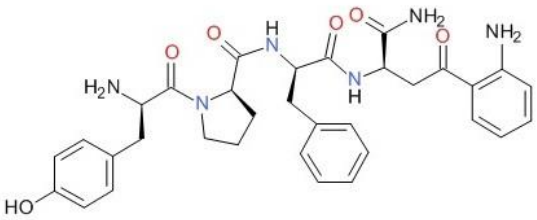

K4: R = OCH_3
K5: R = OH
K6: R = NH_2

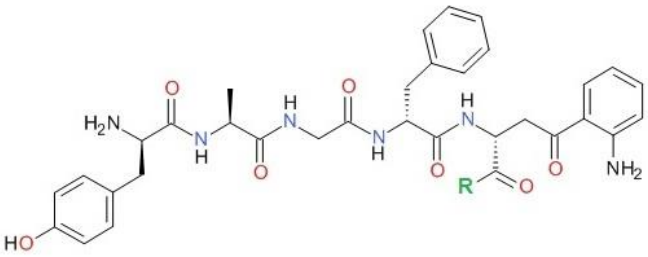

Figure 8. The chemical structure of the oligopeptides.

2 AIMS OF THE STUDY

Opioid ligands still have a crucial role in the MOR-mediated central and peripheral antinociception, although their use can be very dangerous. The aim of this study is to find new ligands, which have higher maximal efficacy at lower concentration than the frequently used morphine to decrease the risk of side effects (such as dependence and tolerance) of analgesic drugs. For this purpose 9 known and 1 new Bentley analogues, and 6 newly synthesized oligopeptides (DAMGO, EM-2 and enkephalin-like peptides containing kynurenines) are described in this thesis to examine which approach for ligand developement is more expedient.

The objectives of the study presented in the thesis were the following:

- To measure the binding affinity of the 10 Bentley compounds towards MOR, DOR and KOR and the 6 new oligopeptides towards MOR, DOR, KOR and NMDA receptor in competition binding assay in rat and guinea pig brain membranes.
- To examine G-protein activation and opioid receptor mediation of the ligands in functional [^{35}S]GTPγS binding.
- To analyse the antiallodynic and antinociceptive effects of the Bentley analogues and the oligopeptides, respectively, *in vivo* test using an animal model of inflammation.
- To compare the final results of biochemical and pharmacological experiments of the examined opioid ligands.

3 MATERIALS AND METHODS

3.1 Chemicals

3.1.1 Radiochemicals

The radiolabelled GTP analogue, [^{35}S]GTPγS (specific activity: 3.7 x 10^{13} Bq/mmol; 1000 Ci/mmol) was purchased from *Hartmann Analytic* (Braunschweig, Germany). [^{3}H]DAMGO [164] (specific activity: 38.8 Ci/mmol), [^{3}H]Ile^{5,6}-deltorphin II [165] (specific activity: 19.6 Ci/mmol) and [^{3}H]HS665 [166] (specific activity: 13.1 Ci/mmol) were radiolabelled by the *Laboratory of Chemical Biology group of the Biological Research Centre* (Szeged, Hungary). [^{3}H]MK-801 [167] (specific activity: 30 Ci/mmol) was acquired from *PerkinElmer* (Boston, MA, USA).

3.1.2 Receptor ligands and fine chemicals

$MgCl_2$ x $6H_2O$, EGTA, Tris-HCl, NaCl, GDP, the GTP analogue GTPγS, and the L-tryptophan metabolite kynurenic acid were purchased from *Sigma-Aldrich* (Budapest, Hungary). The highly selective MOR agonist enkephalin analogue DAMGO was obtained from *Bachem Holding AG* (Bubendorf, Switzerland); EM-2 was kindly provided by *MTA-ELTE Research Group of Peptide Chemistry* (Budapest, Hungary). The highly selective DOR agonist Ile^{5,6}-deltorphin II was synthesized in the *Laboratory of Chemical Biology group of the Biological Research Centre* (Szeged, Hungary). The highly selective KOR agonist diphenethylamine derivative, HS665 [168] were kindly offered by *Dr. Helmut Schmidhammer* (University of Innsbruck, Austria). Naloxone was provided by *Endo Laboratories DuPont de Nemours* (Wilmington, DE, USA). The morphine analogues were provided by *ABX GmbH* (Radeberg, Germany). The oligopeptides were synthesized in the *Department of Pharmacy, University of Chieti-Pescara* (Chieti, Italy). The non-competitive NMDA receptor antagonist, MK-801 and kyn were obtained from *Tocris Bioscience* (Bristol, UK). DAMGO, [Ile^{5,6}]-deltorphin II, HS665 and the oligopeptides were dissolved in water, morphine analogues were dissolved in ethanol and were stored in 1 mM stock solution at −20 °C. The UltimaGold^{TM} MV aqueous scintillation cocktail was purchased from *PerkinElmer* (Boston, MA, USA).

3.2 Animals

3.2.1 *In vitro* studies

For membrane homogenate preparations male and female Wistar rats and guinea pigs were used. Rats were purchased from and housed in the local animal house of the Biological Research Centre (Szeged, Hungary), while guinea pigs were purchased from and housed in LAB-ÁLL Bt. (Budapest, Hungary). All the animals were kept in a temperature controlled room (21–24 °C) under a 12:12 h light/dark cycle and allowed free access to food and water. All housing and experiments were conducted according to the European Communities Council Directives (2010/63/EU) and the Hungarian Act for the Protection of Animals in Research (XXVIII.tv. 32.x). The total number of animals as well as their suffering was minimized.

3.2.2 *In vivo* studies with Bentley analogues

All experiments involving animal subjects were carried out with the approval of the Hungarian Ethical Committee for Animal Research (registration number: XIV/03285/2011). Male Wistar rats (Charles River Laboratories, Bioplan, Budapest, Hungary; 378 ± 5.1 g; n = 6-8/group) were used in the experiments. The animals were group-housed (4 animals/cage) with free access to food and water, and with a 12:12 h light/dark cycle. Animal suffering and the number of animals per group were kept at a minimum; therefore, the drugs were administered in cumulative doses in 30-min intervals (at 0th, 30th and 60th min), and injections were repeated 7 days apart for the same animal, as in our previous study [169].

3.2.3 *In vivo* studies with oligopeptides

In our experiments, we used CD-1 male mice (Harlan, Italy, 25-30 g) maintained in colony, housed in cages (7 mice/cage) under standard light/dark cycle (from 7:00 a.m. to 7:00 p.m.), temperature (21 ± 1 °C) and relative humidity (60% ± 10%) for at least 1 week. Food and water were available ad libitum. The Service for Biotechnology and Animal Welfare of the Istituto Superiore di Sanità and the Italian Ministry of Health authorized the experimental protocol according to Legislative Decree 26/14.

3.3 *In vitro* binding experiments

3.3.1 Preparation of brain samples for binding assays

A crude membrane fraction of Wistar rat and guinea pig brains were prepared for ligand binding experiments according to [170] with changes. After decapitation, brains were rapidly removed and homogenized in 30 volumes (*v/w*) of ice-cold 50 mM Tris–HCl (pH 7.4) buffer with a Teflon-glass Braun homogenizer at 1,500 rpm. After centrifugation at 18,000 rpm for 20 min at 4 °C, the resulting pellet were suspended in 30 volumes (*v/w*) of the same buffer and incubated for 30 min at 37 °C to remove endogenous opioids. Centrifugation was then repeated as described above. The final pellet was suspended in 5 volumes (*v/w*) of 50 mM Tris–HCl (pH 7.4) buffer and stored at −80 °C. Membranes were thawed, diluted with buffer and the resulting pellet were taken up in appropriate fresh buffer and immediately used. For the [^{35}S]GTPγS binding experiments the final pellet of rat and guinea pig brain membrane homogenates were suspended in 5 volumes (*v/w*) of ice-cold TEM (50 mM Tris-HCl pH 7.4, 1 mM EGTA, 5 mM $MgCl_2$) buffer to obtain the appropriate protein content for the assay (~10 µg/ml) and stored at −80 °C for further use.

3.3.2 The principles of in vitro binding assays

The basis of the assays is to add a radioactive compound to a protein homogenate, membrane fraction, cell culture etc. and then incubate them together in certain conditions until the equilibrium binding is reached. The experimental conditions of the equilibrium binding are always defined by the applied radiochemical. Afterwards the bound and free radioactive ligands can be separated from each other; therefore, the amount of bound radioactive ligand can be measured. Two binding assays were used, the radioligand competition and the [^{35}S]GTPγS binding assay to examine ligand binding affinity and agonist activity, respectively.

In the radioligand competition binding experiment a radioactive ligand is applied (in most cases tritium labelled) in fixed concentrations in the presence of increasing concentrations of an unlabelled ligand. If the unlabelled ligand is able to bind to the receptor as the radioligand, the unlabelled ligand displaces the radioligand at the binding site depending on the concentration. The displacement will be shown by the reduced detected

radioactivity in the sample. Then binding affinity data can be received about the applied unlabelled ligand.

In [^{35}S]GTPγS binding assays the target receptor mediated G-protein activation is examined, namely the GDP → GTP exchange of G_{α}, in the presence of an agonist ligand in increasing concentration. The nucleotide exchange is detected by a non-hydrolysable, radioactive, sulphur 35 isotope (^{35}S) labelled GTP analogue called [^{35}S]GTPγS. Due to the bound of γ-thiophosphate, [^{35}S]GTPγS inhibits the GTPase activity of G_{α}, so it cannot be hydrolyzed to GDP and the G protein cannot reassociate into a heterotrimer. As a result the G_{α} bound with [^{35}S]GTPγS accumulates and the incorporated ^{35}S radioactivity can be measured in the samples. The higher the incorporated ^{35}S the higher is the agonist activity of the observed compound, as it stimulated the nucleotide exchange in a greater extent.

3.3.2.1 Competition binding experiments

In MOR, DOR and KOR displacement, aliquots of frozen rat and guinea pig brain membrane homogenates were thawed and suspended in 50 mM Tris-HCl buffer (pH 7.4), in NMDA receptor displacement, the Tris-HCl buffer (pH 7.4) contained 100 µM glycine and 100 µM L-glutamic acid. Samples were incubated in the presence of the unlabelled ligands in increasing concentrations (10^{-10} to 10^{-5} M) for at 35 °C for 45 min with 2 nM [^{3}H]DAMGO, for at 35 °C for 45 min with 2 nM [^{3}H]Ile^{5,6}-deltorphin II, at 25 °C for 30 min with 2 nM [^{3}H]HS665, and at 25 °C for 120 min with 5 nM [^{3}H]MK-801. In homologue displacements using [^{3}H]DAMGO, [^{3}H]Ile^{5,6}-deltorphin II, [^{3}H]HS665 or [^{3}H]MK-801 the level of nonspecific binding was determined in the presence of 10 µM unlabelled naloxone (MOR and DOR), HS665 (KOR) and MK-801 (NMDA receptor), while total binding was determined in the absence of unlabelled ligand. The incubation was followed by rapid filtration under vacuum (Brandel M24R Cell Harvester; Brandel Harvesters), and washed three times with 5mL ice-cold 50mM Tris-HCl. The filtration was accomplished through Whatman GF/C glass fibres. The radioactivity of the filters was measured in UltimaGold MV aqueous scintillation cocktail (Perkin Elmer, Waltham, MA) with Packard Tricarb 2300TR liquid scintillation counter (Perkin Elmer, Waltham, MA). The competition binding assays were performed in duplicates and repeated at least three times.

3.3.2.2 Functional [^{35}S]GTPγS binding experiments

Rat and guinea pig brain membranes (~10 μg of protein/tube) were incubated at 30 ^{o}C for 60 min in Tris–EGTA buffer (50 mM Tris–HCl buffer, 3 mM $MgCl_2$, 1 mM EGTA, 100 mM NaCl, pH 7.4) containing 0.05 nM [^{35}S]GTPγS with increasing concentrations (10^{-10}-10^{-5} M) of opioid ligands tested in the presence of 30 μM GDP in a final volume of 1 mL [171–173]. Total binding was measured in the absence of test compounds, non-specific binding was determined in the presence of 10 μM unlabelled GTPγS and subtracted from total binding. The difference between total and non-specific binding values represents basal activity. The reaction was terminated by rapid filtration under vacuum (Brandel M24R Cell Harvester), and Whatman GF/B glass fiber filters were washed three times with 5 mL ice-cold 50 mM Tris-HCl (pH 7.4) buffer. The radioactivity of the dried filters was detected in Ultima GoldTM MV aqueous scintillation cocktail with Packard TriCarb 2300TR liquid scintillation counter. [^{35}S]GTPγS binding experiments were performed in triplicates and repeated three times.

3.4 Chronic inflammatory pain model and measuring allodynia

The following compounds were applied in these *in vivo* studies: etorphine-hydrochloride (**9**) [156,174] eight 6,14- ethenomorphinan derivatives synthesized as described earlier [147–150,152,153,155], **2a** and **1e**, **1f**, **2b**, **2d**, **4**, **5**, **7** as well as the new compound **2c**. The compounds were freshly diluted (0.01-10 mM) with distilled water from the stock solutions and administered subcutaneously (s.c.) in a volume of 2 mL/kg.

To induce chronic inflammatory pain, an animal model of osteoarthritis was applied. Osteoarthritis was induced by injecting monosodium iodoacetate (MIA) (Sigma-Aldrich Ltd. Budapest, Hungary; 1 mg/30 mL) into the tibiotarsal joint of the right hind leg on two consecutive days. MIA treatments were given to gently restrained conscious animals, using a 27-gauge needle, without anesthesia so as to exclude any drug interaction. These injections did not elicit signs of major distress. Within 14 days MIA had consistently been shown to cause severe end-stage cartilage destruction resulting in osteoarthritis-like joint pain accompanied with moderate edema [169,175,176]. The observer was blind to the drug treatment administered.

The threshold for withdrawal from mechanical stimulation to the plantar aspect of the hindpaws was assessed using a dynamic plantar aesthesiometer (Ugo Basile, Comerio, Italy), which consists of an elevated wire mesh platform to allow access to the ventral surface of the hindpaws. Prior to baseline testing, each rat was habituated to a testing box for at least 20 min. Measurements were done with a straight metal needle (diameter 0.5 mm) that exerts an increasing upward force at a constant rate (6.25 g/s) with a maximum cut-off force of 50 g over an 8 s period. The measurement was stopped when the paw was withdrawn, and the results were expressed as paw withdrawal thresholds in grams.

After MIA injections, baseline pain thresholds (2 times with 15 min interval) were determined 14 days later and their means provided the baseline value. Cumulative-dosing procedure was applied. The control group received distilled water, while the positive control group was treated with **9** (0.1, 0.3, and 1.0 nmol/kg). The higher doses of **9** were also applied in a preliminary experiment (1.0 and 3.0 nmol/kg) but 3.0 nmol/kg dose induced catatonia and respiratory depression in 100% of the animals, thus we determined the maximum dose as 1 nmol/kg. Response latencies were measured at 15 min intervals and the increasing doses of the drugs (three doses) were administered following two recordings. After the highest dose injection the pain threshold was assessed in every 15 min for 1 h, then hourly at the second and third hour to determine the time course of drug effects. Although, the motor behavior and general status of the animals were not investigated and quantified systematically, altered behavior (excitation, flaccidity or motor weakness) or any signs of opioid overdose (catatonia or respiratory depression) were not observed.

3.5 Formalin test: a model for acute inflammatory pain

Oligopeptide **K6** and DAMGO were applied in these *in vivo* studies. In the formalin test, the injection of a dilute solution of formalin (1%, 20 μL/paw) into the dorsal surface of the mouse hind paw evoked biphasic nociceptive behavioural responses, such as licking, biting the injected paw, or both, occurring from 0 to 10 min after formalin injection (the early phase) and a prolonged phase, occurring from 15 to 40 min (the late phase). Before the test, mice were individually placed in a Plexiglas observation cage (30 × 14 × 12 cm) for one hour, to acclimatize to the testing environment. The total time the animal spent licking or biting its paw during the early and late phase of formalin-induced nociception was recorded.

3.6 Data analysis

3.6.1 *In vitro* experiments

Experimental data were presented as means ± S.E.M. Points were fitted with GraphPad Prism 5.0 (GraphPad Prism Software Inc., San Diego, CA, USA), using non-linear regression analysis. In the [^{35}S]GTPγS binding assays the 'Sigmoid dose-response' fitting was used to establish the maximal efficacy (E_{max}) of the receptors' G-protein and the ligand potency (EC_{50}). Stimulation was given as percent of the specific [^{35}S]GTPγS binding observed over the basal activity, which was settled as 100%. An unpaired *t*-test with two-tailed *p* value was performed to determine the significance level. In the competition binding assays the 'One site competition' fitting was used The equilibrium inhibitory constant (K_i) values of the compounds for the receptors were calculated from the competition binding curves and were converted into K_i values, using the Cheng–Prusoff [177] equation. Inhibition was given as percent of the specific binding observed.

3.6.2 *In vivo* experiments with Bentley analogues

Data are presented as means ± SEM. Data sets were examined by repeated measures of ANOVA. Post hoc comparisons were carried out with the Fisher LSD test. The *p* value lower than 0.05 was considered significant. The mean paw withdrawal thresholds obtained 15 and 30 min after the injections (calculated after the individual drug injections) were used for linear regression analysis to determine the effective dose 30 (ED_{30}) values with 95% confidence intervals. Mean of 50 g would mean the complete relief of hyperalgesia, while mean of control value (29 g) means the zero effects, thus the difference (21 g) is the possible maximal effect. ED_{30} is equivalent to the dose that yielded 30% difference (7 g) in the paw withdrawal threshold compared to the baseline (pretreatment) values. Data analyses were performed with the STATISTICA (Statistica Inc., Tulsa, Oklahoma, USA) and GraphPad Prism 4.0 softwares.

3.6.3 *In vivo* experiments with oligopeptides

Experimental data were expressed as mean ± S.E.M. Formalin test data were analysed by using one-way ANOVA, followed by Holm–Sidak′s multiple comparisons test. GraphPad Prism 6.03 software was used for all the analyses. Statistical significance was set at $p < 0.05$.

4 RESULTS

4.1 Competition binding assay

4.1.1 Bentley analogues

Opioid receptor binding affinities of the analogues were examined in [^{3}H]DAMGO, [^{3}H]Ile^{5,6}-deltorphin II and [^{3}H]HS665 homologous displacement experiments for MOR, DOR and KOR, respectively, in rat and guinea pig brain homogenates. All derivatives exhibited higher binding affinity in MOR system than the selective peptide ligand DAMGO (**Figure 9A**), some of them had extremely low K_i values (**Table 3**). For DOR the ligands showed comparable binding affinities than the selective DOR agonist Ile^{5,6}-deltorphin II peptide ligand (**Figure 9B**) except **8** (K_i > 3000 nM). In the KOR binding assays, performed in guinea pig brain membranes, the analogues still displayed nanomolar affinities (**Figure 9C**).

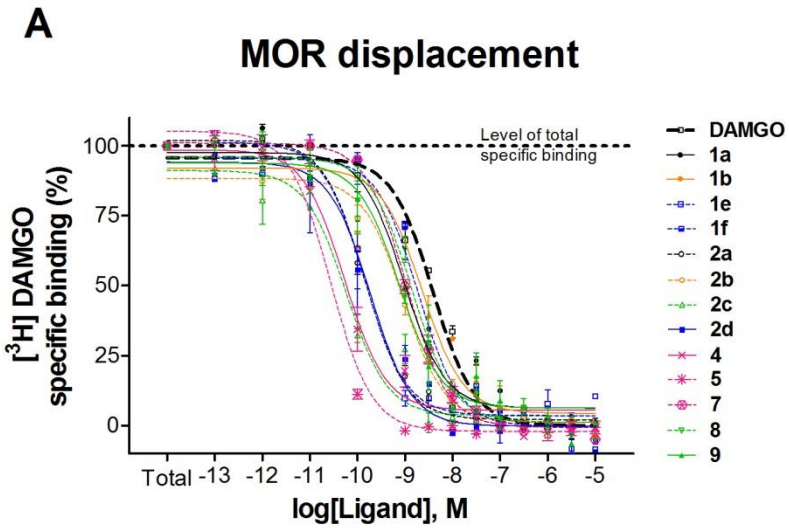

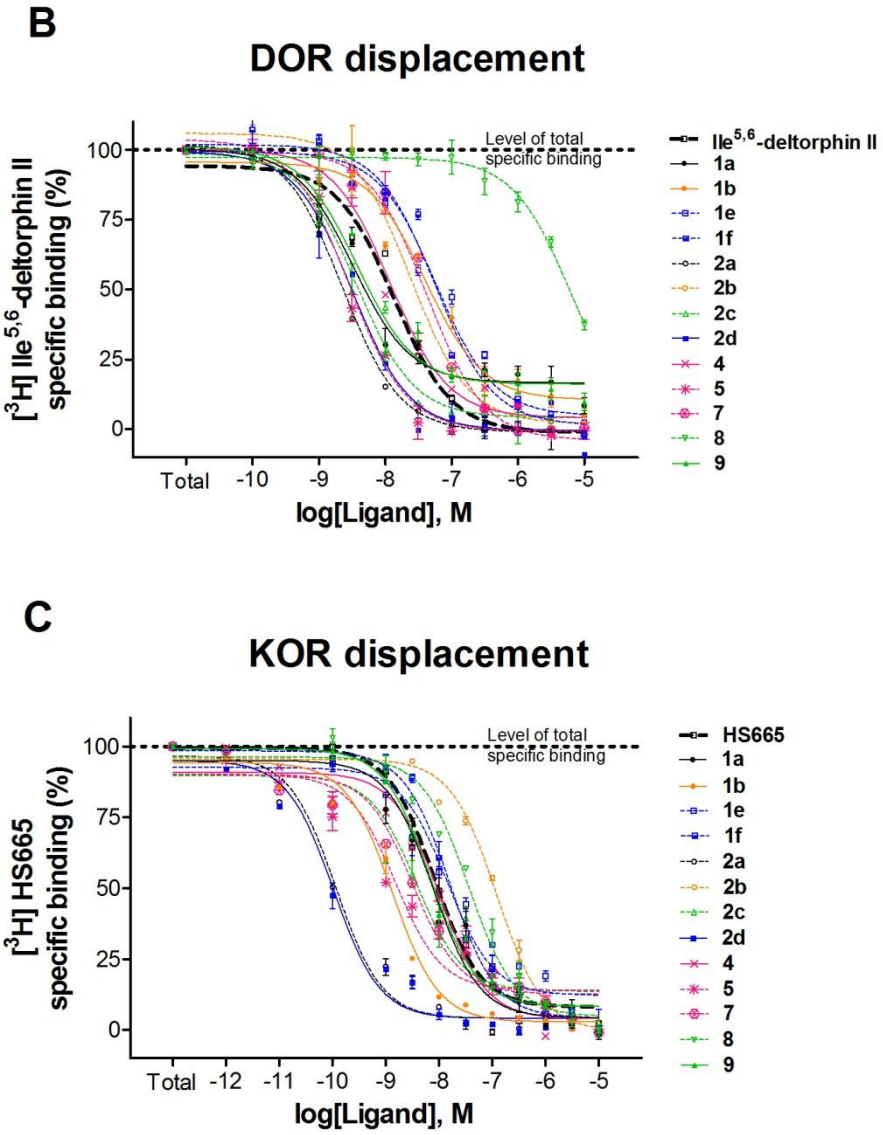

Figure 9. MOR, DOR and KOR displacement of the morphine analogues.

Figure legend: Binding affinity of morphine analogues compared to DAMGO (**A**), Ile^{5,6}-deltorphin II (**B**) and HS665 (**C**), respectively in [^{3}H]DAMGO, [^{3}H]Ile^{5,6}-deltorphin II and [^{3}H]HS665 competition binding assays in rat (MOR, DOR) and guinea pig (KOR) brain membrane homogenates. Membranes were incubated with [^{3}H]DAMGO, [^{3}H]Ile^{5,6}-deltorphin II or [^{3}H]HS665 with increasing concentrations (10^{-13} - 10^{-5} M; 10^{-10} - 10^{-5} M; 10^{-12} - 10^{-5} M, respectively). Values represent mean values $\pm$ S.E.M. for at least three independent experiments performed in duplicate.

Table 3. Displacement of [^{3}H]DAMGO, [^{3}H]Ile^{5,6}-deltorphin II and [^{3}H]HS665 by DAMGO, Ile^{5,6}-deltorphin II, HS665 and morphine derivatives in membranes of rat and guinea pig brain.

Ligand	DAMGO[a]	Ile^{5,6}-deltorphin II[a]	HS665[b]	Selectivity for μ site	
	K_i ± S.E.M. (nM)			(K_i^{δ}/K_i^{μ})	(K_i^{κ}/K_i^{μ})
DAMGO	0.9010 ± 0.27	n.d.	n.d.	n.d.	n.d.
Ile^{5,6}-deltorphin II	n.d.	8.848 ± 0.77	n.d.	n.d.	n.d.
HS665	n.d.	n.d.	1.707 ± 0.02	n.d.	n.d.
1a	0.2142 ± 0.30	2.11 ± 0.77	1.589 ± 0.02	9.85	7.42
1b	0.5315 ± 0.31	26.12 ± 0.77	0.280 ± 0.01	49.14	0.53
1e	0.0325 ± 0.35	37.37 ± 0.75	2.992 ± 0.03	1149.78	92.06
1f	0.4352 ± 0.28	36.56 ± 0.78	3.411 ± 0.01	84.54	7.84
2a	0.0333 ± 0.26	1.49 ± 0.71	0.024 ± 0.02	44.62	0.72
2b	0.2184 ± 0.27	15.72 ± 0.71	0.257 ± 0.01	71.96	1.18
2c	0.0136 ± 0.29	2.41 ± 0.80	0.796 ± 0.03	177.35	56.53
2d	0.0435 ± 0.29	2.06 ± 0.76	0.022 ± 0.02	47.45	0.51
4	0.0125 ± 0.30	7.73 ± 0.77	2.186 ± 0.02	618.30	174.88
5	0.0063 ± 0.27	1.85 ± 0.75	0.321 ± 0.03	294.43	50.95
7	0.2524 ± 0.25	27.53 ± 0.75	0.682 ± 0.02	109.06	2.70
8	0.3260 ± 0.30	3906.3 ± 0.84	7.636 ± 0.01	11982.52	23.42
9	0.1771 ± 0.30	2.44 ± 0.81	1.443 ± 0.01	13.78	8.15

Table legend: [a]: rat brain membrane, [b]: guinea pig brain membrane, n.d.: not determined.

4.1.2 Oligopeptides

KYNA and its analogue (KYNA1) – as previously reported by Zádor et al. - did not directly bind to MOR, DOR and KOR *in vitro* [178]. However, after chronic and acute administration, they altered opioid receptor function *in vivo* and *in vitro* through the NMDA receptor co-localized in the cortex and striatum of mice and rats, though the interaction of opioid and NMDA receptor have been deeply discussed in the literature [178,179]. KYNA is able to bind to the NMDA receptor at micromolar affinity [179]. To test if our novel peptides are able to target both of these systems, they were examined in a receptor binding radioassay using highly specific tritium-labelled primary ligands for opioid and NMDA receptor binding sites. [^{3}H]DAMGO, [^{3}H]Ile^{5,6}-deltorphin II, and [^{3}H]MK-801 equilibrium competition (displacement) studies were conducted in rat brain homogenates, while KOR tests were performed with [^{3}H]HS665 in guinea pig brain homogenates. The novel ligands showed similar K_i value in the μ-opioid system as DAMGO except **K3** (**Table 4, Figure 10A**). In the δ-opioid system, the ligands showed lower binding affinity (higher K_i) compared to the selective DOR selective agonist Ile^{5,6}-deltorphin II (**Figure 10B**). In the κ-opioid receptor system, the compounds showed higher K_i values than that of the selective κ-opioid agonist HS665 (**Figure 10C**). In the NMDA receptor binding assays, the peptides did not produce any affinity in micromolar range (**Figure 10D**). The peptide **KA1** possesses the best binding affinity, with a K_i value very close to that of the reference compound DAMGO (1.08 ± 0.26 nM vs. 0.90 ± 0.28 nM), suggesting that the insertion of KYNA into the DAMGO sequence does not impair its binding potency at the MOR. The peptide **K6**, presenting the enkephalin-like structure linked to kyn C-terminal amide, is able to bind all three opioid receptors with significant affinity, showing a moderate preference for the MOR (affinity ratio 1:18:70 for μ, δ, κ, respectively), whereas compounds **K4** and **K5** are able to bind only MOR and DOR. It is reasonable to believe that the C-terminal amide derivatization in peptide **K6** confers the ability to bind to the KOR. Concerning the EM-2 analogues **K2** and **K3**, the replacement of Phe^3 with kyn improves the binding affinity and selectivity of **K2** for MOR with respect to the standard compound EM-2, with a weak affinity for KOR, while the incorporation of kyn amide in position 4 causes the loss of selectivity for MOR in favor of a modest binding affinity for MOR and KOR. Peptide **K2**

shows a K_i value two-folds lower than that of EM-2 on the MOR, which let us suppose the positive influence of kyn in position 3 on **K2** binding ability.

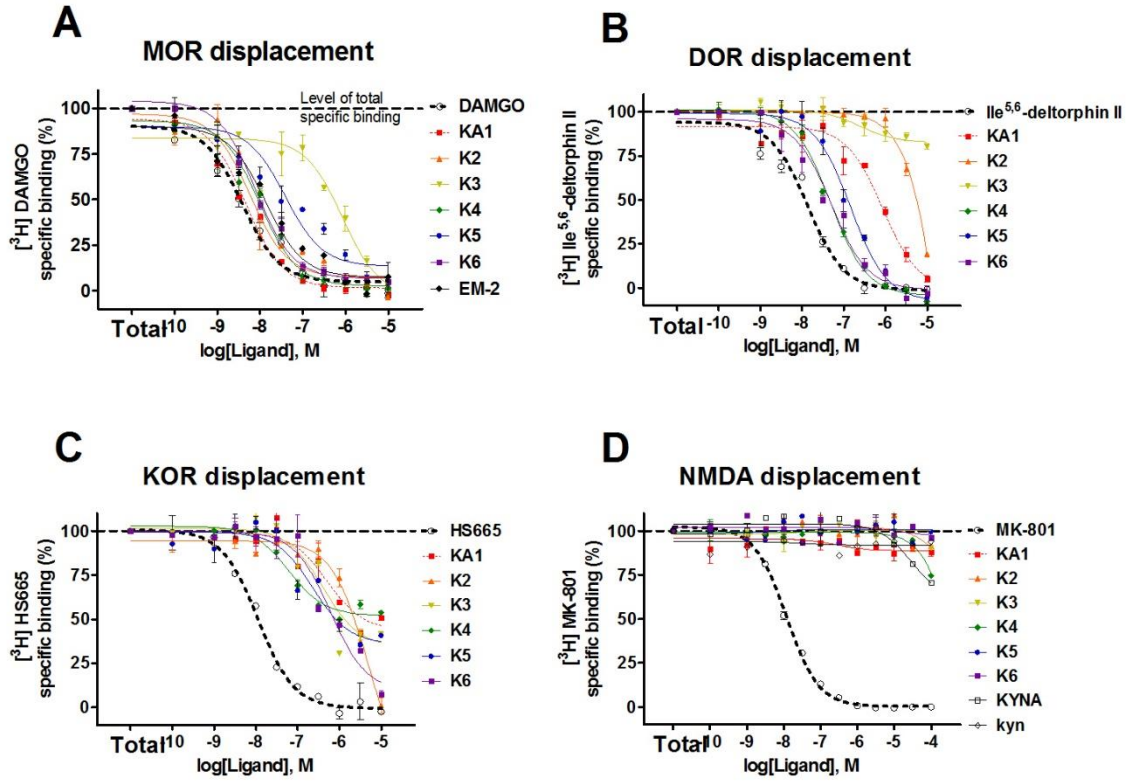

Figure 10. MOR, DOR, KOR and NMDA receptor displacement of the oligopeptides.

Figure legend: Binding affinity of oligopeptides compared to DAMGO (**A**), Ile^{5,6}-deltorphin II (**B**), HS665 (**C**) and MK-801 (**D**), respectively in [^{3}H]DAMGO, [^{3}H]Ile^{5,6}-deltorphin II, [^{3}H]HS665 and [^{3}H]MK-801 competition binding assays in rat (**A, B, D**) and guinea pig (**C**) brain membrane homogenates. Values represent mean values ± S.E.M. for at least three experiments performed in duplicate.

Table 4. Displacement of [^{3}H]DAMGO, [^{3}H]Ile^{5,6}-deltorphin II, [^{3}H]HS665and [^{3}H]MK-801 by DAMGO, Ile^{5,6}-deltorphin II, HS665, MK-801 and oligopeptides in membranes of rat and guinea pig brain.

Ligand	K_i + S.E.M. (nM)			
	Opioid receptor			NMDA receptor
	DAMGO[a]	Ile^{5,6}Delt II[a]	HS665[b]	MK-801[a]
DAMGO	0.90 ± 0.28	n.d.	n.d.	n.d.
Ile^{5,6}Delt II	n.d.	8.85 ± 0.77	n.d.	n.d.
HS665	n.d.	n.d.	2.38 ± 0.25	n.d.
MK-801	n.d.	n.d.	n.d.	11.45 ± 1.04
EM-2	3.16 ± 0.3	n.d.	n.d.	n.d.
KYNA	n.d.	n.d.	n.d.	> 10 000
kyn	n.d.	n.d.	n.d.	> 10 000
KA1	1.08 ± 0.26	554.7 ± 0.8	> 10 000	n.a.
K2	1.39 ± 0.30	> 10 000	1043 ± 0.3	n.a.
K3	197.3 ± 0.36	158.8 ± 1.6	> 10 000	n.a.
K4	2.29 ± 0.28	31.2 ± 0.7	> 10 000	n.a.
K5	9.11 ± 0.32	94.4 ± 0.8	> 10 000	n.a.
K6	1.84 ± 0.27	32.5 ± 0.8	127.7 ± 0.3	n.a.

Table legend: [a]: rat brain membrane; [b]: guinea pig brain membrane; n.d.: not determined; n.a.: no affinity.

4.2 Functional [^{35}S]GTPγS binding stimulation assay

4.2.1 Bentley analogues

The effect of the ligands on receptor-mediated G-protein activation was investigated in [^{35}S]GTPγS binding assays in rat brain membranes (**Figure 11**). The highest stimulations were observed with **2d**, **4**, **5**, **7** and **9**, therefore they can be considered as full agonists. **1a**, **1f**, **2a** and **2b** did not produce a dose-dependent increas, thus they behave as neutral or pure antagonists (**Table 5**). The remaining compounds (**1b**, **1e**, **2c** and **8**) exhibited intermediate levels of G-protein activity, therefore behaving as partial agonist ligands in this *in vitro* system.

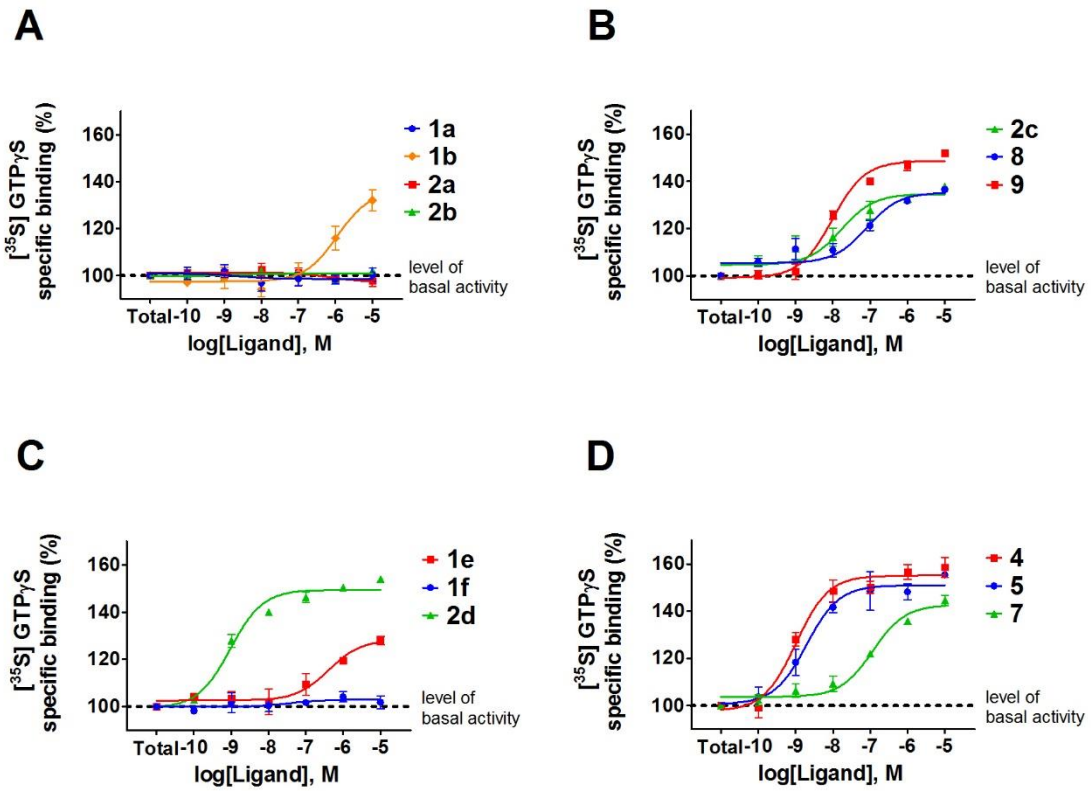

Figure 11. The effect of morphine analogues on G-protein activity compared to the parent ligands in [^{35}S]GTPγS binding assays in rat brain membrane homogenates.

Figure legend: "Total" on the x-axis indicates the basal activity of the monitored G-protein, which is measured in the absence of the ligands and also represents the total specific binding of [^{35}S]GTPγS. The level of basal activity was defined as 100% and it is presented with a dotted line. Points represent means ± S.E.M. for at least three experiments performed in triplicate.

Table 5. The maximal G-protein efficacy (E_{max}) of the morphine analogues in [^{35}S]GTPγS binding assays in rat brain membrane homogenates.

Ligand	Potency log EC_{50} + S.E.M. (M)	Efficacy E_{max} ± S.E.M. (%)
1a	n.d.	98.65 ± 1.40
1b	-5.96 ± 0.22	135.98 ± 5.03
1e	-6.39 ± 0.26	128.31 ± 3.18
1f	n.d.	102.87 ± 1.59
2a	n.d.	101.31 ± 0.98
2b	n.d.	100.81 ± 0.73
2c	-7.77 ± 0.21	134.71 ± 2.05
2d	-9.02 ± 0.11	149.46 ± 1.28
4	-8.99 ± 0.14	155.09 ± 1.83
5	-8.71 ± 0.15	150.95 ± 2.10
7	-6.94 ± 0.12	142.64 ± 2.00
8	-7.09 ± 0.17	135.32 ± 2.07
9	-8.01 ± 0.09	148.61 ± 1.41

The values were calculated according to dose-response binding curves in **Figure 11**.

Table legend: n.d.: not determined.

The neutral opioid antagonist **1a** successfully reversed the efficacy of almost all compounds to basal activity with the exception of **2d** which showed some remaining activation in the presence of equimolar **1a**. Maximal stimulation produced by the ligands was mostly not elevated further when the full agonist **9** was co-administered (**Figure 12A**). However, in the case of **1f** and **2b** the co-presence of **9** was able to effectively stimulate G-protein activation (**Table 6**).

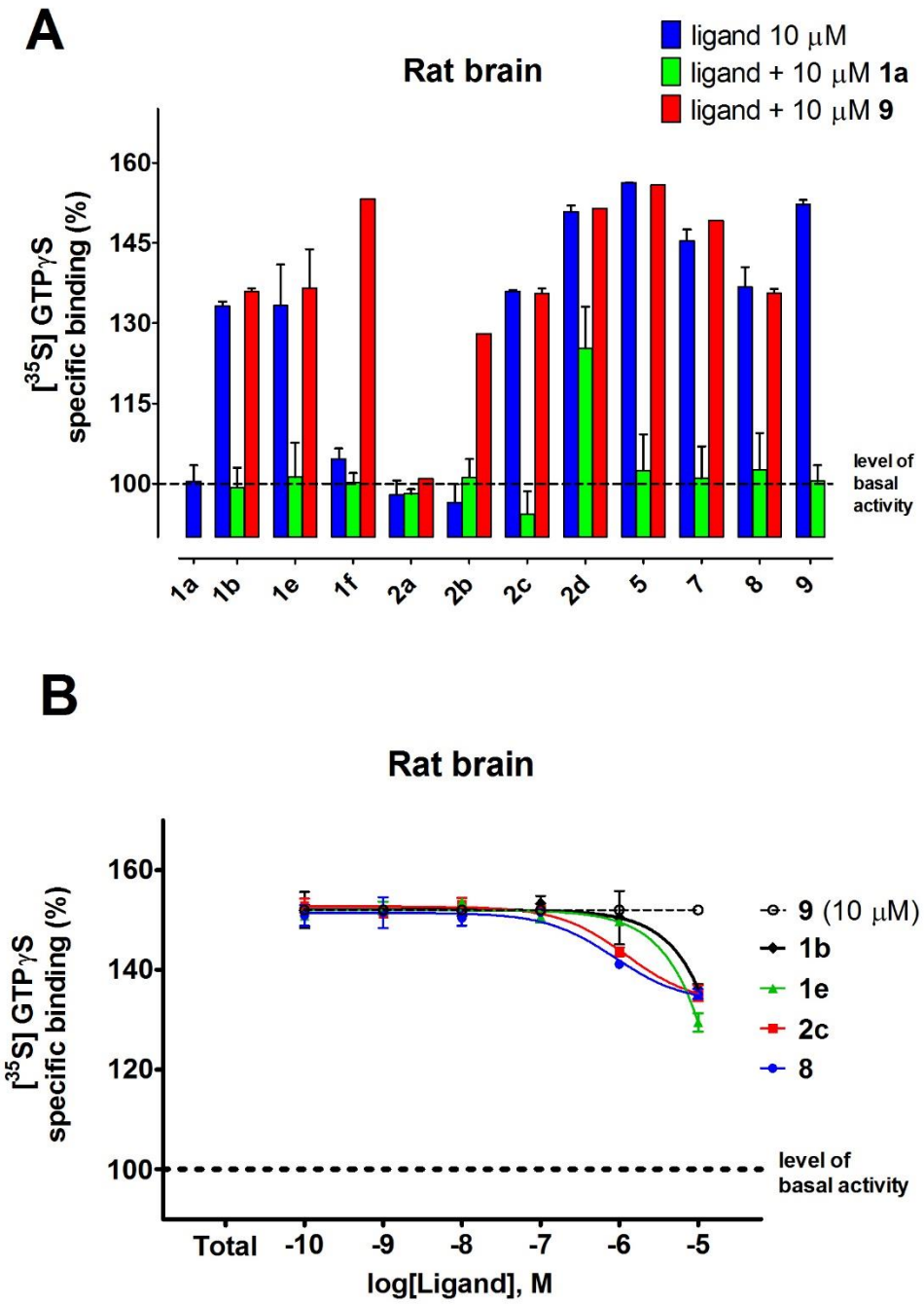

Figure 12. Stimulation of G-protein activation in rat brain membrane homogenates.

Figure legend: blue, 10 μM morphine analogues alone; green, 10 μM morphine analogues and equimolar antagonist **1a**; red, 10 μM morphine analogues and equimolar full agonist **9** (**Figure 12A**). The decrease of the effect of **9** by the indicated partial agonists in [^{35}S]GTPγS binding assays (**Figure 12B**).

Increasing concentrations of the partial agonists were also investigated in the presence of 10 μM **9** producing maximal stimulation (**Figure 12B**). All four compounds were able to inhibit the activation mediated by **9**, although with relatively low efficacy and potency. This weak antagonizing effect in the presence of a full agonist validates that **1b**, **1e**, **2c** and **8** are indeed partial agonist ligands for opioid receptors (**Table 6**).

Table 6. The maximal G-protein efficacy (E_{max}) of morphine analogues in the absence or presence of the opioid antagonist and agonist (1a and 9, respectively) in rat brain membrane homogenates.

Ligand	Efficacy E_{max} ± S.E.M. (%)			
	10 μM ligand	**10 μM ligand + 10 μM of 1a**	**10 μM ligand + 10 μM of 9**	**Ligand (10^{-10}-10^{-5} M) + 10 μM of 9**
1a	100.45 ± 3.05	-	-	-
1b	135.17 ± 0.82	99.30 ± 3.70	135.93 ± 0.58	136.20 ± 1.20
1e	133.27 ± 7.67	101.25 ± 6.45	129.45 ± 1.85	129.45 ± 0.61
1f	104.63 ± 2.00	100.25 ± 1.75	135.20 ± 0.00	-
2a	97.90 ± 2.75	98.10 ± 0.90	101.00 ± 0.00	-
2b	96.50 ± 3.47	101.20 ± 3.40	128.10 ± 0.00	-
2c	135.90 ± 0.30	94.40 ± 4.20	135.50 ± 0.95	136.80 ± 0.58
2d	150.80 ± 1.20	125.30 ± 7.80	151.40 ± 0.00	-
4	158.75 ± 5.15	99.30 ± 2.10	153.20 ± 0.00	-
5	156.20 ± 0.10	102.40 ± 6.90	155.80 ± 0.00	-
7	145.45 ± 2.05	101.05 ± 5.95	149.20 ± 0.00	-
8	136.77 ± 3.67	102.60 ± 6.90	135.63 ± 0.79	135.10 ± 0.87
9	152.15 ± 0.85	100.50 ± 3.00	-	-

The values were calculated according to dose-response binding curves in **Figure 12**.

4.2.2 Oligopeptides

The effect of the bivalent ligands on G-protein stimulation was investigated in functional [^{35}S]GTPγS binding assays in rat and guinea pig brain membranes. All ligands produced dose-dependent increases (**Figures 12**), **K6** showed higher efficacy (E_{max}) than DAMGO (**Table 7**). 10 μM Cyp and 10 μM NTI significantly reversed the agonist effects of the ligands in rat brain membrane homogenates (**Figure 14A**). In guinea pig brain membrane homogenates the ligands did not activate the receptors G-protein, except **K4** and **K6** (**Figure 14B**). Nor-BNI in 10 μM concentrations significantly decreased the agonist effect of **K4**, but did not change the effect of **K6** (**Table 8**). All together these data reveal that peptide **KA1** acts as a selective μ-opioid agonist being able to decrease the [^{35}S]GTPγS binding percentage under the basal level in presence of 10 μM Cyp. Peptides **K2** and **K3** possess a mixed μ/δ agonist activity profile, while peptides **K4**-**K6** showed a modest mix μ/δ-opioid receptor agonism. Probably peptide **K6** is the strongest mixed μ/δ/κ opioid agonist, due to its ability to activate G-protein with an efficacy value over the basal level in the presence of each selective opioid antagonist at 10 μM.

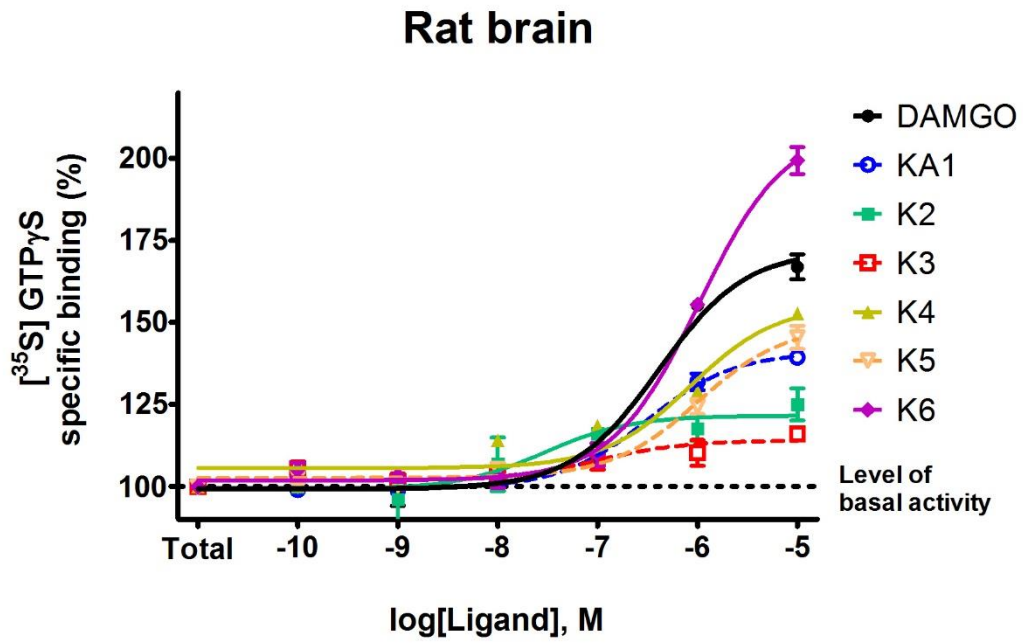

Figure 13. The effect of oligopeptides on G-protein activity compared to DAMGO in [^{35}S]GTPγS binding assay in rat brain membrane homogenates.

Figure represents the specific binding of [^{35}S]GTPγS in percentage in presence of increasing concentrations (10^{-10} - 10^{-5} M) of the indicated ligands. "Total" on the x-axis indicates the basal activity of the monitored G-protein, which is measured in the absence of the ligands and represents the total specific binding of [^{35}S]GTPγS. The level of basal activity was defined as 100% and it is presented with a dotted line. Points represent means ± S.E.M. for at least three experiments performed in triplicate.

Table 7. The maximal G-protein efficacy (E_{max}) DAMGO and oligopeptides in [^{35}S]GTPγS binding assays in rat brain membrane homogenates.

Ligand	Maximal stimulation (efficacy)	Potency
	E_{max} ± S.E.M. (%)	log EC_{50} ± S.E.M. (M)
DAMGO	172.0 ± 3.5	-6.384 ± 0.101
KA1	140.9 ± 1.4	-6.504 ± 0.076
K2	121.6 ± 2.5	-7.535 ± 0.354
K3	114.0 ± 2.1	-6.993 ± 0.422
K4	155.5 ± 4.8	-6.073 ± 0.172
K5	149.2 ± 3.5	-5.990 ± 0.111
K6	209.7 ± 3.4	-5.984 ± 0.054

The values were calculated according to dose-response binding curves in **Figure 13**.

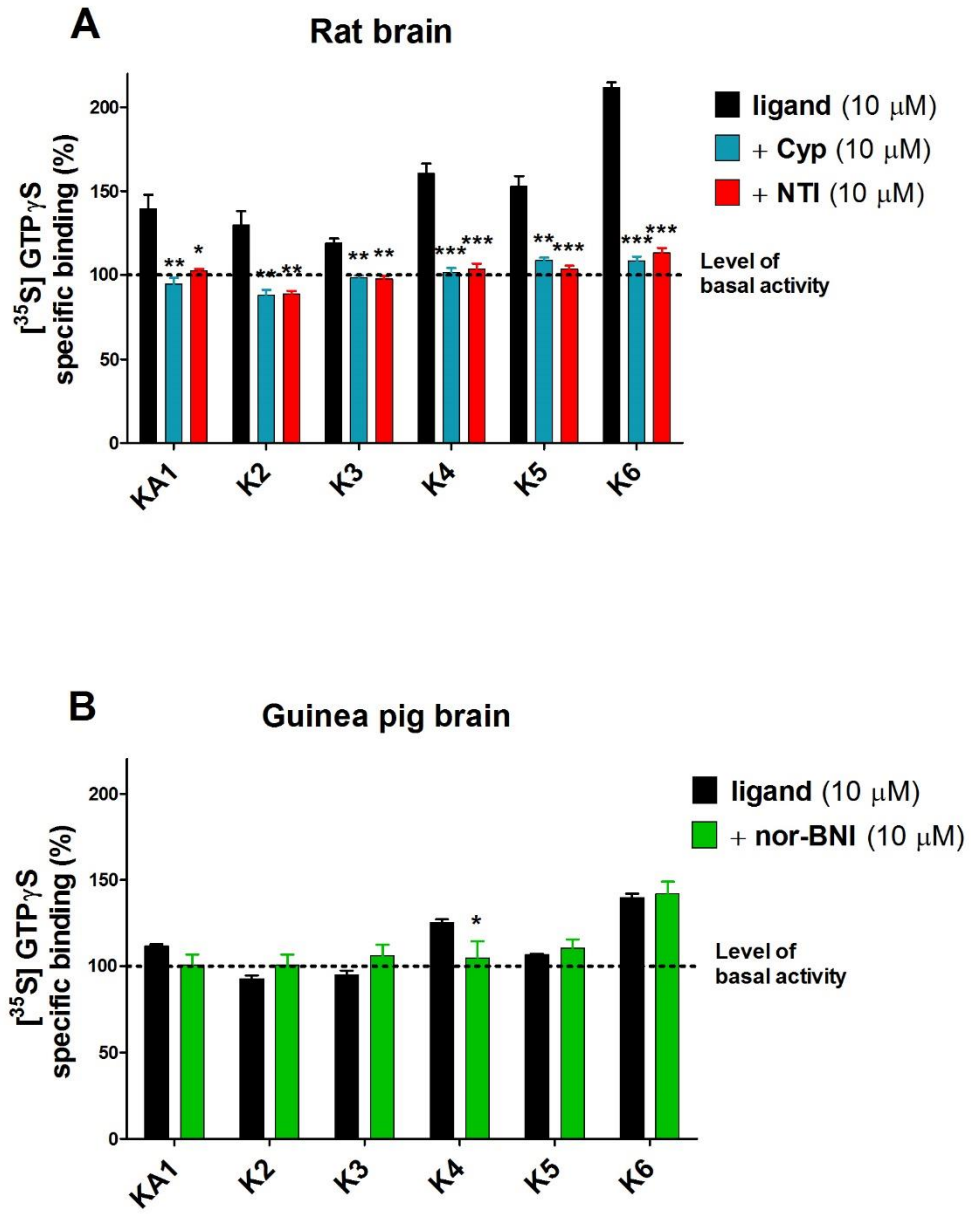

Figure 14. The effect of peptides on G-protein activity in [^{35}S]GTPγS binding assays in the absence or presence of the selective MOR antagonist Cyp and the selective DOR antagonist NTI in rat brain membrane homogenates (A) and the selective KOR antagonist nor-BNI in guinea pig brain membrane homogenates (B).

Figure shows the maximal efficacy (E_{max}) of the oligopeptides in one concentration (10^{-5} M). The level of basal activity was defined as 100% and it is presented with a dotted line. Points represent means ± S.E.M. for at least three experiments performed in triplicate.

Table 8. The maximal G-protein efficacy (E_{max}) of oligopeptides in the absence or presence of the selective MOR antagonist Cyp and the selective DOR antagonist NTI in rat brain membrane homogenates (Figure 14A) and in the absence or presence of the selective KOR antagonist nor-BNI in guinea pig brain membrane homogenates (Figure 14B) in [^{35}S]GTPγS binding assays.

	Ligand[a]	MOR	DOR	Ligand[b]	KOR
		Ligand + Cyp	Ligand + NTI		Ligand + Nor-BNI
KA1	139.6 ± 8.2	94.7 ± 3.7 **	102.5 ± 1.3 *	111.7 ± 1.1	100.7 ± 6.2 ^{ns}
K2	129.9 ± 8.2	88.0 ± 3.3 **	88.8 ± 1.9 **	92.8 ± 2.0	100.7 ± 6.0 ^{ns}
K3	118.9 ± 3.0	98.5 ± 1.2 **	97.8 ± 1.7 **	95.2 ± 2.2	106.0 ± 6.3 ^{ns}
K4	160.6 ± 5.7	101.6 ± 2.6 ***	103.6 ± 3.2 ***	125.2 ± 2.0	104.9 ± 9.5 *
K5	153.1 ± 5.9	108.8 ± 1.6 **	103.8 ± 1.9 ***	106.9 ± 0.3	110.5 ± 5.0 ^{ns}
K6	211.7 ± 3.1	108.5 ± 2.4 ***	113.3 ± 2.9 ***	139.8 ± 2.3	142.1 ± 7.1 ^{ns}

The values were calculated according to bar graphs in **Figure 14**. Experimental data were processed by GraphPad Prism 5.0 using bar graphs. ns: not significant; *: $p < 0.05$; **: $p < 0.01$; ***: $p < 0.001$ based on unpaired *t*-tests.

Table legend: [a]: rat brain membrane; [b]: guinea pig brain membrane.

4.3 Inflammatory pain model

4.3.1 Bentley analogues

The basal withdrawal threshold of the non-inflamed side was 45 ± 0.5 g, and MIA caused significant decrease in paw withdrawal threshold on the injected side (24 ± 0.6 g). Only the largest dose of **9** treatments caused significant enhancement in the pain threshold on the non-inflamed side, therefore, results were analysed only on the inflamed paws. The different ligands showed different potencies, therefore, they were compared to distilled water (as negative control) in the ANOVA analysis, but the curve for **9** was also demonstrated as a positive control group with the lowest ED_{30} value (table of datas are not shown in this thesis).

All of the thevinol derivatives showed a significant antiallodynic effect (**Figure 15**); however, the regression analysis revealed a lower *in vivo* potency compared to **9** as indicated by the ED_{30} values, even it could not be calculated for **7**. Regarding **4**, the treatment was close to significant. Time and their interaction showed significant effects, and the post-hoc analysis showed decreased allodynia in several time-points compared to the control group (**Figure 15A**). ANOVA for repeated measurements showed significant effects of **5** treatments, time and their interaction. The *post hoc* comparison revealed that only the highest doses caused significant antiallodynic effect with similar efficacy as **9** (**Figure 15B**). Similarly, **7** treatments also showed significant effects, and the *post hoc* comparison revealed significant increase in pain threshold at several time points after the highest dose compared to the control group (**Figure 15C**).

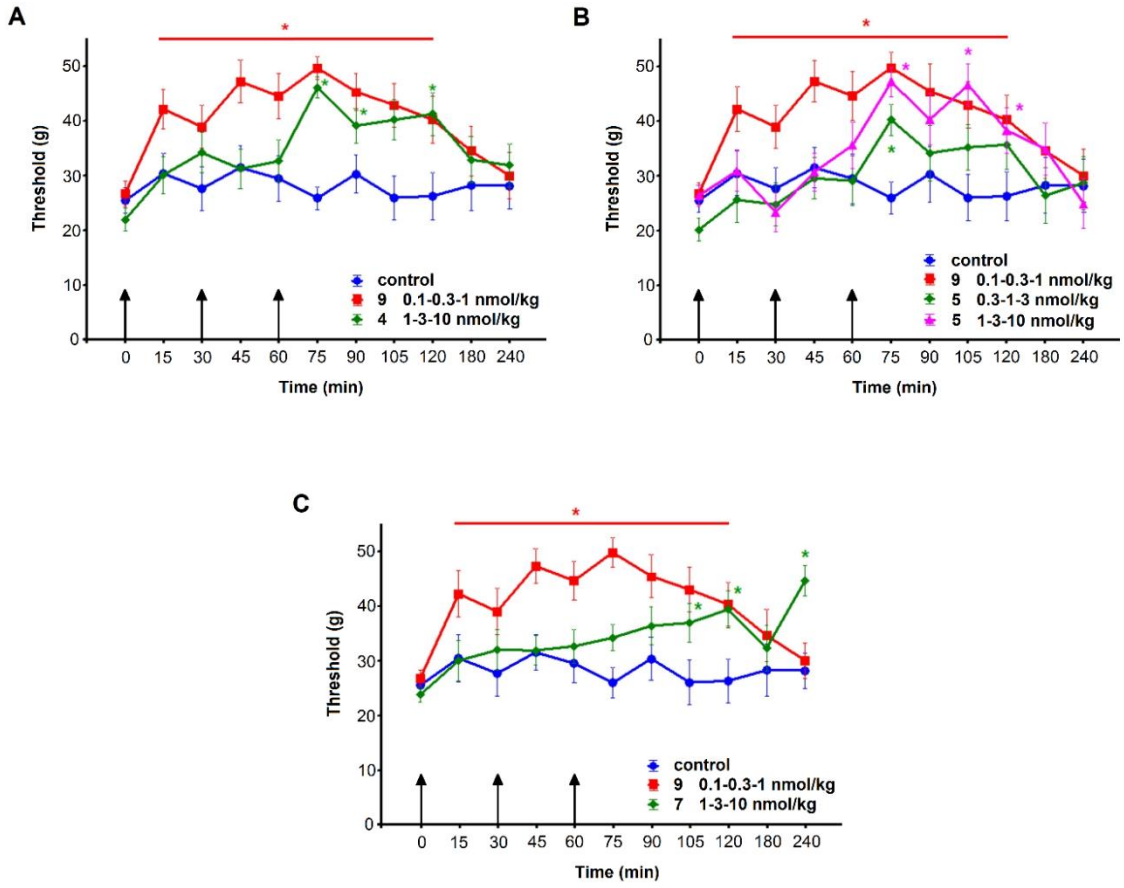

Figure 15. The effects of orvinol derivatives in chronic inflammatory pain model.

Arrows indicate the time points of cumulative drug administrations. *: $p < 0.05$ from control group.

Regarding **2a** and **2b** treatments, there were no significant effects and ED_{30} values could not be calculated (**Figure 16A**, **B**). However, **2c** administration resulted in significant effects of treatment, time, and their interaction, with a relatively low ED_{30} value. The *post hoc* comparison revealed that the largest dose of **2c** caused similar degree of antiallodynic effect as did **9**; even more prolonged effect was observed (**Figure 16C**). **1e, 1f** and **2d** did not produce significant antiallodynic effects (**Figure 16D**, **E**, **F**), and ED_{30} values could not be calculated either.

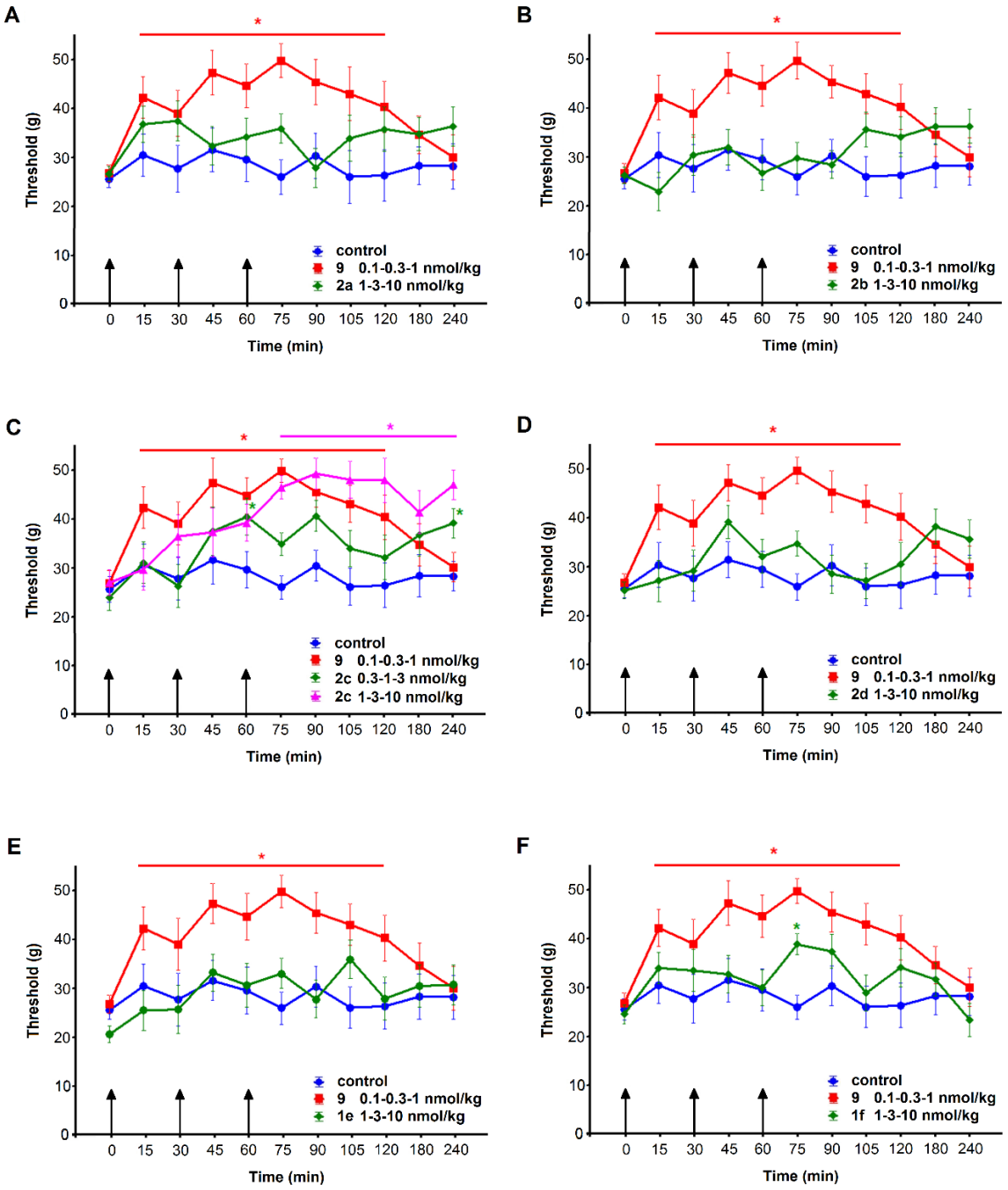

Figure 16. The effects of orvinol derivatives in chronic inflammatory pain model.

Arrows indicate the time points of cumulative drug administrations.

*: $p < 0.05$ from control group

4.3.2 Oligopeptides

Data obtained from binding experiments indicated, that **K6** displayed the best binding properties, thus, formalin test was performed with this compound to evaluate its antinociceptive activity. Since it was reported that some opioid peptides such as DAMGO are also peripheral acting [180], we performed a formalin test administering **K6** and DAMGO subcutaneously in the mouse paw. Compound **K6** was able to reduce the nociceptive response to formalin in the early phase, whereas a light but not significant reduction was induced in the late phase of the formalin test (**Figure 17**). After the DAMGO injection, we observed a reduction of the nociceptive behaviour both in the early and in the late phase of the formalin test (**Figure 17**). The early phase, which depends upon the direct excitement of sensory neurons through TRPA1 cation channel activation [181] of MORs at the peripheral endings of nociceptors, is responsible for most of the analgesic effect [182]. It is also not surprising that **K6** and DAMGO reduced formalin-induced nociception in the early phase of the test. The differences observed in the late phase are probably due to a different metabolic fate of **K6** and DAMGO after subcutaneous administration, depending upon the protease activity that might act in different parts on the chemical structures of **K6** and DAMGO.

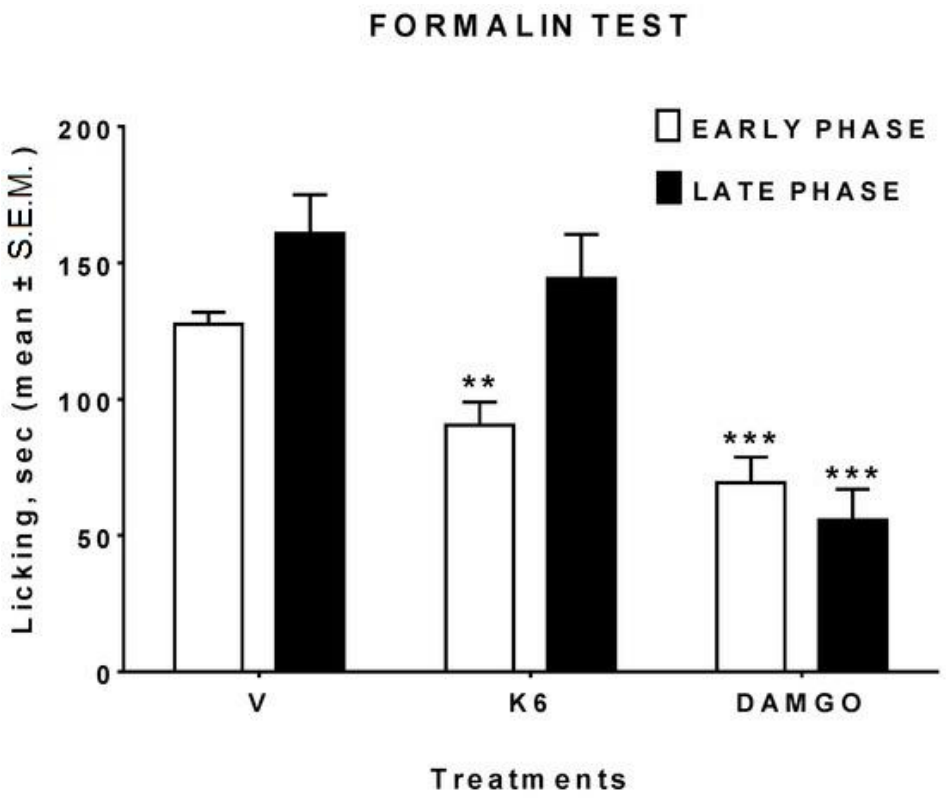

Figure 17. The effect of K6 and DAMGO in the formalin test.

Compounds were administered subcutaneously (s.c.) in the dorsal hind paw of mice at the dose of 100 µg/20 µL, 15 min before a s.c. injection of dilute formalin solution (1% in saline, 20 µL/paw). Early phase represents the formalin-induced nociceptive behaviour recorded from 0 to 10 min after formalin injection; late phase is for the formalin-induced nociceptive behaviour recorded from 15 to 40 min after formalin injection. V is for vehicle-treated animals. Statistical analysis: one-way ANOVA followed by Holm–Sidak′s multiple comparisons test. **: $p < 0.01$; ***: $p < 0.001$ vs. V. n = 7.

5 DISCUSSION

This study presents the pharmacological and biochemical characterization of newly developed or already known but not yet studied opioid receptor ligands. The molecules discussed here were partly morphine-like compounds with a variously modified alkaloid backbone (so called Bentley compounds [150,151] derived from oripavine or thebaine), and partly synthetic opioid oligopeptides containing kynurenine moieties.

The biochemical characterization of 6-*O*-desmethyl-orvinols and 20*R*-phenethyl-orvinols/thevinols have (unanticipated) extremely high potency at MOR. The target compounds are semi synthetic thebaine derivatives and belong to the 6,14-ethenomorphinans (Bentley-compounds). The pharmacologically most important members of this opioid ligand class are diprenorphine (**1a**), buprenorphine (**1b**), dihydroethorphine (**1c**), and phenethyl-orvinol (**1d**). Compound **1a** is an antagonist with approximately the same high affinity for all opioid receptor subtypes. Compound **1b** with a mixed agonist-antagonist (partial MOR-agonist/KOR-antagonist) profile is clinically used as analgesic in the treatment of postoperative and/or cancer-related pain and in the substitution therapy of opioid dependent humans. **1c** and **1d** are nonselective opioid receptor agonists. Biological properties of our thirteen synthetic morphine analogues were investigated by *in vitro* biochemical and in vivo pharmacological experiments. In radioligand binding assays performed using MOR-, DOR- or KOR-selective [^{3}H]labelled primary ligands, all analogues exhibited a high affinity for multiple types of opioid receptors. The observed biochemical potencies of these Bentley compounds were even greater than the previously characterized β-etorphine and β-dihydroetorphine derivatives [156]. At the MOR binding sites **2c**, **4** and **5** were the most potent ligands, but all of the remaining compounds represented quite high affinities. They were also potent competitors in the DOR-selective receptor binding assays, displaying still nanomolar equilibrium dissociation constant (K_i) values with the exception of **8** which had only moderate affinity for DOR. **2a** and **2d** showed the highest affinity at KOR ligand binding sites, although all other analogues produced low nanomolar binding affinities. The mixed KOP/MOP agonist character of the compound, determined in our experiments, was consistent with the results of orvinols reported by Greedy et al. [160]. Taken together, the thevinol and orvinol derivatives are very high affinity opioid ligands, with a general preference for MOR > KOR > DOR binding sites. Receptor mediated G-protein activation experiments were conducted *in vitro* using rat brain membrane preparations and [^{35}S]GTPγS binding stimulation assays. Transmembrane signalling properties of the compounds were variable, and the ligands used can be divided into three biochemical pharmacological groups based on their stimulation features. Full agonists, such as **2d**, **4**, **5**, **7** and **9** produced the highest efficacy (E_{max} values) and they can be characterised by culminating sigmoid stimulation curves with a plateau. Partial agonist ligands, **1b**, **1e**, **2c** and **8**, exhibited submaximal efficacies and rather decreased

potencies in activating $G_{\alpha i}$ regulatory proteins. Another previous term for partial agonists has been mixed agonist-antagonist ligands. When both a full agonist and partial agonist are present, the partial agonist actually acts as a competitive antagonist, competing with the full agonist for receptor occupancy and producing a net decrease in the receptor activation observed with the full agonist alone. The third group of ligands are pure or neutral opiate antagonists, such as **1a**, **2a**, **2b** and **1f**. They are characterised by horizontally linear dose-response curves indicating no changes in the basal G-protein activity. 6-*O*-demethylation usually increased the binding affinity to MOR (**1a** vs. **2a**, **1b** vs. **2b**, **2c** vs. **9**, **4** vs. **5**). In accordance with this finding, increasing the size of the 6-*O*-substituent (**4** vs. **7**) decreased the binding affinity to MOR. The opposite trend was observed for the efficacy in some cases, resulting in a shift of the pharmacological profiles, *i.e.* from partial agonist to antagonist (**1b** vs. **2b**), from agonist to partial agonists (**9** vs. **2c**). In the phenethyl-thevinol series (**2d**, **4**, **5**, **7**) 6-*O*-demethylation did not decrease the efficacy. On the contrary, the bigger 6-*O*-substituent in **7** slightly decreased the efficacy, however, it still can be considered as a full agonist. Behavioural nociceptive properties of the ligands were studied *in vivo*, using Wistar rats in a chronic osteoarthritic inflammatory pain model. **9** at cumulative doses of 0.1-0.3-1.0 nmol/kg remained the most effective compound in decreasing inflammatory pain. **2c**, **4** and **5**, which exhibited the highest ligand binding affinities at the MOR, produced less antinociception than **9** did. The other full (**2d**) or partial antagonists (**1e**, **7**), as well as the two neutral antagonists **2a** and **2b** examined in this test were practically not effective even in ten times higher (1-3-10 nmol) cumulative doses. In *in vivo* tests in osteoarthritis inflammatory model the compound showed a significant antiallodynic effect of thevinol derivatives while orvinol derivatives did not. Despite their outstanding MOR affinities, the Bentley analogues tested did not show a particularly strong effect in the model of osteoarthritis. However, opioid agonists are known to be less effective in inflammatory and neuropathic pain as compared with acute pain situations [183,184].

Chemical modification of endogenous opioid peptides promotes the development of novel analogues with increased potency and improved pharmacokinetic properties, *e.g.*, the synthetic bivalent peptide biphalin enhanced stroke immunohistochemical and behavioural neuroprotection in comparison to DPDPE (D-Pen^2,D-Pen^5 enkephalin) and DAMGO, reducing glutamate toxicity and oxidative stress [185–188]. Metabolites of the kynurenic

pathway, especially KYNA and kyn, play crucial roles in maintaining the normal brain function, preventing the over-activation of excitatory amino acid receptors, thus offering novel therapeutical opportunities for brain neuroprotection. In this study, six novel opioid analogues were synthesized incorporating the kyn and KYNA residues at different positions of several opioid peptide scaffolds. They were characterized *in vitro* and *in vivo* to evaluate their ability to bind the NMDA/opioid receptors and to induce analgesic effects. These novel peptides do not bind to the NMDA receptors in micromolar range, and some of them showed good/high affinity for opioid receptors with different selectivity profiles. In particular, **KA1** exhibits the binding constant (K_i = 1.08 nM) very close to that of DAMGO for the MOR and a pronounced selectivity but medium-low efficacy (E_{max} = 139%); thus the esterification of the ethanolamine portion with KYNA does not add any particular advantage to the parent peptide DAMGO. On the other hand, the presence of kyn residue in place of native Phe in position 3 (**K2**) leads a potent and selective opioid fragment toward MOR (selectivity ration μ/δ/κ = 1:10000:750), whereas the substitution in position 4 (**K3**) leads to a weak and unselective agonist at MOR and DOR. In the analogues **K4–K6**, the KYNA residue was inserted in the fifth position of the YaGP (Tyr-D-Ala-Gly-Phe) peptide, with different C-terminus, respectively, methyl ester, free carboxylic acid, and amide. **K4** and **K5** show a similar mixed binding affinity for MOR and DOR, with a preference for MOR and none or weak affinity for KOR. On the contrary, peptide **K6** shows an interesting behavior since it is able to bind all three opioid receptors with binding affinity ranging from high to modest (K_i^{μ} = 1.84 nM, K_i^{δ} = 32.5 nM, K_i^{κ} = 127.7 nM), with a potency (EC_{50} = 1.037 μM) and efficacy at MOR (E_{max} = 211%) higher than that of DAMGO (E_{max} = 172%). Its activity on the GTPγS binding assay on rat and guinea pig brain membranes is significantly blocked by the co-administration of the selective antagonists for MOR and DOR at 10 μM concentration, prompting us to investigate its anti-nociceptive effect *in vivo*. The formalin test, which is a model for inflammatory pain, revealed that the antinociceptive effect exerted by **K6** after subcutaneous administration is significant only in the early phase, whereas DAMGO is also active in the late phase.

Table 9. Summary of the biochemical and pharmacological properties of the examined ligands.

Examined ligands	Competition radioligand assay				Functional [^{35}S]GTPγS binding assay			*In vivo* experiments
	Affinity in nanomolar range				Effect on G-protein			Antiallodynic effect
	MOR[a]	DOR[a]	KOR[b]	NMDA receptor[a]	MOR[a]	DOR[a]	KOR[b]	
1a	+[#]	+	+	n.d.	ANT – reference ligand			-
1b	+[#]	+	+[#]		PAG – reference ligand			-
1e	+[#]	+	+		PAG			-
1f	+[#]	+	+		ANT			-
2a	+[#]	+	+[#]		ANT			-
2b	+[#]	+	+[#]		ANT			-
2c	+[#]	+	+[#]		PAG			+
2d	+[#]	+	+[#]		AG			-
4	+[#]	+	+		AG			+
5	+[#]	+	+[#]		AG			+
7	+[#]	+	+[#]		AG			+
8	+[#]	-	+		PAG			-
9	+[#]	+	+		AG – reference ligand			+
								Antinocicep-tive effect
DAMGO	+	n.d.	n.d.	n.d.	AG	n.e.	n.e.	+
KA1	+	+	-	n.a.	AG	AG	ANT	n.d.
K2	+	-	-	n.a.	PAG	PAG	ANT	n.d.
K3	+	+	-	n.a.	PAG	PAG	ANT	n.d.
K4	+	+	-	n.a.	AG	AG	PAG	n.d.
K5	+	+	-	n.a.	AG	AG	ANT	n.d.
K6	+	+	+	n.a.	AG	AG	AG*	+

Table legend: [a]: rat brain membrane; [b]: guinea pig brain membrane; [#]: subnanomolar affinity; n.a.: no affinity; n.d.: not determined; n.e.: no effect; AG: agonist; PAG: partial agonist; ANT: antagonist.

*: the effect of G-prtotein activation was not reversed by selective antagonist.

In vivo experiments: **1a**-**9** – osteoarthritis inflammatory model; DAMGO – **K6** – formalin test.

6 SUMMARY

Bentley analogues

In vitro competition binding experiments all derivatives showed low subnanomolar affinity to MOR. For DOR the ligands showed comparable binding affinities than the selective DOR agonist Ile^{5,6}-deltorphin II peptide ligand except **8** (K_i > 3000 nM). In the KOR binding assays the analogues still displayed nanomolar affinities.

In G-protein activity measurements compound **1f**, **2a**, **2b** had antagonistic; **1e**, **2c**, **8** had partial agonistic and **2d**, **4**, **5**, **7** had full agonistic effects.

Ligands were examined in G-protein activation tests in rat brain membranes, the selectivity could not be observed as the receptor selective antagonists such as Cyp, NTI, nor-BNI and the selective agonists such as DAMGO, Ile^{5,6}-deltorphine II, U-69,593 are not able to inhibit the effects of the extremely potent Bentley analogues.

In vivo tests in osteoarthritis inflammatory model the thevinol derivatives showed a significant antiallodynic effect, while orvinol derivatives, except for **2c**, did not display this effect.

Oligopeptides

In competition binding assays the KYNA-containing peptide, **KA1** bound selectively to the MOR with a low K_i value and a high selectivity ratio, the other oligopeptides also showed selectivity to MOR, except **K3**, which bound to MOR and DOR with similar affinity.

In the G-protein activition tests the EM-2 containing compounds, **K2** and **K3** stimulated G-protein with low efficacy, compound **KA1**, **K4**, **K5** behaved as full agonists, while **K6** had efficacy and potency higher than those of the reference compound DAMGO.

In functional binding assays all oligopetides were inhibited by Cyp (MOR) and NTI (DOR) in rat brain membrane. In guinea pig brain membrane **K4** and **K6** stimulated G-protein, the efficacy of **K4** was inhibited by nor-BNI, while the effect of **K6** was not.

K6 exhibited a strong antinociceptive effect in formalin test.

7 FINAL REMARKS

All investigated compounds showed subnanomolar binding affinity to MOR and a preference to MOR over DOR and KOR. The pharmacological effects of the compounds involved agonism, partial agonism and antagonism. Neither binding affinities nor pharmacological features could be directly related to particular organic functional groups.

The *in vitro* pharmacological effects and the *in vivo* antiallodynic effects were in accordance, except the full agonist **2d.** As the only exception, the newly synthesized compound, **2c** despite its partial agonist nature, showed antiallodynic effect equal to that of the full agonist **9**. As thevinols have shown analgesic effects, they should be monitored in further studies, such as their BBB penetration profiles.

The data of the oligopeptides are encouraging to further develop opioid peptides containing kynurenine moieties since the insertion of KYNA and kyn in our opioid model improved, in some cases, the binding affinity and was able to modulate the selectivity. Also, the possible role played in the metabolism of these peptides and their implication in different neuropathic and chronic pain models is unknown and worth further investigation.

Although the Bentley analogues showed extremely high affinity to opioid receptors, just few of them (**2c**, **4**, **5**, **7**) had well measurable effect in the model of osteoarthritis similar to reference compound **9**. The oligopeptide **K6** showed definite selectivity to MOR similar to the reference peptide compound DAMGO with higher efficacy in G-protein activation assay. **K6** exhibited significant antinociceptive effect in the formalin test in the early phase (**Table 9**). Altogether, the newly developed peptide and non-peptide ligands seem to be good candidates for further studies to better understand the binding interactions, G-protein activation and even pharmacological mechanisms of multiple opioid receptors.

8 REFERENCES

[1] R. Fredriksson, M.C. Lagerström, L.G. Lundin, H.B. Schiöth, The G-protein-coupled receptors in the human genome form five main families. Phylogenetic analysis, paralogon groups, and fingerprints, Mol. Pharmacol. 63 (2003) 1256–1272. https://doi.org/10.1124/mol.63.6.1256.

[2] R. Fredriksson, H.B. Schiöth, The repertoire of G-protein-coupled receptors in fully sequenced genomes, Mol. Pharmacol. 67 (2005) 1414–1425. https://doi.org/10.1124/mol.104.009001.

[3] D.M. Perez, From plants to man: The GPCR "tree of life," Mol. Pharmacol. 67 (2005) 1383–1384. https://doi.org/10.1124/mol.105.011890.

[4] T.K. Bjarnadóttir, D.E. Gloriam, S.H. Hellstrand, H. Kristiansson, R. Fredriksson, H.B. Schiöth, Comprehensive repertoire and phylogenetic analysis of the G protein-coupled receptors in human and mouse, Genomics. 88 (2006) 263–273. https://doi.org/10.1016/j.ygeno.2006.04.001.

[5] Y. Saroz, D.T. Kho, M. Glass, E.S. Graham, N.L. Grimsey, Cannabinoid Receptor 2 (CB 2) Signals via G-alpha-s and Induces IL-6 and IL-10 Cytokine Secretion in Human Primary Leukocytes , ACS Pharmacol. Transl. Sci. 2 (2019) 414–428. https://doi.org/10.1021/acsptsci.9b00049.

[6] N. Sharma, A.S. Akhade, A. Qadri, Sphingosine-1-phosphate suppresses TLR-induced CXCL8 secretion from human T cells, J. Leukoc. Biol. 93 (2013) 521–528. https://doi.org/10.1189/jlb.0712328.

[7] G.G.J. Hazell, C.C. Hindmarch, G.R. Pope, J.A. Roper, S.L. Lightman, D. Murphy, A.M. O'Carroll, S.J. Lolait, G protein-coupled receptors in the hypothalamic paraventricular and supraoptic nuclei - serpentine gateways to neuroendocrine homeostasis, Front. Neuroendocrinol. 33 (2012) 45–66. https://doi.org/10.1016/j.yfrne.2011.07.002.

[8] R.T. Dorsam, J.S. Gutkind, G-protein-coupled receptors and cancer, Nat. Rev. Cancer. 7 (2007) 79–94. https://doi.org/10.1038/nrc2069.

[9] K. Palczewski, T. Kumasaka, T. Hori, C.A. Behnke, H. Motoshima, B.A. Fox, I. Le Trong, D.C. Teller, T. Okada, R.E. Stenkamp, M. Yamamoto, M. Miyano, Crystal structure of rhodopsin: A G protein-coupled receptor, Science (80-.). 289 (2000) 739–745. https://doi.org/10.1126/science.289.5480.739.

[10] V. Cherezov, D.M. Rosenbaum, M.A. Hanson, S.G.F. Rasmussen, S.T. Foon, T.S. Kobilka, H.J. Choi, P. Kuhn, W.I. Weis, B.K. Kobilka, R.C. Stevens, High-resolution crystal structure of an engineered human β2-adrenergic G protein-coupled receptor, Science (80-.). 318 (2007) 1258–1265. https://doi.org/10.1126/science.1150577.

[11] S.G.F. Rasmussen, H.J. Choi, D.M. Rosenbaum, T.S. Kobilka, F.S. Thian, P.C. Edwards, M. Burghammer, V.R.P. Ratnala, R. Sanishvili, R.F. Fischetti, G.F.X. Schertler, W.I. Weis, B.K. Kobilka, Crystal structure of the human β2 adrenergic G-

protein-coupled receptor, Nature. 450 (2007) 383–387. https://doi.org/10.1038/nature06325.

[12] D.M. Rosenbaum, V. Cherezov, M.A. Hanson, S.G.F. Rasmussen, S.T. Foon, T.S. Kobilka, H.J. Choi, X.J. Yao, W.I. Weis, R.C. Stevens, B.K. Kobilka, GPCR engineering yields high-resolution structural insights into β2-adrenergic receptor function, Science (80-.). 318 (2007) 1266–1273. https://doi.org/10.1126/science.1150609.

[13] E. Neumann, K. Khawaja, U. Müller-Ladner, G protein-coupled receptors in rheumatology, Nat. Rev. Rheumatol. 10 (2014) 429–436. https://doi.org/10.1038/nrrheum.2014.62.

[14] S. Neves, G protein Signaling G protein pathways :, Science (80-.). 296 (2002) 1–10.

[15] D.E. Clapham, E.J. Neer, G-protein beta gamma subunits, (1997) 1–5.

[16] F.A. Baltoumas, M.C. Theodoropoulou, S.J. Hamodrakas, Interactions of the α-subunits of heterotrimeric G-proteins with GPCRs, effectors and RGS proteins: A critical review and analysis of interacting surfaces, conformational shifts, structural diversity and electrostatic potentials, J. Struct. Biol. 182 (2013) 209–218. https://doi.org/10.1016/j.jsb.2013.03.004.

[17] A. Stewart, R.A. Fisher, Introduction: G Protein-coupled Receptors and RGS Proteins, 1st ed., Elsevier Inc., 2015. https://doi.org/10.1016/bs.pmbts.2015.03.002.

[18] J.W.F. Yuen, L.S.W. Poon, A.S.L. Chan, F.W.Y. Yu, R.K.H. Lo, Y.H. Wong, Activation of STAT3 by specific Gα subunits and multiple Gβγ dimers, Int. J. Biochem. Cell Biol. 42 (2010) 1052–1059. https://doi.org/10.1016/j.biocel.2010.03.017.

[19] S.R. Sprang, Z. Chen, X. Du, Structural Basis of Effector Regulation and Signal Termination in Heterotrimeric Gα Proteins, Adv. Protein Chem. 74 (2007) 1–65. https://doi.org/10.1016/S0065-3233(07)74001-9.

[20] P. Samama, S. Cotecchia, T. Costa, R.J. Lefkowitz, A mutation-induced activated state of the beta 2-adrenergic receptor. Extending the ternary complex model., J. Biol. Chem. 268 (1993) 4625–36. http://www.ncbi.nlm.nih.gov/pubmed/8095262.

[21] A.W. Kahsai, K. Xiao, S. Rajagopal, S. Ahn, A.K. Shukla, J. Sun, T.G. Oas, R.J. Lefkowitz, Multiple ligand-specific conformations of the β2-adrenergic receptor., Nat. Chem. Biol. 7 (2011) 692–700. https://doi.org/10.1038/nchembio.634.

[22] T. Kenakin, Inverse, protean, and ligand- selective agonism: matters of receptor conformation, FASEB J. 15 (2001) 598–611. https://doi.org/10.1096/fj.00-0438rev.

[23] E. Szűcs, J. Marton, Z. Szabó, S. Hosztafi, G. Kékesi, G. Tuboly, L. Bánki, G. Horváth, P.T. Szabó, C. Tömböly, Z.K. Varga, S. Benyhe, F. Ötvös, Synthesis, biochemical, pharmacological characterization and in silico profile modelling of highly potent opioid orvinol and thevinol derivatives, Eur. J. Med. Chem. 191 (2020) 1121–45. https://doi.org/10.1016/j.ejmech.2020.112145.

[24] Michael J. Brownstein, A brief history of opiates, opioid peptides, and opioid receptors, Proc. Natl. Acad. Sci. U. S. A. 90 (1993) 5391–5393. https://www.mendeley.com/viewer/?fileId=2748b363-305f-4311-6a3c-171b74a43332&documentId=6b4dc5ca-8403-3307-9265-ceb50db3e6ec.

[25] C. Meadway, S. George, R. Braithwaite, Opiate concentrations following the ingestion of poppy seed products - Evidence for "the poppy seed defence," Forensic Sci. Int. 96 (1998) 29–38. https://doi.org/10.1016/S0379-0738(98)00107-8.

[26] B.M. Cox, M.J. Christie, L. Devi, L. Toll, J.R. Traynor, Challenges for opioid receptor nomenclature: IUPHAR Review 9, Br. J. Pharmacol. 172 (2015) 317–323. https://doi.org/10.1111/bph.12612.

[27] Y. Feng, X. He, Y. Yang, D. Chao, L.H. Lazarus, Y. Xia, Current research on opioid receptor function., Curr. Drug Targets. 13 (2012) 230–46. https://doi.org/10.2174/138945012799201612.

[28] B.L. Kieffer, C.J. Evans, Opioid receptors: from binding sites to visible molecules in vivo., Neuropharmacology. 56 Suppl 1 (2009) 205–12. https://doi.org/10.1016/j.neuropharm.2008.07.033.

[29] C.W. Stevens, Bioinformatics and Evolution of Vertebrate Nociceptin and Opioid Receptors, 1st ed., Elsevier Inc., 2015. https://doi.org/10.1016/bs.vh.2014.10.002.

[30] G.L. Thompson, E. Kelly, A. Christopoulos, M. Canals, Novel GPCR paradigms at the μ-opioid receptor, Br. J. Pharmacol. 172 (2015) 287–296. https://doi.org/10.1111/bph.12600.

[31] Y. Chen, A. Mestek, J. Liu, J.A. Hurley, L. Yu, Molecular cloning and functional expression of a mu-opioid receptor from rat brain., Mol. Pharmacol. 44 (1993) 8–12. http://www.ncbi.nlm.nih.gov/pubmed/8393525.

[32] B.L. Kieffer, K. Befort, C. Gaveriaux-Ruff, C.G. Hirth, The delta-opioid receptor: isolation of a cDNA by expression cloning and pharmacological characterization., Proc. Natl. Acad. Sci. U. S. A. 89 (1992) 12048–52. https://doi.org/10.1073/pnas.89.24.12048.

[33] K. Yasuda, K. Raynor, H. Kong, C.D. Breder, J. Takeda, T. Reisine, G.I. Bell, Cloning and functional comparison of kappa and delta opioid receptors from mouse brain., Proc. Natl. Acad. Sci. 90 (1993) 6736–6740. https://doi.org/10.1073/pnas.90.14.6736.

[34] J.R. Bunzow, C. Saez, M. Mortrud, C. Bouvier, J.T. Williams, M. Low, D.K. Grandy, Molecular cloning and tissue distribution of a putative member of the rat opioid receptor gene family that is not a μ, δ or κ opioid receptor type, FEBS Lett. 347 (1994) 284–288. https://doi.org/10.1016/0014-5793(94)00561-3.

[35] Y. Chen, Y. Fan, J. Liu, A. Mestek, M. Tian, C.A. Kozak, L. Yu, Molecular cloning, tissue distribution and chromosomal localization of a novel member of the opioid receptor gene family, FEBS Lett. 347 (1994) 279–283. https://doi.org/10.1016/0014-5793(94)00560-5.

[36] J.E. Lachowicz, Y. Shen, F.J. Monsma, D.R. Sibley, Molecular Cloning of a Novel G

Protein-Coupled Receptor Related to the Opiate Receptor Family, J. Neurochem. 64 (1995) 34–40. https://doi.org/10.1046/j.1471-4159.1995.64010034.x.

[37] C. Mollereau, M. Parmentier, P. Mailleux, J.-L. Butour, C. Moisand, P. Chalon, D. Caput, G. Vassart, J.-C. Meunier, ORL1, a novel member of the opioid receptor family, FEBS Lett. 341 (1994) 33–38. https://doi.org/10.1016/0014-5793(94)80235-1.

[38] M.J. Wick, S.R. Minnerath, X. Lin, R. Elde, P.Y. Law, H.H. Loh, Isolation of a novel cDNA encoding a putative membrane receptor with high homology to the cloned μ, δ, and κ opioid receptors, Mol. Brain Res. 27 (1994) 37–44. https://doi.org/10.1016/0169-328X(94)90181-3.

[39] J.C. Meunier, Nociceptin/orphanin FQ and the opioid receptor-like ORL1 receptor, Eur. J. Pharmacol. 340 (1997) 1–15. https://doi.org/10.1016/S0014-2999(97)01411-8.

[40] W. Stevens, Craig, The evolution of vertebrate opioid receptors, Front. Biosci. Volume (2009) 1247–69. https://doi.org/10.2741/3306.

[41] D.M.F. Cooper, C. Londos, D.L. Gill, M. Rodbell, Opiate Receptor-Mediated Inhibition of Adenylate Cyclase in Rat Striatal Plasma Membranes, J. Neurochem. 38 (1982) 1164–1167. https://doi.org/10.1111/j.1471-4159.1982.tb05365.x.

[42] E. Bourinet, T.W. Soong, A. Stea, T.P. Snutch, Determinants of the G protein-dependent opioid modulation of neuronal calcium channels., Proc. Natl. Acad. Sci. 93 (1996) 1486–1491. https://doi.org/10.1073/pnas.93.4.1486.

[43] T. Ivanina, D. Varon, S. Peleg, I. Rishal, Y. Porozov, C.W. Dessauer, T. Keren-Raifman, N. Dascal, Gα i1 and Gα i3 Differentially Interact with, and Regulate, the G Protein-activated K + Channel, J. Biol. Chem. 279 (2004) 17260–17268. https://doi.org/10.1074/jbc.M313425200.

[44] S. Benyhe, F. Zádor, F. Ötvös, Biochemistry of opioid (morphine) receptors: Binding, structure and molecular modelling, Acta Biol. Szeged. 59 (2015) 17–37. http://www.sci.u-szeged.hu/ABS REVIEW.

[45] N.T. Burford, D. Wang, W. Sadée, G-protein coupling of mu-opioid receptors (OP3): elevated basal signalling activity., Biochem J. 348 (2000) 531–7. https://doi.org/10.1042/0264-6021:3480531.

[46] M. Capogna, B.H. Gähwiler, S.M. Thompson, Mechanism of mu-opioid receptor-mediated presynaptic inhibition in the rat hippocampus in vitro., J. Physiol. 470 (1993) 539–558. https://doi.org/10.1113/jphysiol.1993.sp019874.

[47] A. Mansour, C.A. Fox, H. Akil, S.J. Watson, Opioid-receptor mRNA expression in the rat CNS: anatomical and functional implications, Trends Neurosci. 18 (1995) 22–29. https://doi.org/10.1016/0166-2236(95)93946-U.

[48] M.J. Brownstein, A brief history of opiates, opioid peptides, and opioid receptors., Proc. Natl. Acad. Sci. 90 (1993) 5391–5393. https://doi.org/10.1073/pnas.90.12.5391.

[49] L.J. Sim, S.R. Childers, Anatomical distribution of mu, delta, and kappa opioid- and nociceptin/orphanin FQ-stimulated [35S]Guanylyl-5?-O-(?-Thio)-triphosphate binding

in guinea pig brain, J. Comp. Neurol. 386 (1997) 562–572. https://doi.org/10.1002/(SICI)1096-9861(19971006)386:4<562::AID-CNE4>3.0.CO;2-0.

[50] C. Stein, M. Schäfer, H. Machelska, Attacking pain at its source: new perspectives on opioids, Nat. Med. 9 (2003) 1003–1008. https://doi.org/10.1038/nm908.

[51] J. Hughes, T.W. Smith, H.W. Kosterlitz, L. Fothergill, B. Morgan, H.R. Morris, Identification of two related pentapeptides from the brain with potent opiate agonist activity, Nature. 258 (1975) 577–579. https://doi.org/10.1038/258577a0.

[52] C.H. Li, D. Chung, Isolation and structure of an untriakontapeptide with opiate activity from camel pituitary glands., Proc. Natl. Acad. Sci. U. S. A. 73 (1976) 1145–8. https://doi.org/10.1073/pnas.73.4.1145.

[53] a Goldstein, W. Fischli, L.I. Lowney, M. Hunkapiller, L. Hood, Porcine pituitary dynorphin: complete amino acid sequence of the biologically active heptadecapeptide., Proc. Natl. Acad. Sci. U. S. A. 78 (1981) 7219–23. http://www.pubmedcentral.nih.gov/articlerender.fcgi?artid=349228&tool=pmcentrez&rendertype=abstract.

[54] C.W. Pittius, N. Kley, J.P. Loeffler, V. Höllt, Quantitation of proenkephalin A messenger RNA in bovine brain, pituitary and adrenal medulla: correlation between mRNA and peptide levels., EMBO J. 4 (1985) 1257–60. http://www.ncbi.nlm.nih.gov/pubmed/4006917.

[55] R. Guillemin, T. Vargo, J. Rossier, S. Minick, N. Ling, C. Rivier, W. Vale, F. Bloom, beta-Endorphin and adrenocorticotropin are selected concomitantly by the pituitary gland., Science. 197 (1977) 1367–9. https://doi.org/10.1126/science.197601.

[56] B. Sharp, K. Linner, What do we know about the expression of proopiomelanocortin transcripts and related peptides in lymphoid tissue?, Endocrinology. 133 (1993) 1921A–1921B. https://doi.org/10.1210/endo.133.5.8404637.

[57] H.S. Sharma, P. Alm, Nitric oxide synthase inhibitors influence dynorphin A (1-17) immunoreactivity in the rat brain following hyperthermia, Amino Acids. 23 (2002) 247–259. https://doi.org/10.1007/s00726-001-0136-0.

[58] J.E. Zadina, L. Hackler, L.-J. Ge, A.J. Kastin, A potent and selective endogenous agonist for the μ-opiate receptor, Nature. 386 (1997) 499–502. https://doi.org/10.1038/386499a0.

[59] S.K. Michelhaugh, A.R. Guastella, S. Mittal, Overview of the Kynurenine Pathway of Tryptophan Metabolism, in: Target. Broadly Pathog. Kynurenine Pathw., Springer International Publishing, Cham, 2015: pp. 3–9. https://doi.org/10.1007/978-3-319-11870-3_1.

[60] A.T. van der Goot, E.A.A. Nollen, Tryptophan metabolism: entering the field of aging and age-related pathologies, Trends Mol. Med. 19 (2013) 336–344. https://doi.org/10.1016/j.molmed.2013.02.007.

[61] R. Schwarcz, J.P. Bruno, P.J. Muchowski, H.Q. Wu, Kynurenines in the mammalian

brain: When physiology meets pathology, Nat. Rev. Neurosci. 13 (2012) 465–477. https://doi.org/10.1038/nrn3257.

[62] M. Huengsberg, J.B. Winer, M. Gompels, R. Round, J. Ross, M. Shahmanesh, Serum kynurenine-to-tryptophan ratio increases with progressive disease in HIV-infected patients, Clin. Chem. 44 (1998) 858–862. https://doi.org/10.1093/clinchem/44.4.858.

[63] K. Schroecksnadel, S. Kaser, M. Ledochowski, G. Neurauter, E. Mur, M. Herold, D. Fuchs, Increased degradation of tryptophan in blood of patients with rheumatoid arthritis., J. Rheumatol. 30 (2003) 1935–9. http://www.ncbi.nlm.nih.gov/pubmed/12966593.

[64] Y. Suzuki, T. Suda, K. Furuhashi, M. Suzuki, M. Fujie, D. Hahimoto, Y. Nakamura, N. Inui, H. Nakamura, K. Chida, Increased serum kynurenine/tryptophan ratio correlates with disease progression in lung cancer, Lung Cancer. 67 (2010) 361–365. https://doi.org/10.1016/j.lungcan.2009.05.001.

[65] B. Widner, E.R. Werner, H. Schennach, H. Wachter, D. Fuchs, Simultaneous measurement of serum tryptophan and kynurenine by HPLC., Clin. Chem. 43 (1997) 2424–6. http://www.ncbi.nlm.nih.gov/pubmed/9439467.

[66] D. Fuchs, A.A. Möller, G. Reibnegger, E. Stöckle, E.R. Werner, H. Wachter, Decreased serum tryptophan in patients with HIV-1 infection correlates with increased serum neopterin and with neurologic/psychiatric symptoms., J. Acquir. Immune Defic. Syndr. 3 (1990) 873–6. http://www.ncbi.nlm.nih.gov/pubmed/2166783.

[67] M. Misztal, T. Frankiewicz, C.G. Parsons, W. Danysz, Learning deficits induced by chronic intraventricular infusion of quinolinic acid — protection by MK-801 and memantine, Eur. J. Pharmacol. 296 (1996) 1–8. https://doi.org/10.1016/0014-2999(95)00682-6.

[68] G.J. Guillemin, D.G. Smith, G.A. Smythe, P.J. Armati, G.J. Brew, Expression of The Kynurenine Pathway Enzymes in Human Microglia and Macrophages, in: 2003: pp. 105–112. https://doi.org/10.1007/978-1-4615-0135-0_12.

[69] L. Vécsei, L. Szalárdy, F. Fülöp, J. Toldi, Kynurenines in the CNS: Recent advances and new questions, Nat. Rev. Drug Discov. 12 (2013) 64–82. https://doi.org/10.1038/nrd3793.

[70] M. Yeganeh Salehpour, A. Mollica, S. Momtaz, N. Sanadgol, M.H. Farzaei, Melatonin and Multiple Sclerosis: From Plausible Neuropharmacological Mechanisms of Action to Experimental and Clinical Evidence, Clin. Drug Investig. 39 (2019) 607–624. https://doi.org/10.1007/s40261-019-00793-6.

[71] M.N. Perkins, T.W. Stone, Actions of kynurenic acid and quinolinic acid in the rat hippocampus in vivo, Exp. Neurol. 88 (1985) 570–579. https://doi.org/10.1016/0014-4886(85)90072-X.

[72] J. Wang, N. Simonavicius, X. Wu, G. Swaminath, J. Reagan, H. Tian, L. Ling, Kynurenic acid as a ligand for orphan G protein-coupled receptor GPR35, J. Biol. Chem. 281 (2006) 22021–22028. https://doi.org/10.1074/jbc.M603503200.

[73] P.H. Reggio, D.M. Shore, The therapeutic potential of orphan GPCRs, GPR35 and GPR55, Front. Pharmacol. 6 (2015) 1–22. https://doi.org/10.3389/fphar.2015.00069.

[74] P.J. Birch, C.J. Grossman, A.G. Hayes, Kynurenate and FG9041 have both competitive and non-competitive antagonist actions at excitatory amino acid receptors, Eur. J. Pharmacol. 151 (1988) 313–315. https://doi.org/10.1016/0014-2999(88)90814-X.

[75] N.J. Kapolka, G.J. Taghon, J.B. Rowe, W.M. Morgan, J.F. Enten, N.A. Lambert, D.G. Isom, DCyFIR: a high-throughput CRISPR platform for multiplexed G protein-coupled receptor profiling and ligand discovery, Proc. Natl. Acad. Sci. 117 (2020) 13117–13126. https://doi.org/10.1073/pnas.2000430117.

[76] A. Peters, P. Krumbholz, E. Jäger, A. Heintz-Buschart, M.V. Çakir, S. Rothemund, A. Gaudl, U. Ceglarek, T. Schöneberg, C. Stäubert, Metabolites of lactic acid bacteria present in fermented foods are highly potent agonists of human hydroxycarboxylic acid receptor 3, PLOS Genet. 15 (2019) e1008145. https://doi.org/10.1371/journal.pgen.1008145.

[77] I. Cervenka, L.Z. Agudelo, J.L. Ruas, Kynurenines: Tryptophan's metabolites in exercise, inflammation, and mental health, Science (80-.). 357 (2017). https://doi.org/10.1126/science.aaf9794.

[78] Y. Ye, Z. Xia, D. Zhang, Z. Sheng, P. Zhang, H. Zhu, N. Xu, S. Liang, Multifunctional pharmaceutical effects of the antibiotic daptomycin, Biomed Res. Int. 2019 (2019). https://doi.org/10.1155/2019/8609218.

[79] P.H. Chuang, P.W. Hsieh, Y.L. Yang, K.F. Hua, F.R. Chang, J. Shiea, S.H. Wu, Y.C. Wu, Cyclopeptides with anti-inflammatory activity from seeds of Annona montana, J. Nat. Prod. 71 (2008) 1365–1370. https://doi.org/10.1021/np8001282.

[80] S.T. Ellis-Steinborner, D. Scanlon, I.F. Musgrave, T.T.N. Tran, S. Hack, T. Wang, A.D. Abell, M.J. Tyler, J.H. Bowie, An unusual kynurenine-containing opioid tetrapeptide from the skin gland secretion of the Australian red tree frog Litoria rubella. Sequence determination by electrospray mass spectrometry, Rapid Commun. Mass Spectrom. 25 (2011) 1735–1740. https://doi.org/10.1002/rcm.5041.

[81] G.J. Guillemin, S.J. Kerr, G.A. Smythe, D.G. Smith, V. Kapoor, P.J. Armati, J. Croitoru, B.J. Brew, Kynurenine pathway metabolism in human astrocytes: A paradox for neuronal protection, J. Neurochem. 78 (2001) 842–853. https://doi.org/10.1046/j.1471-4159.2001.00498.x.

[82] S. Fukui, R. Schwarcz, S.I. Rapoport, Y. Takada, Q.R. Smith, Blood-Brain Barrier Transport of Kynurenines: Implications for Brain Synthesis and Metabolism, J. Neurochem. 56 (1991) 2007–2017. https://doi.org/10.1111/j.1471-4159.1991.tb03460.x.

[83] G. Oláh, J. Herédi, Á. Menyhárt, Z. Czinege, D. Nagy, J. Fuzik, K. Kocsis, L. Knapp, L. Gellért, Z. Kis, T. Farkas, F. Fülöp, Á. Párdutz, J. Tajti, L. Vécsei, J. Toldi, Unexpected effects of peripherally administered kynurenic acid on cortical spreading depression and related blood-brain barrier permeability, Drug Des. Devel. Ther. 7 (2013) 981–987. https://doi.org/10.2147/DDDT.S44496.

[84] F.P. Bonina, L. Arenare, R. Ippolito, G. Boatto, G. Battaglia, V. Bruno, P. De Caprariis, Synthesis, pharmacokinetics and anticonvulsant activity of 7-chlorokynurenic acid prodrugs, Int. J. Pharm. 202 (2000) 79–88. https://doi.org/10.1016/S0378-5173(00)00421-X.

[85] H. Luhavaya, R. Sigrist, J.R. Chekan, S.M.K. McKinnie, B.S. Moore, Biosynthesis of l-4-Chlorokynurenine, an Antidepressant Prodrug and a Non-Proteinogenic Amino Acid Found in Lipopeptide Antibiotics, Angew. Chemie - Int. Ed. 58 (2019) 8394–8399. https://doi.org/10.1002/anie.201901571.

[86] S. Manfredini, B. Pavan, S. Vertuani, M. Scaglianti, D. Compagnone, C. Biondi, A. Scatturin, S. Tanganelli, L. Ferraro, P. Prasad, A. Dalpiaz, Design, synthesis and activity of ascorbic acid prodrugs of nipecotic, kynurenic and diclophenamic acids, liable to increase neurotropic activity, J. Med. Chem. 45 (2002) 559–562. https://doi.org/10.1021/jm015556r.

[87] H. Baran, K. Jellinger, L. Deecke, Kynurenine metabolism in Alzheimer's disease, J. Neural Transm. 106 (1999) 165–181. https://doi.org/10.1007/s007020050149.

[88] Z. Hartai, A. Juhász, Á. Rimanóczy, T. Janáky, T. Donkó, L. Dux, B. Penke, G.K. Tóth, Z. Janka, J. Kálmán, Decreased serum and red blood cell kynurenic acid levels in Alzheimer's disease, Neurochem. Int. 50 (2007) 308–313. https://doi.org/10.1016/j.neuint.2006.08.012.

[89] M.P. Heyes, K. Saito, J.S. Crowley, L.E. Davis, M.A. Demitrack, M. Der, L.A. Dilling, J. Elia, M.J.P. Kruesi, A. Lackner, S.A. Larsen, K. Lee, H.L. Leonard, S.P. Markey, A. Martin, S. Milstein, M.M. Mouradian, M.R. Pranzatelli, B.J. Quearry, A. Salazar, M. Smith, S.E. Strauss, T. Sunderland, S.W. Swedo, W.W. Tourtellotte, Quinolinic acid and kynurenine pathway metabolism in inflammatory and non-inflammatory neurological disease, Brain. 115 (1992) 1249–1273. https://doi.org/10.1093/brain/115.5.1249.

[90] T. Ogawa, W.R. Matson, M.F. Beal, R.H. Myers, E.D. Bird, P. Milbury, S. Saso, Kynurenine pathway abnormalities in Parkinson's disease, Neurology. 42 (1992) 1702–1702. https://doi.org/10.1212/WNL.42.9.1702.

[91] M.F. Beal, W.R. Matson, E. Storey, P. Milbury, E.A. Ryan, T. Ogawa, E.D. Bird, Kynurenic acid concentrations are reduced in Huntington's disease cerebral cortex, J. Neurol. Sci. 108 (1992) 80–87. https://doi.org/10.1016/0022-510X(92)90191-M.

[92] M.F. Beal, W.R. Matson, K.J. Swartz, P.H. Gamache, E.D. Bird, Kynurenine Pathway Measurements in Huntington's Disease Striatum: Evidence for Reduced Formation of Kynurenic Acid, J. Neurochem. 55 (1990) 1327–1339. https://doi.org/10.1111/j.1471-4159.1990.tb03143.x.

[93] D. Jauch, E.M. Urbańska, P. Guidetti, E.D. Bird, J.P.G. Vonsattel, W.O. Whetsell, R. Schwarcz, Dysfunction of brain kynurenic acid metabolism in Huntington's disease: focus on kynurenine aminotransferases, J. Neurol. Sci. 130 (1995) 39–47. https://doi.org/10.1016/0022-510X(94)00280-2.

[94] K. Rejdak, A. Petzold, T. Kocki, J. Kurzepa, P. Grieb, W.A. Turski, Z. Stelmasiak,

Astrocytic activation in relation to inflammatory markers during clinical exacerbation of relapsing-remitting multiple sclerosis, J. Neural Transm. 114 (2007) 1011–1015. https://doi.org/10.1007/s00702-007-0667-y.

[95] K. Rejdak, H. Bartosik-Psujek, B. Dobosz, T. Kocki, P. Grieb, G. Giovannoni, W.A. Turski, Z. Stelmasiak, Decreased level of kynurenic acid in cerebrospinal fluid of relapsing-onset multiple sclerosis patients, Neurosci. Lett. 331 (2002) 63–65. https://doi.org/10.1016/S0304-3940(02)00710-3.

[96] H. Yamamoto, I. Shindo, B. Egawa, K. Horiguchi, Kynurenic acid is decreased in cerebrospinal fluid of patients with infantile spasms, Pediatr. Neurol. 10 (1994) 9–12. https://doi.org/10.1016/0887-8994(94)90060-4.

[97] H. Yamamoto, Studies on CSF tryptophan metabolism in infantile spasms, Pediatr. Neurol. 7 (1991) 411–414. https://doi.org/10.1016/0887-8994(91)90023-E.

[98] P.J. Langlais, M.L. Wardlow, H. Yamamoto, Changes in CSF neurotransmitters in infantile spasms, Pediatr. Neurol. 7 (1991) 440–445. https://doi.org/10.1016/0887-8994(91)90028-J.

[99] H. Yamamoto, H. Murakami, K. Horiguchi, B. Egawa, Studies on cerebrospinal fluid kynurenic acid concentrations in epileptic children, Brain Dev. 17 (1995) 327–329. https://doi.org/10.1016/0387-7604(95)00065-J.

[100] S.N. Raja, D.B. Carr, M. Cohen, N.B. Finnerup, H. Flor, S. Gibson, F.J. Keefe, J.S. Mogil, M. Ringkamp, K.A. Sluka, X.-J. Song, B. Stevens, M.D. Sullivan, P.R. Tutelman, T. Ushida, K. Vader, The revised International Association for the Study of Pain definition of pain, Pain. Publish Ah (2020). https://doi.org/10.1097/j.pain.0000000000001939.

[101] H. Merskey, M.R. Bond, D.B. Boyd, Classification of chronic pain. Descriptions of chronic pain syndromes and definitions of pain terms. Prepared by the International Association for the Study of Pain, Subcommittee on Taxonomy., Pain. Suppl. 3 (1986) S1-226. http://www.ncbi.nlm.nih.gov/pubmed/3461421.

[102] T.S. Jensen, N.B. Finnerup, Allodynia and hyperalgesia in neuropathic pain: clinical manifestations and mechanisms, Lancet Neurol. 13 (2014) 924–935. https://doi.org/10.1016/S1474-4422(14)70102-4.

[103] S. Lolignier, N. Eijkelkamp, J.N. Wood, Mechanical allodynia, Pflügers Arch. - Eur. J. Physiol. 467 (2015) 133–139. https://doi.org/10.1007/s00424-014-1532-0.

[104] A.A. Pradhan, M.L. Smith, B.L. Kieffer, C.J. Evans, Ligand-directed signalling within the opioid receptor family, Br. J. Pharmacol. 167 (2012) 960–969. https://doi.org/10.1111/j.1476-5381.2012.02075.x.

[105] C.F. Semenkovich, A.S. Jaffe, Adverse effects due to morphine sulfate. Challenge to previous clinical doctrine, Am. J. Med. 79 (1985) 325–330. https://doi.org/10.1016/0002-9343(85)90311-0.

[106] J.L. Whistler, H. Chuang, P. Chu, L.Y. Jan, M. von Zastrow, Functional Dissociation of μ Opioid Receptor Signaling and Endocytosis, Neuron. 23 (1999) 737–746.

https://doi.org/10.1016/S0896-6273(01)80032-5.

[107] World Health Organization, Model list of essential medicines, Ment. Holist. Heal. Some Int. Perspect. 21 (2019) 119–134.

[108] H. Hedegaard, B.A. Bastian, J.P. Trinidad, M. Spencer, M. Warner, Drugs Most Frequently Involved in Drug Overdose Deaths: United States, 2011-2016., Natl. Vital Stat. Rep. 67 (2018) 1–14. http://www.ncbi.nlm.nih.gov/pubmed/30707673.

[109] W.R. Martin, H.F. Fraser, A comparative study of physiological and subjective effects of heroin and morphine administered intravenously in postaddicts., J. Pharmacol. Exp. Ther. 133 (1961) 388–99. http://www.ncbi.nlm.nih.gov/pubmed/13767429.

[110] T.H. Stanley, The history and development of the fentanyl series, J. Pain Symptom Manage. 7 (1992) S3–S7. https://doi.org/10.1016/0885-3924(92)90047-L.

[111] J. Pergolizzi, Jr., R. Taylor Jr, J.A. LeQuang, R.B. Raffa, Managing severe pain and abuse potential: the potential impact of a new abuse-deterrent formulation oxycodone/naltrexone extended-release product, J. Pain Res. Volume 11 (2018) 301–311. https://doi.org/10.2147/JPR.S127602.

[112] J. Homsi, D. Walsh, K.A. Nelson, S.B. LeGrand, M. Davis, Hydrocodone for cough in advanced cancer, Am. J. Hosp. Palliat. Med. 17 (2000) 342–346. https://doi.org/10.1177/104990910001700512.

[113] E. Prommer, MD, Role of codeine in palliative care, J. Opioid Manag. 7 (2011) 401–406. https://doi.org/10.5055/jom.2011.0081.

[114] S. Friedrichsdorf, A. Postier, Management of breakthrough pain in children with cancer, J. Pain Res. (2014) 117. https://doi.org/10.2147/JPR.S58862.

[115] J.D. Toombs, L.A. Kral, Methadone treatment for pain states., Am. Fam. Physician. 71 (2005) 1353–8. http://www.ncbi.nlm.nih.gov/pubmed/15832538.

[116] M. Grissinger, Keeping patients safe from methadone overdoses., P T. 36 (2011) 462–6. http://www.ncbi.nlm.nih.gov/pubmed/21935293.

[117] J. Schumacher, Side Effects of Etorphine and Carfentanil in Nondomestic Hoofstock, in: Zoo Wild Anim. Med., Elsevier, 2008: pp. 455–461. https://doi.org/10.1016/B978-141604047-7.50059-2.

[118] C.G. Pollock, E.C. Ramsay, Serial immobilization of a brazilian tapir (Tapirus Terrestrus) with oral detomidine and oral carfentanil, J. Zoo Wildl. Med. 34 (2003) 408–410. https://doi.org/10.1638/01-061.

[119] P. Sloan, Review of oral oxymorphone in the management of pain, Ther. Clin. Risk Manag. Volume 4 (2008) 777–787. https://doi.org/10.2147/TCRM.S1784.

[120] S. Grond, A. Sablotzki, Clinical Pharmacology of Tramadol, Clin. Pharmacokinet. 43 (2004) 879–923. https://doi.org/10.2165/00003088-200443130-00004.

[121] M.J. Hoffert, J.R. Couch, S. Diamond, A.H. Elkind, J. Goldstein, N.J. Kohlerman, J.R. Saper, S. Solomon, Transnasal Butorphanol in the Treatment of Acute Migraine,

Headache J. Head Face Pain. 35 (1995) 65–69. https://doi.org/10.1111/j.1526-4610.1995.hed3502065.x.

[122] M. Bush, S.B. Citino, W.R. Lance, The use of butorphanol in anesthesia protocols for zoo and wild mammals, Elsevier Inc., 2011. https://doi.org/10.1016/b978-1-4377-1986-4.00077-9.

[123] A. Schnabel, S.U. Reichl, P.K. Zahn, E. Pogatzki-Zahn, Nalbuphine for postoperative pain treatment in children, Cochrane Database Syst. Rev. (2014). https://doi.org/10.1002/14651858.CD009583.pub2.

[124] P. Gharagozlou, H. Demirci, J. David Clark, J. Lameh, Activity of opioid ligands in cells expressing cloned mu opioid receptors., BMC Pharmacol. 3 (2003) 1. https://doi.org/10.1186/1471-2210-3-1.

[125] L. Gowing, R. Ali, J.M. White, D. Mbewe, Buprenorphine for managing opioid withdrawal, Cochrane Database Syst. Rev. (2017). https://doi.org/10.1002/14651858.CD002025.pub5.

[126] B. Holmes, A. Ward, Meptazinol A Review of its Pharmacodynamic and Pharmacokinetic Properties and Therapeutic Efficacy, Drugs. 30 (1985) 285–312. https://doi.org/10.2165/00003495-198530040-00001.

[127] B.T. Alford, R.L. Burkhart, W.P. Johnson, Etorphine and diprenorphine as immobilizing and reversing agents in captive and free-ranging mammals., J. Am. Vet. Med. Assoc. 164 (1974) 702–5. http://www.ncbi.nlm.nih.gov/pubmed/4817959.

[128] D.A. Jessup, W.E. Clark, K.R. Jones, R. Clark, W.R. Lance, Immobilization of free-ranging desert bighorn sheep, tule elk, and wild horses, using carfentanil and xylazine: reversal with naloxone, diprenorphine, and yohimbine., J. Am. Vet. Med. Assoc. 187 (1985) 1253–4. http://www.ncbi.nlm.nih.gov/pubmed/4077657.

[129] L. Gowing, R. Ali, J.M. White, Opioid antagonists with minimal sedation for opioid withdrawal. Cochrane Database of Systematic Reviews: Reviews, Cochrane Database Syst. Rev. (2017). https://doi.org/10.1002/14651858.CD002021.pub4.www.cochranelibrary.com.

[130] A.A.-B. Badawy, M. Evans, The mechanism of the antagonism by naloxone of acute alcohol intoxication, Br. J. Pharmacol. 74 (1981) 514–516. https://doi.org/10.1111/j.1476-5381.1981.tb10458.x.

[131] C. Cenk Tek, Naltrexone HCI/bupropion HCI for chronic weight management in obese adults: patient selection and perspectives, Patient Prefer. Adherence. (2016) 751. https://doi.org/10.2147/PPA.S84778.

[132] F. Paille, H. Martini, Nalmefene: a new approach to the treatment of alcohol dependence, Subst. Abuse Rehabil. (2014) 87. https://doi.org/10.2147/SAR.S45666.

[133] E.W. Boyer, Management of Opioid Analgesic Overdose, N. Engl. J. Med. 367 (2012) 146–155. https://doi.org/10.1056/NEJMra1202561.

[134] C. Berna, R.J. Kulich, J.P. Rathmell, Tapering Long-term Opioid Therapy in Chronic

Noncancer Pain, Mayo Clin. Proc. 90 (2015) 828–842. https://doi.org/10.1016/j.mayocp.2015.04.003.

[135] A. Signla, MD, P. Sloan, MD, Review article. Pharmacokinetic evaluation of hydrocodone/acetaminophen for pain management, J. Opioid Manag. 9 (2013) 71–80. https://doi.org/10.5055/jom.2013.0149.

[136] M.K. Park, J.H. Lee, G.Y. Yang, K.A. Won, M.J. Kim, Y.Y. Park, Y.C. Bae, D.K. Ahn, Peripheral administration of NR2 antagonists attenuates orofacial formalin-induced nociceptive behavior in rats, Prog. Neuro-Psychopharmacology Biol. Psychiatry. 35 (2011) 982–986. https://doi.org/10.1016/j.pnpbp.2011.01.018.

[137] G.Y. Yang, Y.W. Woo, M.K. Park, Y.C. Bae, D.K. Ahn, E. Bonfa, Intracisternal administration of NR2 antagonists attenuates facial formalin-induced nociceptive behavior in rats., J. Orofac. Pain. 24 (2010) 203–11. http://www.ncbi.nlm.nih.gov/pubmed/20401359.

[138] E. Vamos, A. Pardutz, P. Klivenyi, J. Toldi, L. Vecsei, The role of kynurenines in disorders of the central nervous system: Possibilities for neuroprotection, J. Neurol. Sci. 283 (2009) 21–27. https://doi.org/10.1016/j.jns.2009.02.326.

[139] E. Knyihár-Csillik, J. Toldi, A. Mihály, B. Krisztin-Péva, Z. Chadaide, H. Németh, R. Fenyo, L. Vécsei, Kynurenine in combination with probenecid mitigates the stimulation-induced increase of c-fos immunoreactivity of the rat caudal trigeminal nucleus in an experimental migraine model, J. Neural Transm. 114 (2007) 417–421. https://doi.org/10.1007/s00702-006-0545-z.

[140] G. Nagy-Grócz, F. Zádor, S. Dvorácskó, Z. Bohár, S. Benyhe, C. Tömböly, Á. Párdutz, L. Vécsei, Interactions between the kynurenine and the endocannabinoid system with special emphasis on migraine, Int. J. Mol. Sci. 18 (2017) 1–22. https://doi.org/10.3390/ijms18081617.

[141] H. Ohshiro, H. Tonai-Kachi, K. Ichikawa, GPR35 is a functional receptor in rat dorsal root ganglion neurons, Biochem. Biophys. Res. Commun. 365 (2008) 344–348. https://doi.org/10.1016/j.bbrc.2007.10.197.

[142] C. Cosi, G. Mannaioni, A. Cozzi, V. Carlà, M. Sili, L. Cavone, D. Maratea, F. Moroni, G-protein coupled receptor 35 (GPR35) activation and inflammatory pain: Studies on the antinociceptive effects of kynurenic acid and zaprinast, Neuropharmacology. 60 (2011) 1227–1231. https://doi.org/10.1016/j.neuropharm.2010.11.014.

[143] J.D. Mezrich, J.H. Fechner, X. Zhang, B.P. Johnson, W.J. Burlingham, C.A. Bradfield, An Interaction between Kynurenine and the Aryl Hydrocarbon Receptor Can Generate Regulatory T Cells, J. Immunol. 185 (2010) 3190–3198. https://doi.org/10.4049/jimmunol.0903670.

[144] F. Moroni, A. Cozzi, M. Sili, G. Mannaioni, Kynurenic acid: A metabolite with multiple actions and multiple targets in brain and periphery, J. Neural Transm. 119 (2012) 133–139. https://doi.org/10.1007/s00702-011-0763-x.

[145] T.W. Stone, N. Stoy, L.G. Darlington, An expanding range of targets for kynurenine

metabolites of tryptophan, Trends Pharmacol. Sci. 34 (2013) 136–143. https://doi.org/10.1016/j.tips.2012.09.006.

[146] S. Hosztafi, Chemical structures of alkaloids. In Poppy, The Genus Papaver, Harwood Acad. Publ. Amsterdam. (1998) 105–158.

[147] J.R. Lever, R.F. Dannals, A.A. Wilson, H.T. Ravert, H.N. Wagner, Synthesis of carbon-11 labeled diprenorphine: A radioligand for positron emission tomographic studies of opiate receptors, Tetrahedron Lett. 28 (1987) 4015–4018. https://doi.org/10.1016/S0040-4039(01)83849-1.

[148] J.R. Lever, S.M. Mazza, R.F. Dannals, H.T. Ravert, A.A. Wilson, H.N. Wagner, Facile synthesis of [11C]buprenorphine for positron emission tomographic studies of opioid receptors, Int. J. Radiat. Appl. Instrumentation. Part. 41 (1990) 745–752. https://doi.org/10.1016/0883-2889(90)90022-9.

[149] S.K. Luthra, F. Brady, D.R. Turton, D.J. Brown, K. Dowsett, S.L. Waters, A.K.P. Jones, R.W. Matthews, J.C. Crowder, Automated radiosyntheses of [6-O-methyl-11C]diprenorphine and [6-O-methyl-11C]buprenorphine from 3-O-trityl protected precursors, Appl. Radiat. Isot. 45 (1994) 857–873. https://doi.org/10.1016/0969-8043(94)90217-8.

[150] J. Marton, B.W. Schoultz, T. Hjoernevik, A. Drzezga, B.H. Yousefi, H.J. Wester, F. Willoch, G. Henriksen, Synthesis and evaluation of a full-agonist orvinol for PET-imaging of opioid receptors: [11C]PEO, J. Med. Chem. 52 (2009) 5586–5589. https://doi.org/10.1021/jm900892x.

[151] J. Marton, G. Henriksen, Design and synthesis of an 18F-labeled version of phenylethyl orvinol ([18F]FE-PEO) for PET-imaging of opioid receptors, Molecules. 17 (2012) 11554–11569. https://doi.org/10.3390/molecules171011554.

[152] K.W. Bentley, D.G. Hardy, B. Meek, Novel Analgesics and Molecular Rearrangements in the Morphine-Thebaine Group. II. Alcohols Derivd from 6,14-endo-Ethno-and 6,14-endo-Ethanotetrahydrothebaine, J. Am. Chem. Soc. 89 (1967) 3273–3280.

[153] K.W. Bentley, D.G. Hardy, Novel analgesics and molecular rearrangements in the morphine-thebaine group. III. Alcohols of the 6,14-endo-ethenotetrahydrooripavine series and derived analogs of N-allylnormorphine and -norcodeine, J. Am. Chem. Soc. 89 (1967) 3281–3292. https://doi.org/10.1021/ja00989a032.

[154] A. Coop, J.W. Janetka, J.W. Lewis, K.C. Rice, L-Selectride as a General Reagent for the O-Demethylation and N-Decarbomethoxylation of Opium Alkaloids and Derivatives 1, J. Org. Chem. 63 (1998) 4392–4396. https://doi.org/10.1021/jo9801972.

[155] J.W. Lewis, M.J. Readhead, Novel analgetics and molecular rearrangements in the morphine-thebaine group. 18. 3-deoxy-6,14-endo-etheno-6,7,8,14-tetrahydrooripavines., J. Med. Chem. 13 (1970) 525–7. http://www.ncbi.nlm.nih.gov/pubmed/5441135.

[156] D. Biyashev, S. Garadnay, J. Marton, S. Makleit, A. Borsodi, S. Benyhe, Biochemical characterisation of newly developed beta-etorphine and beta-dihydroetorphine

derivatives., Eur. J. Pharmacol. 442 (2002) 23–7. http://www.ncbi.nlm.nih.gov/pubmed/12020678.

[157] J.W. Lewis, S.M. Husbands, The orvinols and related opioids--high affinity ligands with diverse efficacy profiles., Curr. Pharm. Des. 10 (2004) 717–32. https://doi.org/10.2174/1381612043453027.

[158] S.M. Husbands, Buprenorphine and Related Orvinols, in: 2013: pp. 127–144. https://doi.org/10.1021/bk-2013-1131.ch007.

[159] A. Coop, I. Berzetei-Gurske, J. Burnside, L. Toll, J.R. Traynor, S.M. Husbands, J.W. Lewis, Structural Determinants of Opioid Activity in the Orvinols and Related Structures. Ethers of 7,8-Cyclopenta-Fused Analogs of Buprenorphine, Helv. Chim. Acta. 83 (2000) 687–693. https://doi.org/10.1002/(SICI)1522-2675(20000412)83:4<687::AID-HLCA687>3.0.CO;2-W.

[160] B.M. Greedy, F. Bradbury, M.P. Thomas, K. Grivas, G. Cami-Kobeci, A. Archambeau, K. Bosse, M.J. Clark, M. Aceto, J.W. Lewis, J.R. Traynor, S.M. Husbands, Orvinols with Mixed Kappa/Mu Opioid Receptor Agonist Activity, J. Med. Chem. 56 (2013) 3207–3216. https://doi.org/10.1021/jm301543e.

[161] T.W. Stone, C.M. Forrest, L.G. Darlington, Kynurenine pathway inhibition as a therapeutic strategy for neuroprotection, FEBS J. 279 (2012) 1386–1397. https://doi.org/10.1111/j.1742-4658.2012.08487.x.

[162] G.S. Deora, S. Kantham, S. Chan, S.N. Dighe, S.K. Veliyath, G. McColl, M.O. Parat, R.P. McGeary, B.P. Ross, Multifunctional Analogs of Kynurenic Acid for the Treatment of Alzheimer's Disease: Synthesis, Pharmacology, and Molecular Modeling Studies, ACS Chem. Neurosci. 8 (2017) 2667–2675. https://doi.org/10.1021/acschemneuro.7b00229.

[163] D. Zádori, G. Nyiri, A. Szonyi, I. Szatmári, F. Fülöp, J. Toldi, T.F. Freund, L. Vécsei, P. Klivényi, Neuroprotective effects of a novel kynurenic acid analogue in a transgenic mouse model of Huntington's disease, J. Neural Transm. 118 (2011) 865–875. https://doi.org/10.1007/s00702-010-0573-6.

[164] H.A. Oktem, J. Moitra, S. Benyhe, G. Tóth, A. Lajtha, A. Borsodi, Opioid receptor labeling with the chloromethyl ketone derivative of [3H]Tyr-D-Ala-Gly-(Me)Phe-Gly-ol (DAMGO) II: Covalent labeling of mu opioid binding site by 3H-Tyr-D-Ala-Gly-(Me)Phe chloromethyl ketone., Life Sci. 48 (1991) 1763–8.

[165] S.T. Nevin, L. Kabasakal, F. Ötvös, G. Tóth, A. Borsodi, Binding characteristics of the novel highly selective delta agonist, [3H]IIe5,6deltorphin II., Neuropeptides. 26 (1994) 261–5. https://doi.org/10.1016/0143-4179(94)90080-9.

[166] E. Guerrieri, J.R. Mallareddy, G. Tóth, H. Schmidhammer, M. Spetea, Synthesis and Pharmacological Evaluation of [3 H]HS665, a Novel, Highly Selective Radioligand for the Kappa Opioid Receptor, ACS Chem. Neurosci. 6 (2015) 456–463. https://doi.org/10.1021/cn5002792.

[167] N. Basu, A.M. Scheuhammer, K. Rouvinen-Watt, N. Grochowina, R.D. Evans, M.

O'Brien, H.M. Chan, Decreased N-methyl-d-aspartic acid (NMDA) receptor levels are associated with mercury exposure in wild and captive mink, Neurotoxicology. 28 (2007) 587–593. https://doi.org/10.1016/j.neuro.2006.12.007.

[168] M. Spetea, I.P. Berzetei-Gurske, E. Guerrieri, H. Schmidhammer, Discovery and pharmacological evaluation of a diphenethylamine derivative (HS665), a highly potent and selective ?? opioid receptor agonist, J. Med. Chem. 55 (2012) 10302–10306. https://doi.org/10.1021/jm301258w.

[169] G. Kovács, Z. Petrovszki, J.R. Mallareddy, G. Tóth, G. Benedek, G. Horváth, Characterization of antinociceptive potency of endomorphin-2 derivatives with unnatural amino acids in rats, Acta Physiol. Hung. 99 (2012) 353–363. https://doi.org/10.1556/APhysiol.99.2012.3.12.

[170] S. Benyhe, J. Farkas, G. Tóth, M. Wollemann, Met5-enkephalin-Arg6-Phe7, an endogenous neuropeptide, binds to multiple opioid and nonopioid sites in rat brain, J. Neurosci. Res. 48 (1997) 249–258. https://doi.org/10.1002/(SICI)1097-4547(19970501)48:3<249::AID-JNR7>3.0.CO;2-F.

[171] L.J. Sim, D.E. Selley, S.R. Childers, In vitro autoradiography of receptor-activated G proteins in rat brain by agonist-stimulated guanylyl 5'-[gamma-[35S]thio]-triphosphate binding., Proc Natl Acad Sci USA. 92 (1995) 7242–46.

[172] J.R. Traynor, S.R. Nahorski, Modulation by mu-opioid agonists of guanosine-5'-O-(3-[35S]thio)triphosphate binding to membranes from human neuroblastoma SH-SY5Y cells., Mol. Pharmacol. 47 (1995) 848–54.

[173] E. Szűcs, A. Büki, G. Kékesi, G. Horváth, S. Benyhe, Mu-Opioid (MOP) receptor mediated G-protein signaling is impaired in specific brain regions in a rat model of schizophrenia, Neurosci. Lett. 619 (2016) 29–33. https://doi.org/10.1016/j.neulet.2016.02.060.

[174] J. Marton, Z. Szabó, S. Garadnay, S. Miklós, S. Makleit, Studies on the synthesis of β-thevinone derivatives, Tetrahedron. 54 (1998) 9143–9152. https://doi.org/10.1016/S0040-4020(98)00551-1.

[175] S.E. Bove, S.L. Calcaterra, R.M. Brooker, C.M. Huber, R.E. Guzman, P.L. Juneau, D.J. Schrier, K.S. Kilgore, Weight bearing as a measure of disease progression and efficacy of anti-inflammatory compounds in a model of monosodium iodoacetate-induced osteoarthritis, Osteoarthr. Cartil. 11 (2003) 821–830. https://doi.org/10.1016/S1063-4584(03)00163-8.

[176] D.A. Kalbhen, Chemical model of osteoarthritis--a pharmacological evaluation., J. Rheumatol. 14 (1987) 130–1. http://www.ncbi.nlm.nih.gov/pubmed/3625668.

[177] Y.-C. Cheng, W.H. Prusoff, relationship between the constant (Ki) and the concentration of inhibitor which causes 50 percent inhibition (I50) of an enzymatic reaction, 22 (1973) 3099–3108.

[178] F. Zádor, R. Samavati, E. Szlávicz, B. Tuka, E. Bojnik, F. Fülöp, J. Toldi, L. Vécsei, A. Borsodi, Inhibition of opioid receptor mediated G-protein activity after chronic

administration of kynurenic acid and its derivative without direct binding to opioid receptors., CNS Neurol. Disord. Drug Targets. 13 (2014) 1520–9. http://www.ncbi.nlm.nih.gov/pubmed/25478797.

[179] J.A. Kemp, S. Grimwood, A.C. Foster, Characterization of the antagonism of excitatory amino acid receptors in rat cortex by kynurenic acid., Br. J. Pharmacol. 91 (1987) 314–24.

[180] H.S. Smith, Peripherally-acting opioids., Pain Physician. 11 (2008) S121-32. http://www.ncbi.nlm.nih.gov/pubmed/18443636.

[181] C.R. McNamara, J. Mandel-Brehm, D.M. Bautista, J. Siemens, K.L. Deranian, M. Zhao, N.J. Hayward, J.A. Chong, D. Julius, M.M. Moran, C.M. Fanger, TRPA1 mediates formalin-induced pain, Proc. Natl. Acad. Sci. U. S. A. 104 (2007) 13525–13530. https://doi.org/10.1073/pnas.0705924104.

[182] C. Stein, Opioid receptors, Annu. Rev. Med. 67 (2016) 433–451. https://doi.org/10.1146/annurev-med-062613-093100.

[183] J.M. Berthelot, C. Darrieutort-Lafitte, B. Le Goff, Y. Maugars, Strong opioids for noncancer pain due to musculoskeletal diseases: Not more effective than acetaminophen or NSAIDs, Jt. Bone Spine. 82 (2015) 397–401. https://doi.org/10.1016/j.jbspin.2015.08.003.

[184] M.M. Garcia, C. Goicoechea, M. Avellanal, S. Traseira, M.I. Martín, E.M. Sánchez-Robles, Comparison of the antinociceptive profiles of morphine and oxycodone in two models of inflammatory and osteoarthritic pain in rat, Eur. J. Pharmacol. 854 (2019) 109–118. https://doi.org/10.1016/j.ejphar.2019.04.011.

[185] L. Yang, H. Wang, K. Shah, V.T. Karamyan, T.J. Abbruscato, Opioid receptor agonists reduce brain edema in stroke, Brain Res. 1383 (2011) 307–316. https://doi.org/10.1016/j.brainres.2011.01.083.

[186] L. Yang, K. Shah, H. Wang, V.T. Karamyan, T.J. Abbruscato, Characterization of neuroprotective effects of biphalin, an opioid receptor agonist, in a model of focal brain ischemia, J. Pharmacol. Exp. Ther. 339 (2011) 499–508. https://doi.org/10.1124/jpet.111.184127.

[187] L. Yang, M.R. Islam, V.T. Karamyan, T.J. Abbruscato, In vitro and in vivo efficacy of a potent opioid receptor agonist, biphalin, compared to subtype-selective opioid receptor agonists for stroke treatment, Brain Res. 1609 (2015) 1–11. https://doi.org/10.1016/j.brainres.2015.03.022.

[188] T.P. Davis, T.J. Abbruscato, R.D. Egleton, Peptides at the blood brain barrier: Knowing me knowing you, Peptides. 72 (2015) 50–56. https://doi.org/10.1016/j.peptides.2015.04.020.

APPENDIX: OFF-PRINTS OF THE THESIS RELATED PUBLICATIONS

I.

Edina Szűcs, János Marton, Zoltán Szabó, Sándor Hosztafi, Gabriella Kékesi, Gábor Tuboly, László Bánki, Gyöngyi Horváth, Pál T. Szabó, Csaba Tömböly, Zsuzsanna Varga, Sándor Benyhe, Ferenc Ötvös (2020) **Synthesis, biochemical, pharmacological characterization and in silico profile modelling of highly potent opioid orvinol and thevinol derivatives.** EUR. J. MED. CHEM., 191:1121-45.

European Journal of Medicinal Chemistry 191 (2020) 112145

Contents lists available at ScienceDirect

European Journal of Medicinal Chemistry

journal homepage: http://www.elsevier.com/locate/ejmech

Research paper

Synthesis, biochemical, pharmacological characterization and *in silico* profile modelling of highly potent opioid orvinol and thevinol derivatives

Edina Szűcs [a, b, 1], János Marton [c, 1], Zoltán Szabó [d], Sándor Hosztafi [e], Gabriella Kékesi [f], Gábor Tuboly [g], László Bánki [h], Gyöngyi Horváth [f], Pál T. Szabó [i], Csaba Tömböly [a], Zsuzsanna Katalin Varga [a, b], Sándor Benyhe [a], Ferenc Ötvös [a, *]

[a] Institute of Biochemistry, Biological Research Center, Temesvári krt. 62, H-6726, Szeged, Hungary
[b] Doctoral School of Theoretical Medicine, Faculty of Medicine, University of Szeged, Dóm tér 10, H-6720, Szeged, Hungary
[c] ABX Advanced Biochemical Compounds, Biomedizinische Forschungsreagenzien GmbH, Heinrich-Glaeser-Strasse 10-14, D-01454, Radeberg, Germany
[d] Royal Institute of Technology (KTH), School of Engineering Sciences in Chemistry, Biotechnology and Health, Department of Chemistry, Organic Chemistry, S-100 44, Stockholm, Sweden
[e] Institute of Pharmaceutical Chemistry, Semmelweis Medical University, Hőgyes Endre utca 9, H-1092, Budapest, Hungary
[f] Department of Physiology, Faculty of Medicine, University of Szeged, Dóm tér 10, H-6720, Szeged, Hungary
[g] Department of Neurology, Faculty of Medicine, University of Szeged, Semmelweis u 6, H-6725, Szeged, Hungary
[h] Department of Traumatology, Faculty of Medicine, University of Szeged, Semmelweis u 6, H-6725, Szeged, Hungary
[i] Research Centre for Natural Sciences, MS Metabolomics Research Laboratory, H-1117, Budapest, Magyar tudósok krt. 2, Hungary

ARTICLE INFO

Article history:
Received 12 November 2019
Received in revised form
22 January 2020
Accepted 12 February 2020
Available online 15 February 2020

This study is dedicated to the memory of our wonderful colleague, the late professor Mária Wollemann, MD, PhD, DSc (1923-2019) at the Institute of Biochemistry, Biological Research Centre of the Hungarian Academy of Science, Szeged, Hungary.

Keywords:
G-protein
Efficacy
Binding
Mu-opioid
Osteoarthritis inflammation model
Interaction fingerprint
6,14-Ethenomorphinan derivatives

ABSTRACT

Morphine and its derivatives play inevitably important role in the μ-opioid receptor (MOR) targeted antinociception. A structure-activity relationship study is presented for novel and known orvinol and thevinol derivatives with varying 3-*O*, 6-*O*, 17-*N* and 20-alkyl substitutions starting from agonists, antagonists and partial agonists. In vitro competition binding experiments with [^{3}H]DAMGO showed low subnanomolar affinity to MOR. Generally, 6-*O*-demethylation increased the affinity toward MOR and decreased the efficacy changing the pharmacological profile in some cases. *In vivo* tests in osteoarthritis inflammation model showed significant antiallodynic effects of thevinol derivatives while orvinol derivatives did not. The pharmacological character was modelled by computational docking to both active and inactive state models of MOR. Docking energy difference for the two states separates agonists and antagonists well while partial agonists overlapped with them. An interaction pattern of the ligands, involving the interacting receptor atoms, showed more efficient separation of the pharmacological profiles. In rats, thevinol derivatives showed antiallodynic effect *in vivo*. The orvinol derivatives, except for 6-O-desmethyl-dihydroetorfin (**2c**), did not show antiallodynic effect.

1. Introduction

Pain modulation is mainly regulated through the activation of the three classical types of opioid receptors, *i.e.* the μ-, δ- and κ-opioid receptors (MOR, DOR and KOR, respectively) expressed in the neurons of the central and peripheral nervous system. The opioid receptors are members of the G-protein coupled receptors

* Corresponding author. Institute of Biochemistry, Biological Research Center, Hungarian Academy of Sciences, Szeged, Hungary.
E-mail address: otvos@brc.hu (F. Ötvös).
[1] Edina Szűcs and János Marton contributed equally to this work.

https://doi.org/10.1016/j.ejmech.2020.112145
0223-5234/

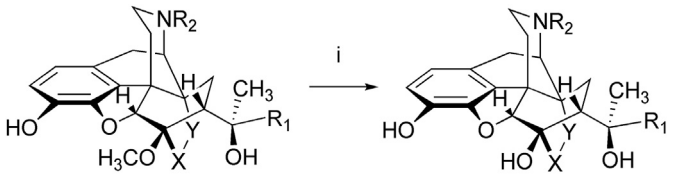

a: R_1 = CH_3, R_2 = CPM, X-Y = CH_2CH_2
b: R_1 = *tert*-Bu, R_2 = CPM, X-Y = CH_2CH_2
c: R_1 = *n*-Pr, R_2 = CH_3, X-Y = CH_2CH_2
d: R_1 = CH_2CH_2Ph, R_2 = CH_3, X-Y = CH=CH
e: R_1 = CH_3, R_2 = CH_3, X-Y = CH=CH
f: R_1 = CH_3, R_2 = CH_3, X-Y = CH_2CH_2

Scheme 1. Synthesis of 6-*O*-desmethyl-orvinol analogues
Figure legend: **Reagents and conditions:** (i): $LiAlH_4$, CCl_4, THF, reflux.

(GPCRs), the largest receptor family in the human genome, sharing the distinctive seven helical hydrophobic transmembrane helix domain [1–5]. Their activation leads to the inhibition of adenylyl cyclase which results in hyperpolarisation and inhibits neurotransmitter release [6,7]. The main target of the antinociceptive drugs in the treatment of pain is MOR.

Endogenous opioid peptides such as Met- and Leu-enkephalin [8], β-endorphin [9] and dynorphin-A [10] are produced in the brain. Two endomorphin tetrapeptides, endomorphin-1 and endomorphin-2 [11] were found to be highly selective endogenous agonists for MOR. Morphine is a prototype opioid agonist binding to MOR and is still the most frequently used drug in pain medication. Beside pain relief and analgesia, it has serious side effects including decreased respiratory effort, low blood pressure and it also has a high potential for addiction and abuse [12–14]. Therefore, it is very important to find new ligands with higher affinity, selectivity and stability to get more effective drugs to decrease the side effects.

Natural morphine alkaloids (*e.g.* morphine, codeine, thebaine, neopine, oripavine) [15] can be converted into a variety of pharmacologically more advantageous compounds, such as the so called nal-compounds (naloxone, naltrexone, nalbuphine) and the ring-C bridged derivatives (6,14-ethenomorphinans or Bentley-compounds, *e.g.* etorphine (**9**), buprenorphine, diprenorphine). In this study nine previously synthesized orvinol and thevinol-type MOR-selective ligands [16–25] were examined (compounds **1e**, **1f**, **2a**, **2b**, **2d**, **4**, **5**, **7**, **8** (3-methoxyetorphine)). 6-*O*-Desmethyl-dihydroethorphine (**2c**) is a new compound synthesized for this study.

A number of structure-activity relationship studies dealing with thevinol and orvinol derivates are available [26,27], but the biochemical and pharmacological properties of our target compounds have not been reported except for **8** [25], The aim of present study was to compare the receptor binding properties and the MOR, DOR and KOR selectivity of some Bentley compounds in rat and guinea pig brain membrane preparations. The ligands were also investigated in [^{35}S]GTPγS functional binding assays to examine G-protein activation *via* opioid receptors. The effect of the investigated derivates was observed *in vivo* nociceptive tests.

The presence or absence of specific functional groups in the orvinol and thevinol derivatives can not be straightforwardly related to their pharmacological profiles. As an example, the 17-*N*-substituent serves as an acknowledged pharmacological switch between agonists and antagonists being methyl or cyclopropylmethyl, respectively. However, it is highly ambiguous within this class of opioids, regarding that 17-*N*-cyclopropylmethyl derivative can be full agonist as well [28,29] which may be a consequence of the bigger size of these opiates resulting in a more complex interaction pattern with the receptor. According to this, it

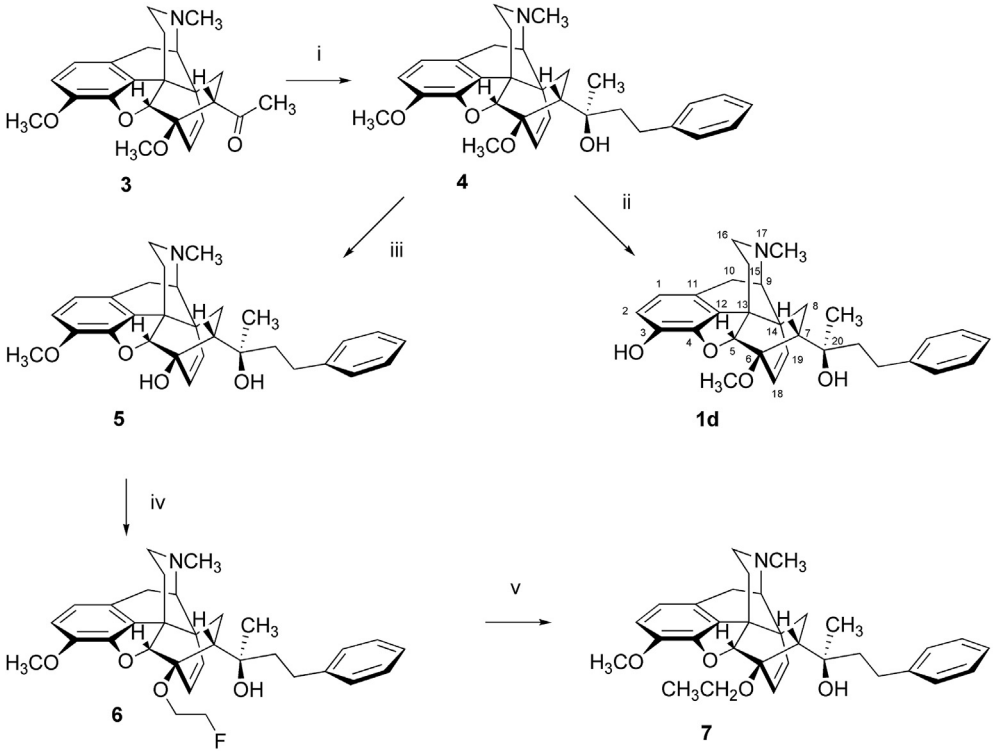

Scheme 2. Synthesis of phenethyl-thevinol- and -orvinol derivatives
Figure legend: **Reagents and conditions**: (i): 2-phenylethymagnesium bromide, toluene-THF, 2 h; (ii): KOH diethyleneglycol, 210 °C or L-Selectride, THF, reflux, 5 h; (iii): $LiAlH_4$, CCl_4, THF; reflux; (iv): $BrCH_2CH_2F$, NaH, DMF, RT, 48 h; (v): L-Selectride, THF, reflux, 3 h.

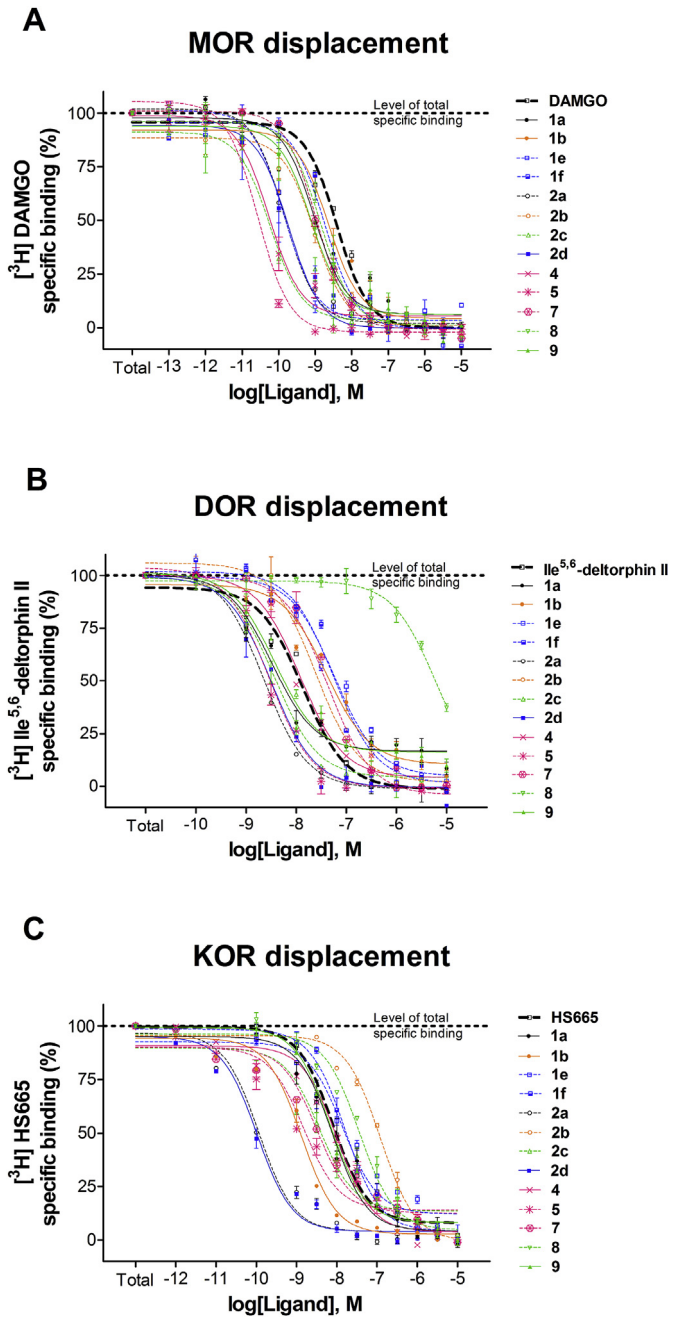

Fig. 1. MOR (A), DOR (B) and KOR (C) binding affinity of the morphine analogues
Figure legend: MOR (A), DOR (B) and KOR (C) binding affinity of morphine analogues compared to DAMGO, Ile^{5,6}-deltorphin II and HS665, respectively in [^{3}H]DAMGO, [^{3}H] Ile^{5,6}-deltorphin II and [^{3}H]HS665 competition binding assays in rat (MOR, DOR) and guinea pig (KOR) brain membrane homogenates. Membranes were incubated with 2 nM [^{3}H]DAMGO or [^{3}H]Ile^{5,6}-deltorphin II for 45 min at 35 °C with increasing concentrations (10^{-13} - 10^{-5} M; 10^{-10} - 10^{-5} M, respectively) or 2 nM [^{3}H]HS665 for 30 min at 25 °C (10^{-12} - 10^{-5} M) of each competing ligand. Values represent mean values ± S.E.M. for at least three independent experiments performed in duplicate.

seems plausible to investigate the interacting residues or atoms of the receptor leading to the specific response, *i.e.* pharmacological feature.

Former computational studies attempted to identify the interacting residues in MOR responsible for different pharmacological actions. However, no distinguishable interaction pattern was found for a structurally highly diverse set of agonist, partial agonist and antagonist to predict pharmacological activities using the inactive receptor state [30].

2. Results and discussion

2.1. Chemistry

In this study we report the biochemical characterization of 6-*O*-desmethyl-orvinols and 20*R*-phenethyl-orvinols/thevinols having (unanticipated) extremely high potency at MOR. The target compounds are semisythetic thebaine derivatives and belong to the 6,14-ethenomorphinans (Bentley-compounds). The pharmacologicaly most important members of this opioid ligand class are diprenorpine (**1a**), buprenorphine (**1b**), dihydroethorphine (**1c**), and phenethyl-orvinol (**1d**). Compound **1a** is an antagonist with approximatelly the same high affinity for opioid receptor subtypes. Compound **1b** with a mixed agonist-antagonist (partial μ-agonist/κ-antagonist) profile is clinicaly used as analgesic in the treatment of postoperative and/or cancer-related pain and in the substitution therapy of opioid dependent humans. **1c** and **1d** are nonselective opioid receptor agonists.

For our pharmacological investigations, the target compounds, 18,19-dihydro-6,14-ethenomorphinans (6,14-endoethano-6,7,8,14-tetrahydrooripavines, Scheme 1), 20*R*-phenethyl-orvinol and -thevinol derivatives (Scheme 2) were synthesized from thebaine. These compounds can be synthesized by the original method of Bentley [21,22] or by later developed modification [31,32] of the initial procedure starting from thebaine.

20-Methyl-orvinol (**1e**) [22] and 20-methyl-dihydroorvinol (**1f**) were prepared as reference substances for our biological investigations. **1e** was synthesized from thebaine in a three-step procedure. The Diels-Alder adduct of thebaine and methyl-vinyl ketone, thevinone, was reacted with methylmagnesium iodide to give 20-methyl-thevinol. The latter was 3-*O*-demethylated with KOH in diethylene glycol at 210 °C to yield **1e**. **1f** was prepared from dihydrothevinone in a similar manner [24].

The synthesis of 18,19-dihydro-6-*O*-desmethyl-6,14-ethenomorphinan derivatives (**2a-d**) are depicted in Scheme 1. 6-*O*-desmethyl-diprenorphine (**2a**) was synthesized in an eight-step procedure from thebaine as described earlier [16]. 6-*O*-desmethyl-buprenorphine (**2b**) was prepared analogously in an eight-step synthesis [17]. The new etorphine derivative, 6-*O*-desmethyl-dihydroetorphine (**2c**) was prepared in five steps. In brief, the Grignard reaction of dihydrothevinone with *n*-propylmagnesium bromide resulted in the main product 20*R*-dihydroetorphine-3-*O*-methylether. Following 3-*O*-demethylation and 6-*O*-demethylation **2c** was prepared in a 18% overall yield fom thebaine. Complete assignments of ^{1}H and ^{13}C NMR spectra of the prepared compounds are given in the Supplementary Information.

Introducing a phenyl group in the position-20 (20*R*-phenyl-orvinols [nepenthone derivatives] and 20*S*-phenyl-orvinols [thevinone derivatives]) can be advantageous [33,34] while a 20-β-phenethyl group results in products with extremely high affinity to opioid receptors [35]. Phenethyl-thevinol (**4**) and **1d** have been playing an important role in the 1970s in the development of new opioid receptor model [35,36]. The synthesis of phenethyl-thevinol- and phenethyl-orvinol derivatives are demonstrated in Scheme 2. Grignard addition of 2-phenetylmagnesium bromide to thevinone (**3**) resulted in 20*R*-phenethyl-thevinol (**4**) [22], which was converted either by 3-*O*-demethylation to 20*R*-phenethyl-orvinol (**1d**) or by 6-*O*-demethylation to 6-*O*-desmethyl-phenethyl-thevinol (**5**). 6-*O*-Demethylation of **1d** gave 6-*O*-desmethyl-phenethyl-orvinol (**2d**). Alkylation of **5** with 2-fluoroethyl bromide in *N*,*N*-dimethylformamide in the presence of sodium hydride yielded 6-(2-fluoroethyl)-phenethyl-thevinol (**6**), which was reacted with L-Selectride in THF.

Table 1
Displacement of [^{3}H]DAMGO, [^{3}H]Ile^{5,6}-deltorphin II and [^{3}H]HS665 by DAMGO, Ile^{5,6}-deltorphin II, HS665 and morphine derivatives in membranes of rat and guinea pig brain. The IC_{50} values for the MOR, DOR and KOR according to the competition binding curves (see Fig. 1) were converted into equilibrium inhibitory constant (K_i) values, using the Cheng–Prusoff equation.

Ligand	DAMGO[a]	Ile^{5,6}-deltorphin II[a]	HS665[b]	Selectivity for μ site	
	K_i ± S.E.M. (nM)			(Ki_δ/Ki_μ)	(Ki_κ/Ki_μ)
DAMGO	0.9010 ± 0.27	n.d.[c]	n.d.[c]	n.d.[c]	n.d.[c]
Ile^{5,6}-deltorphin II	n.d.[c]	8.848 ± 0.77	n.d.[c]	n.d.[c]	n.d.[c]
HS665	n.d.[c]	n.d.[c]	1.707 ± 0.02	n.d.[c]	n.d.[c]
1a	0.2142 ± 0.30	2.11 ± 0.77	1.589 ± 0.02	9.85	7.42
1b	0.5315 ± 0.31	26.12 ± 0.77	0.280 ± 0.01	49.14	0.53
1e	0.0325 ± 0.35	37.37 ± 0.75	2.992 ± 0.03	1149.78	92.06
1f	0.4352 ± 0.28	36.56 ± 0.78	3.411 ± 0.01	84.54	7.84
2a	0.0333 ± 0.26	1.49 ± 0.71	0.024 ± 0.02	44.62	0.72
2b	0.2184 ± 0.27	15.72 ± 0.71	0.257 ± 0.01	71.96	1.18
2c	0.0136 ± 0.29	2.41 ± 0.80	0.796 ± 0.03	177.35	56.53
2d	0.0435 ± 0.29	2.06 ± 0.76	0.022 ± 0.02	47.45	0.51
4	0.0125 ± 0.30	7.73 ± 0.77	2.186 ± 0.02	618.30	174.88
5	0.0063 ± 0.27	1.85 ± 0.75	0.321 ± 0.03	294.43	50.95
7	0.2524 ± 0.25	27.53 ± 0.75	0.682 ± 0.02	109.06	2.70
8	0.3260 ± 0.30	3906.3 ± 0.84	7.636 ± 0.01	11982.52	23.42
9	0.1771 ± 0.30	2.44 ± 0.81	1.443 ± 0.01	13.78	8.15

[a] Rat brain membrane.
[b] Guinea pig brain membrane.
[c] Not determined.

Unexpectedly, 6-*O*-ethyl-6-*O*-desmethyl-phenethyl thevinol (**7**) was isolated from the product mixture as solely product in 90% as result of reductive defluorination.

In the present study we performed a selective 6-*O*-demethylation of several compounds in order to study the structure-activity relationships. Binding affinities of 6-*O*-desmethyl-orvinols to opioid receptors were not yet investigated and their pharmacological/biochemical characterisation is currently not available in the scientific literature. In contrast to 3-*O*-demethylation the 6-*O*-demethylation of Bentley compounds is less explored. 6,14-Ethenomorphinans with a free tertiary hydroxyl group in position-6 were inaccessible before 1986. The first selective 6-*O*-demethylation of 7α-aminomethyl- and 7α-aldoxime-type 6,14-ethenomorphinan derivatives was reported by Kopcho & Schaeffer [37]. Lithium aluminium hydride in tetrahydrofuran containing a halogenated co-solvent (CCl_4) was utilized as demethylating system. A six membered ring aluminum complex was hypothesized to play an important role in this unusual *O*-dealkylation. Subsequently, Lever et al. [16,17] extended this special 6-*O*-demethylation method for other 6,14-ethenomorphinans with

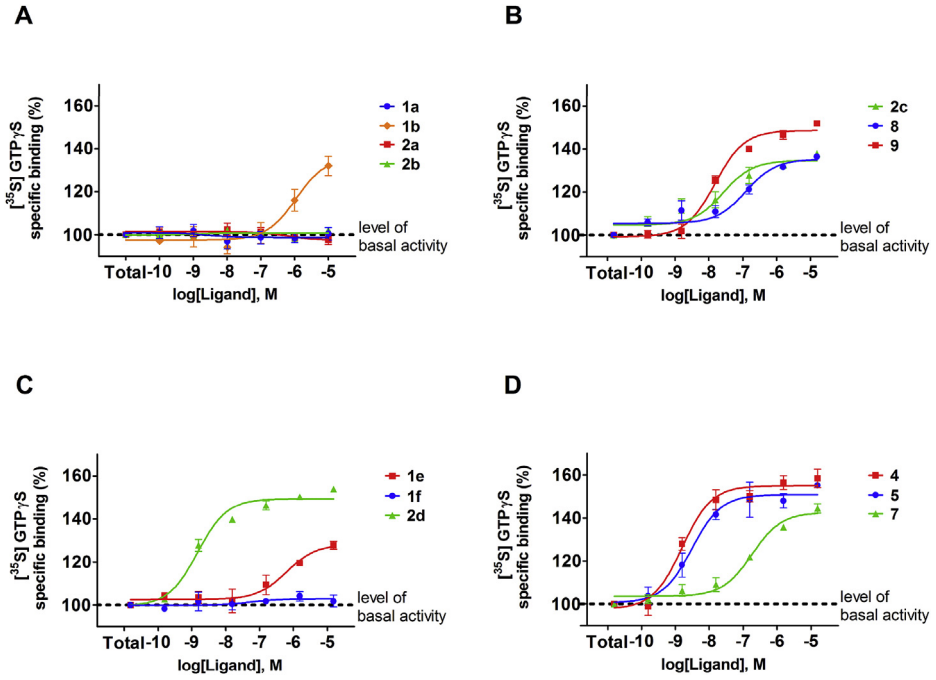

Fig. 2. The effect of morphine analogues on G-protein activity compared to the parent ligands in [^{35}S]GTPγS binding assays in rat brain membrane homogenates.
Figure legend: "Total" on the x-axis indicates the basal activity of the monitored G-protein, which is measured in the absence of the ligands and also represents the total specific binding of [^{35}S]GTPγS. The level of basal activity was defined as 100% and it is presented with a dotted line. Points represent means ± S.E.M. for at least three experiments performed in triplicate.

Table 2
The maximal G-protein efficacy (E_{max}) of the morphine analogues in [^{35}S]GTPγS binding assays in rat brain membrane homogenates. The values were calculated according to dose-response binding curves in Fig. 2.

Ligand	Potency log EC_{50} + S.E.M. (M)	Efficacy E_{max} ± S.E.M. (%)
1a	n.d.[a]	98.65 ± 1.40
1b	−5.96 ± 0.22	135.98 ± 5.03
1e	−6.39 ± 0.26	128.31 ± 3.18
1f	n.d.[a]	102.87 ± 1.59
2a	n.d.[a]	101.31 ± 0.98
2b	n.d.[a]	100.81 ± 0.73
2c	−7.77 ± 0.21	134.71 ± 2.05
2d	−9.02 ± 0.11	149.46 ± 1.28
4	−8.99 ± 0.14	155.09 ± 1.83
5	−8.71 ± 0.15	150.95 ± 2.10
7	−6.94 ± 0.12	142.64 ± 2.00
8	−7.09 ± 0.17	135.32 ± 2.07
9	−8.01 ± 0.09	148.61 ± 1.41

[a] Not determined.

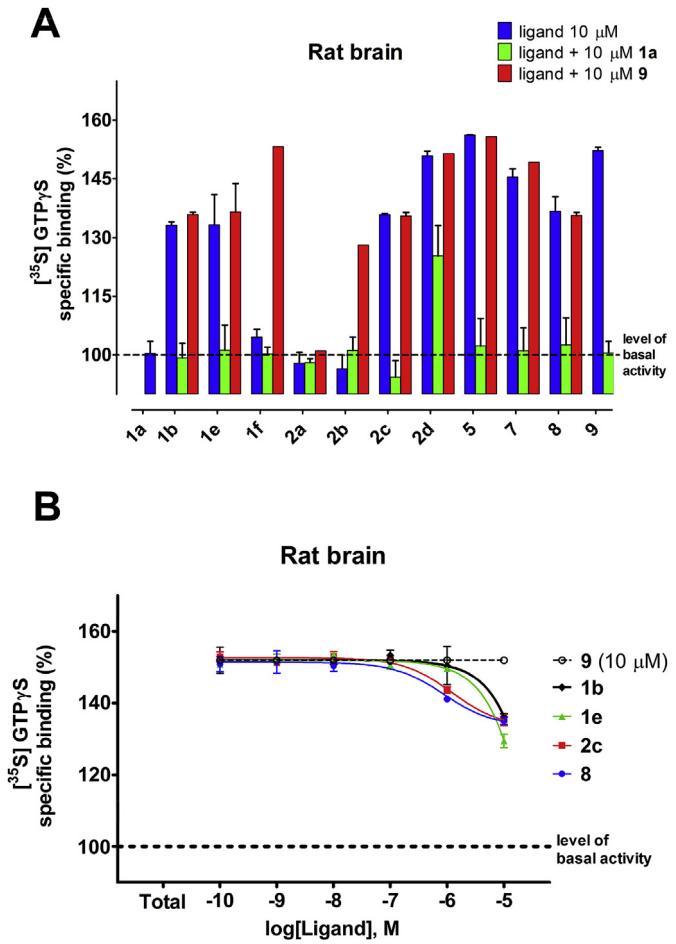

Fig. 3. Stimulation of G-protein activation in rat brain membrane homogenates. Figure legend: blue, 10 μM morphine analogues alone; green, 10 μM morphine analogues and equimolar antagonist **1a**; red, 10 μM morphine analogues and equimolar full agonist **9** (A). The decrease of the effect of **9** by partial agonists in [^{35}S]GTPγS binding assays (B). . (For interpretation of the references to colour in this figure legend, the reader is referred to the Web version of this article.)

tert-alcohol functions in the position-20. Another method for the 6-*O*-demethylation of 6,14-ethenomorphinans has been developed by Breeden et al. [38], in 1999.

2.2. In vitro studies

2.2.1. Competition binding assay

Opioid receptor binding affinities of the analogues were examined in [^{3}H]DAMGO, [^{3}H]Ile^{5,6}-deltorphin II and [^{3}H]HS665 homologous displacement experiments for MOR, DOR and KOR, respectively, in rat and guinea pig brain homogenates. All derivatives exhibited higher binding affinity in μ-opioid receptor system than the selective peptide ligand DAMGO (Fig. 1A), some of them had extremely low K_i values (Table 1). For DOR the ligands showed comparable binding affinities than the selective DOR agonist Ile^{5,6}-deltorphin II peptide ligand (Fig. 1B) except **8** (K_i > 3000 nM). In the KOR binding assays, performed in guinea pig brain membranes, the analogues still displayed nanomolar affinities (Fig. 1C).

2.2.2. Functional GTPγS binding stimulation assay

The effect of the ligands on receptor-mediated G-protein activation was investigated in [^{35}S]GTPγS binding assays in rat brain membranes (Fig. 2). The highest stimulations were observed with **2d**, **4**, **5**, **7** and **9**, therefore they can be considered as full agonists. **1a**, **1f**, **2a** and **2b** did not produced dose-dependent increases, so they behave as neutral or pure antagonists (Table 2). The remaining compounds (**1b**, **1e**, **2c** and **8**) exhibiting intermediate levels of G-protein activation are partial agonist ligands in this *in vitro* system.

The pure opioid antagonist **1a** successfully reversed the efficacy of almost all compounds to basal activity with the exception of **2d** which showed some remaining activation in the presence of equimolar **1a**. Maximal stimulation produced by the ligands was mostly not elevated further when the full agonist **9** was co-administered (Fig. 3A). However, in the case of **1f** and **2b** the co-presence of **9** was able to effectively stimulate G-protein activation (Table 3).

Increasing concentrations of the partial agonists were also investigated in the presence of 10 μM **9** producing maximal stimulation (Fig. 3B). All four compounds were able to inhibit the activation mediated by **9**, although with relatively low efficacy and potency. This weak antagonizing effect in the presence of a full agonist validates that **1b**, **1e**, **2c** and **8** are indeed partial agonist ligands for opioid receptors (Table 3).

2.3. In vivo studies

The basal withdrawal threshold of the non-inflamed side was 45 ± 0.5 g, and MIA caused significant decrease in paw withdrawal threshold on the injected side (24 ± 0.6 g). Only the largest dose of **9** treatments caused significant enhancement in the pain threshold on the non-inflamed side, therefore, results were analysed only on the inflamed paws. The different ligands showed different potencies, therefore, they were compared to distilled water (as negative control) in the ANOVA analysis, but the curve for **9** was also demonstrated as a positive control group with the lowest ED_{30} value (Table 4).

All of the thevinol derivatives showed significant antiallodynic effects (Fig. 4); however, the regression analysis revealed a lower *in vivo* potency compared to **9** as indicated by the ED_{30} values, even it could not be calculated for **7** (Table 4). Regarding **4**, the treatment was close to significant (Table 4). Time and their interaction showed significant effects, and the post-hoc analysis showed decreased allodynia in several time-points compared to the control group (Fig. 4A). ANOVA for repeated measurements showed

Table 3
The maximal G-protein efficacy (E_{max}) the morphine analogues in the absence or presence of the opioid antagonist and agonist, **1a** and **9**, respectively in rat brain membrane homogenates. The values were calculated according to dose-response binding curves in Fig. 3.

Ligand	Efficacy E_{max} ± S.E.M. (%)			
	10 μM ligand	10 μM ligand +10 μM of 1a	10 μM ligand +10 μM of 9	Ligand (10^{-10}-10^{-5} M) +10 μM of 9
1a	100.45 ± 3.05	–	–	–
1b	135.17 ± 0.82	99.30 ± 3.70	135.93 ± 0.58	136.20 ± 1.20
1e	133.27 ± 7.67	101.25 ± 6.45	129.45 ± 1.85	129.45 ± 0.61
1f	104.63 ± 2.00	100.25 ± 1.75	135.20 ± 0.00	–
2a	97.90 ± 2.75	98.10 ± 0.90	101.00 ± 0.00	–
2b	96.50 ± 3.47	101.20 ± 3.40	128.10 ± 0.00	–
2c	135.90 ± 0.30	94.40 ± 4.20	135.50 ± 0.95	136.80 ± 0.58
2d	150.80 ± 1.20	125.30 ± 7.80	151.40 ± 0.00	–
4	158.75 ± 5.15	99.30 ± 2.10	153.20 ± 0.00	–
5	156.20 ± 0.10	102.40 ± 6.90	155.80 ± 0.00	–
7	145.45 ± 2.05	101.05 ± 5.95	149.20 ± 0.00	–
8	136.77 ± 3.67	102.60 ± 6.90	135.63 ± 0.79	135.10 ± 0.87
9	152.15 ± 0.85	100.50 ± 3.00	–	–

significant effects of **5** treatment, time and their interaction. The *post hoc* comparison revealed that only the highest doses caused significant antiallodynic effect with similar efficacy as **9** (Fig. 4B). Similarly, **7** treatment also showed significant effects, and the *post hoc* comparison revealed significant increase in pain threshold at several time points after the highest dose compared to the control group (Fig. 4C).

Regarding **2a** and **2b** treatments, there were no significant effects and ED_{30} values could not be calculated (Fig. 5A and B, Table 4). However, **2c** administration resulted in significant effects of treatment, time, and their interaction, with a relatively low ED_{30} value (Table 4). The *post hoc* comparison revealed that the largest dose of **2c** caused similar degree of antiallodynic effect as did **9**; even more prolonged effect was observed (Fig. 5C). **1e, 1f** and **2d** did not produce significant antinociceptive effects (Fig. 5D, E, F), and ED_{30} values could not be calculated either.

2.4. In silico studies

2.4.1. Docking

Almost all of the investigated compounds showed higher binding affinity to MOR and thus they are expected to exert G-protein activation through MOR. According to this, their pharmacological behaviour was modelled on the MOR crystal structures. The target compounds are members of three pharmacological types showing agonism, antagonism or partial agonism at MOR. Thus the target compounds and several known agonists, antagonists and partial agonists, composing a set of 48 compounds (Tables S3–1, Tables S3–2) [25,26,28,29,39], were docked to both the active and inactive receptor models to reveal whether their characteristics in docking experiments can be related to that of ligands with known pharmacological character. However, a simple visual inspection of the docked positions did not reveal specific features to explain the pharmacological diversity neither at the active nor at the inactive receptor state, therefore, the ligands were further characterized with their docking energies and the contacting receptor atoms. It is noteworthy that among the lowest energy docking poses only 16 out of 96 (48 ligands docked to both receptor states) originated from energy minimized conformers (see Experimental section 4.4.3.) suggesting the role of the flexibility of aliphatic rings.

2.4.2. Analysis of the docking energies and ligand efficiencies obtained for the active and inactive receptor states

Three kinds of docking energy measures were investigated: docking energies calculated by AutoDock Vina (E), ligand efficiency (docking energy divided by the number of non-hydrogen atoms of the ligand, LE) [40] and a similar value obtained from the docking energy divided by the count of the interacting atoms of the ligand

Table 4
The applied drugs and the cumulative dose procedure, the number of the animals and ANOVA results in each group and their *in vivo* potency as ED_{30} with confidence interval (CI).

Drug	Doses (nmol/kg)						ED_{30} (CI) nmol/kg	ANOVA		
	0.1	0.3	1.0	3.0	10.0	N		Group	Time	Interaction
Distilled water						6				
1e			+	+	+	7		NS	NS	NS
1f			+	+	+	8		NS	NS	NS
2a			+	+	+	8		NS	NS	NS
2b			+	+	+	7		NS	NS	NS
2c[a]		+	+	+		6	4.5 (2.59–6.11)	NS	10,100 = 2.11 p < 0.05	NS
2c[b]			+	+	+	6		1,100 = 15.48 p < 0.005	10,100 = 2.96 p < 0.005	10,100 = 3.42 p < 0.001
2d			+	+	+	8		NS	NS	NS
4			+	+	+	7	8.0 (5.16–10.88)	1,110 = 4.50 p = 0.06	10,110 = 2.21 p < 0.05	10,110 = 2.85 p < 0.005
5[a]		+	+	+		6	7.2 (5.11–9.35)	NS	NS	NS
5[b]			+	+	+	7		1,110 = 5.02 p < 0.05	10,110 = 2.61 p < 0.01	10,110 = 3.30 p < 0.001
7			+	+	+	8	uncountable	1,120 = 5.32 p < 0.05	NS	NS
9	+	+	+			6	0.1 (0.01–0.49)	1,100 = 20.80 p < 0.005	10,100 = 3.03 p < 0.005	10,100 = 2.05 p < 0.05

[a] Dose: 0.3-1-3 nmol/kg.
[b] Dose: 1-3-10 nmol/kg.

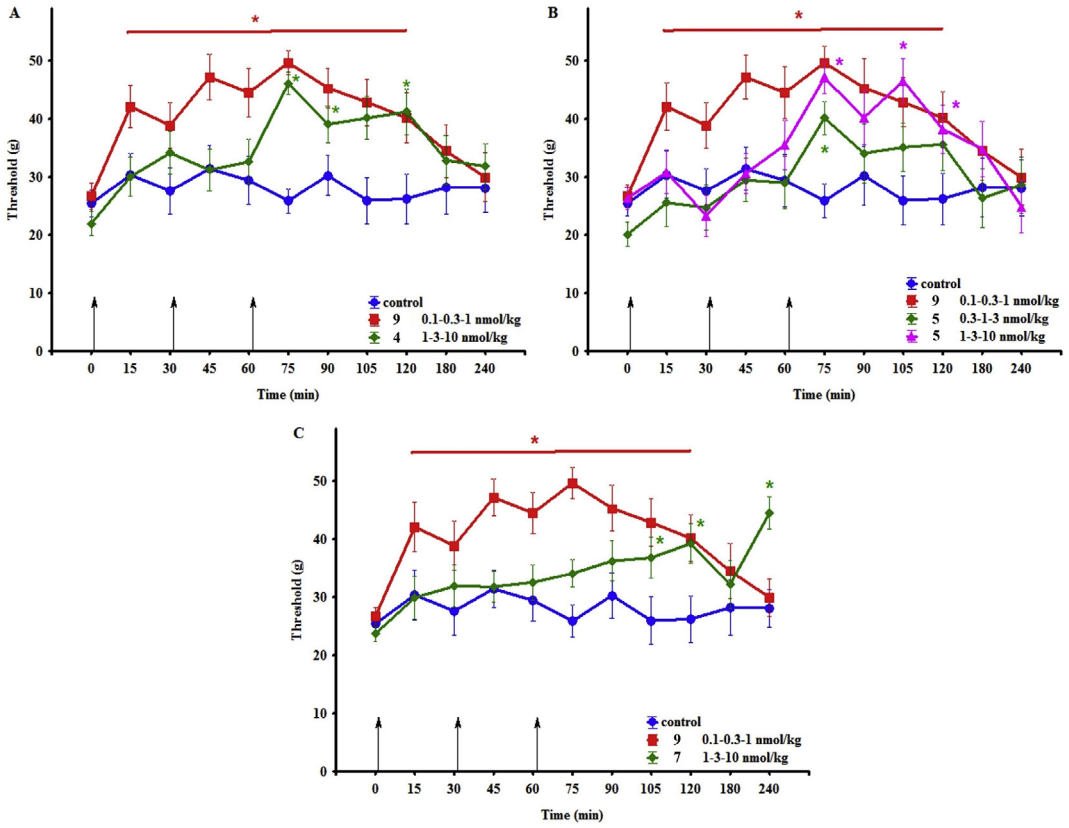

Fig. 4. The effects of thevinol derivates in behavioral nociceptive test. Arrows indicate the time points of cumulative drug administrations. * signs $p < 0.05$ from control group.

(LEIAC). The effect of the receptor state on the docking energy measures was analysed by two-sided paired t-tests (Table 5.). According to this, agonists and partial agonists clearly differentiate between the receptor states by docking energies and LE while antagonists do not. In case of LEIAC agonists could not distinguish the receptor states. The energetic preference of the different ligand types for the receptor states, *i.e.* the difference between the docking energies obtained for the active and inactive states, was also investigated (Table S4). The energy difference would be negative for agonists showing their physically feasible preference for the active receptor and it should be the opposite (positive) for antagonists. Although this expectation was only partially fulfilled within the series of compounds investigated here, agonists were well separated from antagonists and partial agonists by two-sided unpaired t-tests using docking energy and LE values (Table 6.). Antagonists and partial agonists did not differ significantly. This is an interesting result however, because the geometric differencies between the receptor states do not seem significant (Table S5, Fig. S23), nevertheless the ligands distinguished them by binding energy.

2.4.3. *Multivariate statistical analysis of docking energy values*

Because both the receptor preference of the ligand types (Table 5.) and the difference between the types (Table 6.) were partially fulfilled, principal component analysis (PCA) was performed with five principal components to reveal the relationships between docking energy values and pharmacological features. Input data were the docking energies (E), LE and LEIAC values and their differences for the two receptor (Table S4). Additionally, the energy contributions decomposed for the specific interacting atom pair types, calculated by BINANA, were also involved. The different energy measures, however, did not contribute equally well in PCA to separate the experimentally determined pharmacological types. The efficiency of clustering was assessed by considering hierarchical clustering, J_2 statistics [41] and pairwise cluster overlap statistics using the program package "pca-utils" [42] for the five PCA components. Hierarchical clustering statistics and pairwise cluster overlap probabilities conformed each other showing that the separation of agonists from antagonists and partial agonists performed well while distinguishing antagonists from partial agonists highly depended on the energy measures used in PCA (Table 7. J_2 statistics). J_2 measures the fuzziness of the clusters, less J_2 means more compact cluster. It is interesting that using the decomposed energy contributions (ES) resulted in more efficient cluster separation but less compact clusters (Table 7. J_2 statistics, cluster overlapping statistics). Considering all three quality matrix, the best classification was obtained by the use of the docking energies and their active-inactive receptor differences (Ea, Ei, Ea-Ei, LEa-LEi, LEIACa-LEIACi). Results for the first two PCA dimensions and the distance matrix for five PCA variables are shown in (Fig. 6). The results show that the ligands can be classified to their known pharmacological groups using docking energies and related measures, albeit with significant overlap (Fig. 6A). However, a closer look on 3D representation of the first three PCA dimensions (Fig. 7) revealed better separation of the ligand types. There is a little overlap between agonists and antagonists while partial agonists overlap with both. According to PCA results **2c**, a newly synthesized partial agonist, is among antagonists and close to established partial agonists (BU08028 (**11**), BU61 (**14**)). However, **1f**, despite being antagonist experimentally, showed up among agonists in all kinds of PCA calculations. Furthermore, compound **30**, considered to be a full agonist despite its *N*-cyclopropylmethyl substituent [29], was among antagonists in this model. It is worth to note that the use of

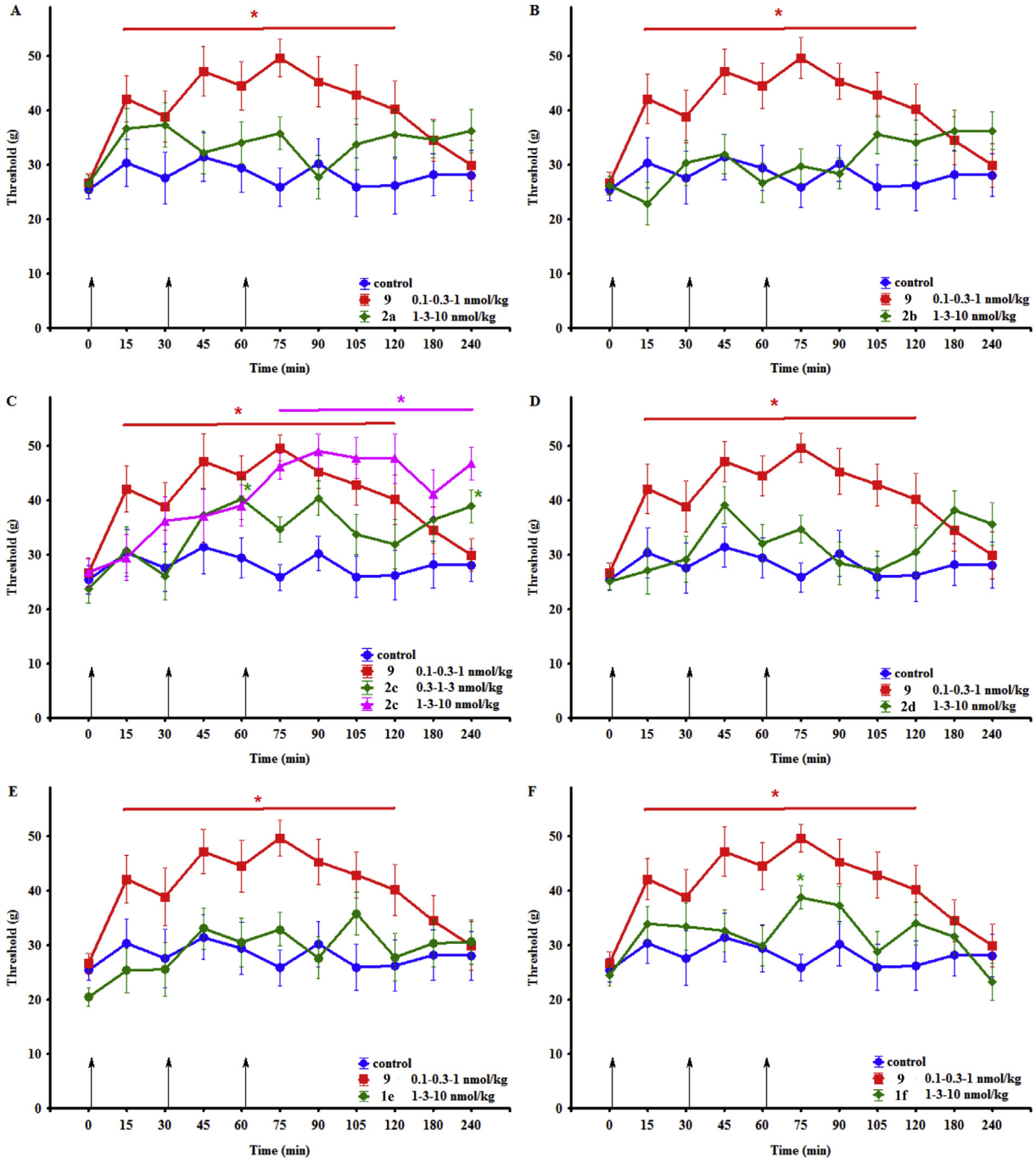

Fig. 5. The effects of orvinol derivates in behavioral nociceptive test. Arrows indicate the time points of cumulative drug administrations. * signs $p < 0.05$ from control group.

Table 5
Paired *t*-test/Welch-test of docking energies for active and inactive receptors.

Ligand type	F-test	*t*-test
Agonists	0.632	7.89×10^{-12}
Antagonists	0.545	0.227
Partial agonists	0.192	0.008

energy differences alone gave almost the same classification efficiency.

Table 6
Comparison of docking energy differences between ligand types.

Ligand types	F-test	*t*-test
agonist - antagonist	0.020	2.00×10^{-5}*
agonist - partial agonist	0.023	2.98×10^{-4}*
partial agonist - antagonist	0.845	0.371

2.4.4. Characterization of the ligands by the interacting receptor atoms

Because the ligands exert their effects through interactions with the receptor, the details of these interactions (interaction pattern)

Table 7
Assessment of ligand type classification by PCA.

VARIABLES	Dendogram statistics		J_2 statistics			Overlap probabilities		
	AG vs. (PAG, ANTAG)	PAG vs. ANTAG	AG	PAG	ANTAG	AG − PAG	AG − ANTAG	PAG − ANTAG
Ediffs*	1.20E-03	0.72	2.02	7.44	6.45	2.81E-03	3.13E-04	7.24E-01
E,LE*	9.30E-04	0.53	42.77	32.37	1.28	6.24E-04	1.03E-03	5.32E-01
E,LE,LEIAC*	5.10E-03	0.54	2.11	21.44	2.10	6.87E-03	2.61E-03	5.38E-01
E,ES*	0.01	0.02	0.87	915.79	8.79	8.55E-03	1.44E-02	2.33E-02
E,LE,ES*	9.50E-03	0.04	0.82	900.51	9.44	7.68E-03	9.14E-03	3.80E-02
E,Ediffs	7.90E-03	0.81	6.75	5.46	22.13	1.45E-02	2.85E-03	8.08E-01
E,LEIAC*	3.50E-03	0.9	2.67	4.42	2.06	7.97E-03	9.28E-04	9.01E-01
E,LE,LEIAC, Ediffs*	5.30E-03	0.54	2.13	21.68	2.15	7.29E-03	2.63E-03	5.38E-01
E,LE,LEIAC, Ediffs,ES*	1.00E-03	0.06	1.23	899.80	9.45	3.70E-03	1.54E-04	6.14E-02
atomname,sd,a,i**	1.00E-04	0.01	8.16	171.02	5.75	1.91E-04	3.07E-05	1.32E-02
atomname,sd,a**	1.90E-04	8.30E-03	6.52	508.23	1.88	4.04E-04	5.06E-05	8.28E-03
atomname,sd,i**	1.50E-04	0.05	2.19	20.43	70.44	8.78E-04	1.37E-05	4.65E-02
atomname**	2.20E-05	0.02	58.60	2805.44	1.24	1.55E-04	1.64E-06	1.53E-02
residue,sd**	4.80E-03	0.1	37.01	633.30	0.72	3.19E-03	5.48E-03	9.90E-02

AG: agonist, PAG: partial agonist, ANTAG: antagonist, *: PCA, **: MCA, a: active receptor state, i: inactive receptor state, sd: stabilizing/destabilizing interaction types involved, atom: atom based interaction pattern, residue: residue level interaction pattern.

may reflect the pharmacological features. The interaction pattern of a ligand is the list of the interacting receptor atoms depicted in both receptor states. Additionally, each atom is marked whether it was involved in stabilizing (attractive) and/or destabilizing (repulsive) interaction. The interacting receptor atoms were extracted from the output of BINANA [43] analysis of the receptor-ligand complex listing up all particular interacting ligand-receptor atom pairs using the default parameters of BINANA. The stabilizing/destabilizing nature of an interaction between the ligand and receptor depends on the type of the interacting atoms. There are compatible and incompatible atom types (or atom classes) [44] resulting in stabilizing and destabilizing interactions, respectively. The atom class scheme was adopted to the AutoDock atomtypes from Sobolev et al. [44]. The classification of the ligands using their interaction patterns was performed by multiple correspondence analysis (MCA). A variety of interaction patterns, holding different information of the interactions, were created to find the most useful one for pharmacological classification of the ligands: i) both receptors, individual atoms, stabilization flags, ii) active receptor, individual atoms, stabilization flags, iii) inactive receptor, individual atoms, stabilization flags, iv) both receptors, individual atoms, without stabilization flags, v) both receptors, residues only, stabilization flags. As it was expected, the best classification was obtained with the most information rich input, *i.e.* with both receptors, individual atoms, stabilization flags (i) and the worst separation was obtained using only the interacting residues and stabilization flags (Table 7 J2). The MCA results are shown in Fig. 8 and the 3D representation in Fig. 9.

Comparing the energy based PCA and the interaction pattern based MCA results suggests that the interaction patterns resulted in better pharmacological classification of the ligands, although the antagonist **1f** was an outliner in both cases being close to the agonist group. It is worth to note that the cluster separation statistics was better for all kinds of MCA results compared with PCA, although the fuzziness of the clusters increased (Table 7).

Biological properties of our thirteen synthetic morphine analogues were investigated by *in vitro* biochemical and *in vivo* pharmacological experiments. In radioligand binding assays performed using MOR-, DOR- or KOR-selective [^{3}H]labelled primary ligands, all analogues exhibited excellent affinities for the multiple types of opioid receptors. At the MOR binding sites **2c**, **4** and **5** were the most potent ligands, but all of the remaining compounds represented quite high affinities. They were also potent competitors in the DOR-selective receptor binding assays, displaying still

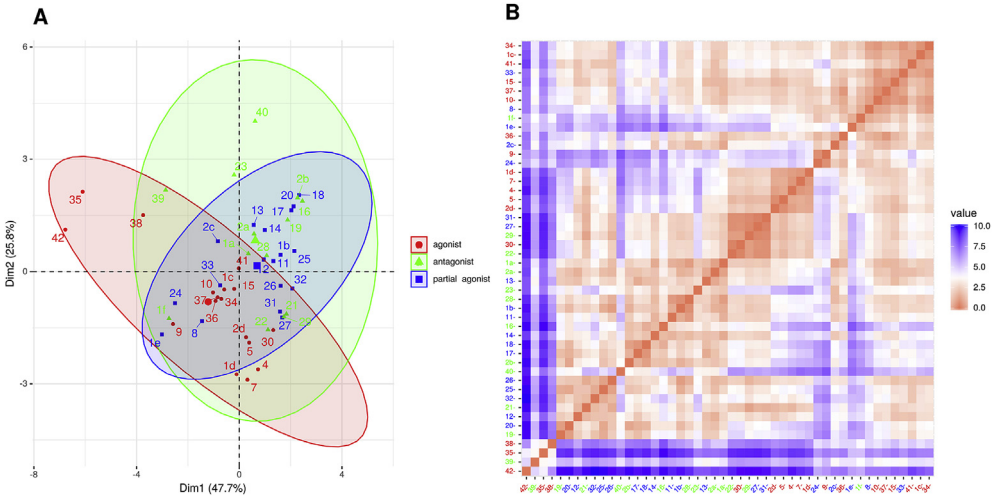

Fig. 6. Classification of the compounds by PCA of the docking energy measures
Figure legend: Individuals scores plot in the first two principal components (A), distance matrix calculated with five principal components (B).

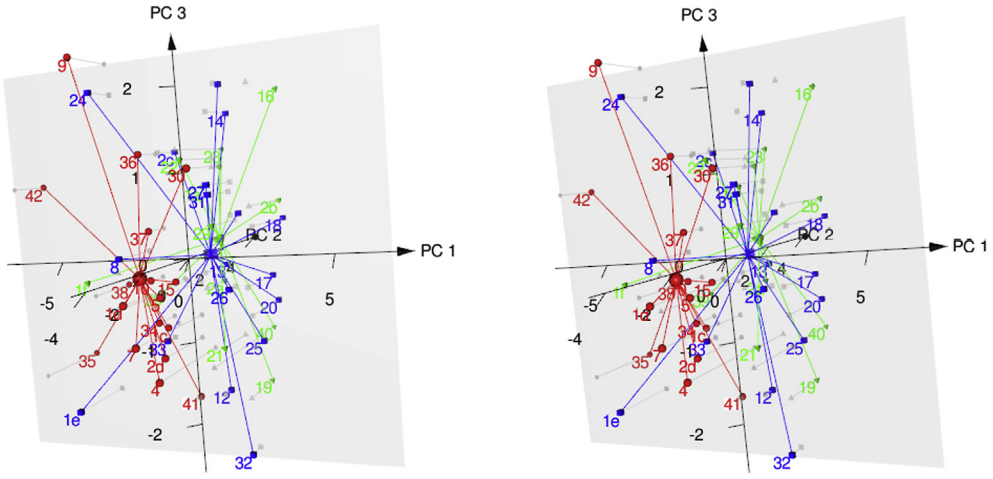

Fig. 7. Stereo view of 3D scores plot of PCA of the docking energy measures
Figure legend: red: agonists, green: antagonists, blue: partial agonists. (For interpretation of the references to colour in this figure legend, the reader is referred to the Web version of this article.)

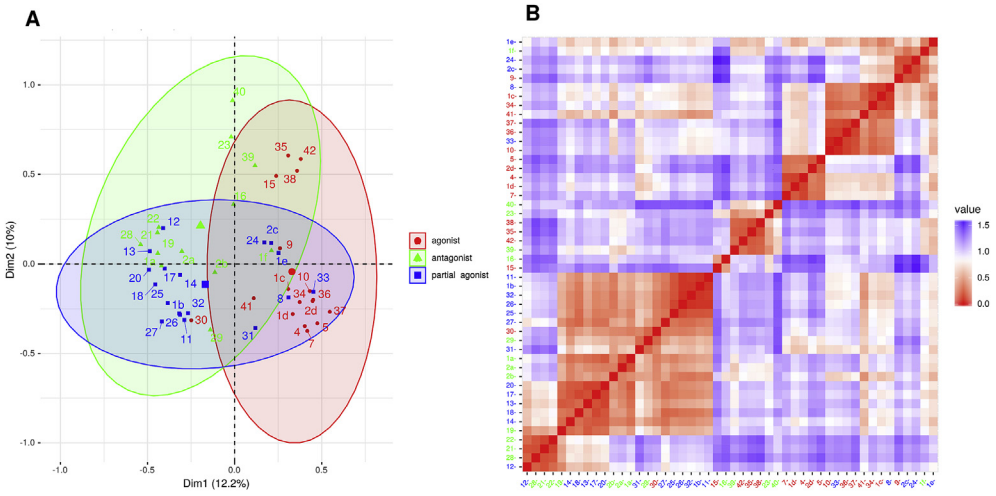

Fig. 8. Classification of the compounds by MCA of the interaction pattern
Figure legend: A: Individuals scores plot in the first two principal components, B: distance matrix calculated with five principal components.

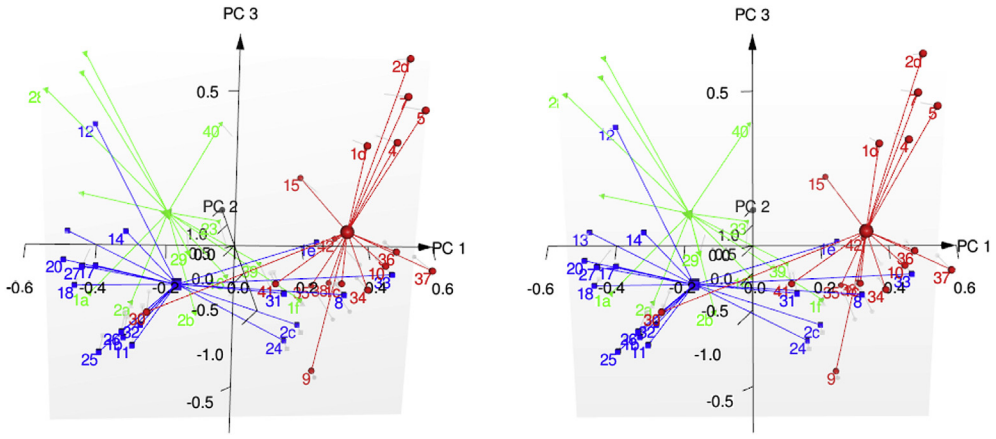

Fig. 9. Stereo view of 3D scores plot of MCA of the docking interaction pattern
Red: agonists, green: antagonists, blue: partial agonists. (For interpretation of the references to colour in this figure legend, the reader is referred to the Web version of this article.)

nanomolar equilibrium dissociation constant (K_i) values with the exception of **8** which had only moderate affinity for DOR. **2a** and **2d** showed the highest affinities at KOR ligand binding sites, although all other analogues produced low nanomolar binding affinities. Taken together, the thevinol and orvinol derivatives are very high affinity opioid ligands, with a general preference for MOR > KOR > DOR binding sites.

Receptor mediated G-protein activation experiments were conducted *in vitro* using rat brain membrane preparations and [^{35}S] GTPγS binding stimulation assays. Transmembrane signalling properties of the compounds were variable, and the ligands used can be divided into three biochemical pharmacological groups based on their stimulation features. Full agonists, such as **2d**, **4**, **5**, **7** and **9** produced the highest efficacy (E_{max} values) and they can be characterised by culminating sigmoid stimulation curves with a plateau. Partial agonist ligands, **1b**, **1e**, **2c** and **8**, exhibited submaximal efficacies and rather decreased potencies in activating G_i/G_o regulatory proteins. Another previous term for partial agonists has been mixed agonist-antagonist ligands. When both a full agonist and partial agonist are present, the partial agonist actually acts as a competitive antagonist, competing with the full agonist for receptor occupancy and producing a net decrease in the receptor activation observed with the full agonist alone (Fig. 6B). The third cluster of ligands are pure or neutral opiate antagonists, such as **1a**, **2a**, **2b** and **1f**. They are characterised by horizontally linear dose-response curves indicating no changes in the basal G-protein activity.

6-*O*-demethylation usually increased the binding affinity to MOR (**1a** vs. **2a**, **1b** vs. **2b**, **2c** vs. **9**, **4** vs. **5**). In accordance with this finding, increasing the size of the 6-*O*-substituent (**4** vs. **7**) decreased the binding affinity to MOR (Table 1). The opposite trend was observed for the efficacy in some cases, resulting in a shift of the pharmacological profiles, i.*e.* from partial agonist to antagonist (**1b** vs. **2b**), from agonist to partial agonists (**2c** vs. **9**). In the phenethyl thevinol series (**2d**, **4**, **5**, **7**) 6-*O*-demethylation did not decrease the efficacy. On the contrary, the bigger 6-*O*-substituent in **7** slightly decreased the efficacy, however, it still can be considered as a full agonist (Table 3). The changes in the pharmacological features caused by the different substituents are graphically summarized in Fig. S37.

Behavioural nociceptive properties of the ligands were studied *in vivo*, using Wistar rats in a chronic osteoarthritic inflammatory pain model. **9** at cumulative doses of 0.1-0.3−1.0 nmol/kg remained the most effective compound in decreasing inflammatory pain. **2c**, **4** and **5**, which exhibited the highest ligand binding affinities at the MOR, produced less antinociception than **9** did. The other full (**2d**) or partial antagonists (**1e**, **7**), as well as the two neutral antagonists **2a** and **2b** examined in this test were practically not effective even in ten times higher (1-3-10 nmol) cumulative doses.

Docking the ligands to both the active and inactive receptor states makes possible reasonable pharmacological classification of the ligands by docking energies. The positive effect of the differences of the docking energy measures on the pharmacological classification of the ligands also emphasize that, despite the moderate geometric difference between the active and inactive receptor states within the binding pocket, the docking energies can predict the pharmacological features of the ligands. Pharmacological classification was also attempted by the interaction pattern of the docked ligands, *i.e.* by the interacting receptor atoms and the type of the interactions (stabilizing or distabilizing). More information (*i.e.* more kinds of docking energy measures, two receptor states instead of single one) resulted in better classification in both cases.

Agonists and antagonist are separated quite well while partial agonists overlap with the others which is in accordance with molecular dynamics results comparing interactions of agonists, antagonists and partial agonists; nevertheless, pharmacological classification by the docking algorithm in the present paper is still closer to the high throughput methodology.

3. Conclusions

All investigated compounds showed subnanomolar binding affinity to MOR and a preference to MOR over DOR and KOR. The pharmacological effects of the compounds involved agonism, partial agonism and antagonism. Neither binding affinities nor pharmacological features could be directly related to particular organic functional groups.

The *in vitro* pharmacological effects and the *in vivo* antiallodynic effects were in accordance except the full agonist **2d.** As the only exception, the newly synthesized compound, **2c** despite its partial agonist feature, showed antiallodynic effect equal tot hat of the full agonist **9**.

Due to the harmony between the *in vitro* and *in vivo* results, the *in silico* calculations were expected to explain the pharmacological profiles of the compounds. The unsupervised multivariate classification methods (using either docking energies or interaction fingerprints) applied to the docking results, obtained from active and inactive receptor states, were able to separate the agonists from antagonists with a good accuracy. Additionally, the third group, partial agonists, were partially differentiated from the other two groups. Due to the effectivity of the multivariates classification, their further improvement seems to be promising. Differentiating between ORs needs accurate docking calculations, however, if it is accurate enough it can differentiate between the receptor states as well. If it is so, the first step in the modelling scenario should be the pharmacophoric featuring (receptor state selection) for binding affinity prediction.

4. Experimental section

4.1. General procedure

Reagents and solvents were obtained from commercial suppliers and were used without further purifications. Melting points were measured with a Büchi-535 instrument and the data are uncorrected. Column chromatography was performed on Kieselgel 60 Merck 1.09385 (0.040−0.063 mm). Analytical TLC was accomplished on Macherey-Nagel Alugram® Sil G/UV_{254} 40 × 80 mm aluminium sheets [0.25 mm silica gel with fluorescent indicator] with the following eluent systems (each (v/v)): [A]: chloroform-methanol 9:1, [B]: ethyl acetate-methanol 8:2, [C]: hexane-ethyl acetate 7:3, [D]: hexane-ethyl acetate 1:1. The spots were visualized with a 254 nm UV lamp or with 5% phosphomolybdic acid in ethanol.

NMR spectra: All the 1D and 2D NMR experiments were recorded on a Bruker AV 500 (Avance 500 MHz) spectrometer at 298 K, using BBO probehead (hp workstation xw 5000, software: Bruker TOPSPIN 1.3). For ^{1}H experiment: 10 mg of the appropriate orvinol was dissolved in 500 μL of deuterated chloroform ($CDCl_3$). For measuring ^{13}C NMR spectra: 20 mg sample of the corresponding derivative was dissolved in 500 μL $CDCl_3$. Chemical shifts (δ) are reported in parts per million (ppm), and coupling constants (J) reported in Hertz. ^{1}H and ^{13}C NMR chemical shifts were referenced to the residual peak of $CDCl_3$ at δ 7.26 and 77.16 ppm, for proton and carbon, respectively.

4.1.1. General procedure for the 3-O-demethylation of thevinol derivatives (preparation of 1e, 1f and 1d)

Potassium hydroxide (3.2 g, 57 mmol) was dissolved in diethylene glycol (20 mL) at 110 °C. The solution was allowed to cool to 70 °C and the corresponding 3-*O*-methyl-thevinol derivative

(2 mmol) was added. The reaction mixture was stirred under argon atmosphere at 210 °C (internal temperature) for 90 min. The brownish product mixture was allowed to cool to room temperature and poured into a saturated ammonium chloride solution (40 mL). The suspension was extracted with diethyl ether (4 × 45 mL). The combined organic layer was extracted successively with 5% sodium hydrogen sulfite solution (2 × 30 mL) and water (2 × 30 mL). The organic phase was dried (Na_2SO_4) and the solvent was evaporated under reduced pressure. The residue was purified by means of column chromatography on silica gel using the appropriate solvent system.

1d: prepared from 20*R*-phenethyl-thevinol (**4**, 975 mg, 2 mmol). Eluent system: hexane-ethyl acetate 8:2 (v/v). Yield: 590 mg (62%).

4.1.1.1. (5R,6R,7R,9R,13S,14S)-4,5-Epoxy-3-hydroxy-α,α,17-trimethyl-6,14-ethenomorphinan-7-methanol (1e). **1e** was synthesized from 20-methyl-thevinol (795 mg, 2 mmol). Eluent system: chloroform-methanol 9:1 (v/v). Yield: 440 mg (57%). ^{1}H NMR ($CDCl_3$) δ = 0.77 (dd, $^2J_{8\alpha,8\beta}$ = 12.9 Hz, $^3J_{8\alpha,7\beta}$ = 8.2 Hz, 1H, 8α-H), 1.01 (s, 3H, 20-CH_3), 1.08 (s, 3H, 20-CH_3), 1.84 (dd, $^2J_{15eq,15ax}$ = 13.1 Hz, $^3J_{15eq,16ax}$ = 2.6 Hz, 1H, 15-H_{eq}), 1.96 (app t, $^3J_{7\beta,8\alpha}$ = 8.8 Hz, 1H, 7β-H), 1.99 (td, $^2J_{15ax,15eq}$ = 13.1 Hz, $^3J_{15ax,16eq}$ = 5.7 Hz, 1H, 15-H_{ax}), 2.36 (m, 1H, 10α-H), 2.37 (s, 3H, NCH_3), 2.41 (m, 1H, 16-H_{ax}), 2.52 (dd, $^2J_{16eq,16ax}$ = 12.1 Hz, $^3J_{16eq,15ax}$ = 5.3 Hz, 1H, 16-H_{eq}), 2.87 (ddd, $^2J_{8\beta,8\alpha}$ = 12.9 Hz, $^3J_{8\beta,7\beta}$ = 9.1 Hz, 1H, 8β-H), 3.12 (d, $^3J_{9\alpha,10\alpha}$ = 6.5 Hz, 1H, 9α-H), 3.20 (d, $^2J_{10\beta,10\alpha}$ = 18.5 Hz, 1H, 10β-H), 3.75 (s, 3H, 6-OCH_3), 4.50 (br s, 1H, 3-*OH*), 4.57 (s, 1H, 5β-H), 4.77 (br s, 1H, 20-*OH*), 5.42 (d, $^3J_{19,18}$ = 9.1 Hz, 1H, 19-H), 5.93 (d, $^3J_{18,19}$ = 9.1 Hz, 1H, 18-H), 6.47 (d, $J_{1,2}$ = 8.2 Hz, 1H, 1-H), 6.59 (d, $J_{2,1}$ = 8.2 Hz, 1H, 2-H). ^{13}C NMR ($CDCl_3$) δ = 22.2 (C-10), 25.2 (20CH_3), 28.6 (20CH_3), 30.9 (C-8), 33.4 (C-15), 42.9 (C-14); 43.5 (NCH_3), 45.5 (C-16), 47.5 (C-13), 48.5 (C-7), 55.1 (6OCH_3), 59.9 (C-9), 73.5 (C-20), 84.1 (C-6), 99.2 (C-5), 116.0 (C-2), 119.6 (C-1), 124.4 (C-18), 127.9 (C-11), 134.0 (C-12), 135.3 (C-19), 137.2 (C-3), 146.5 (C-4). HRMS (TOF): Calcd. for $C_{23}H_{29}NO_4$ $[M+H]^+$: 384.2169; Found: 384.2178.

4.1.1.2. (5R,6R,7R,9R,13S,14S)-4,5-Epoxy-18,19-dihydro-3-hydroxy-α,α,17-trimethyl-6,14-etheno morphinan-7-methanol (1f). **1f**: prepared from 20-methyl-dihydrothevinol (800 mg, 2 mmol). Eluent system: chloroform-methanol 9:1 (v/v). Yield: 470 mg (60%). ^{1}H NMR ($CDCl_3$) δ = 0.75 (m, 1H, 19-H_{syn}), 1.02 (m, 1H, 19-H_{anti}), 1.08 (dd, $^2J_{8\alpha,8\beta}$ = 12.8 Hz, $^3J_{8\alpha,7\beta}$ = 9.2 Hz, 1H, 8α-H), 1.18 (s, 3H, 20-CH_3), 1.37 (s, 3H, 20-CH_3), 1.66 (dd, $^2J_{15eq,15ax}$ = 13.2 Hz, $^3J_{15eq,16ax}$ = 2.6 Hz, 1H, 15-H_{eq}), 1.75–1.78 (m, 2H, 18-H_{anti}, 18-H_{syn}), 1.91 (app t, $^3J_{7\beta,8\alpha}$ = 9.2 Hz, 1H, 7β-H), 2.04 (td, $^2J_{15ax,15eq}$ = 12.7 Hz, $^3J_{15ax,16eq}$ = 5.4 Hz, 1H, 15-H_{ax}), 2.20 (dd, $^2J_{10\alpha,10\beta}$ = 18.3 Hz, $^3J_{10\alpha,9\alpha}$ = 6.2 Hz, 1H, 10α-H), 2.30 (m, 1H, 16-H_{ax}), 2.31 (s, 3H, NCH_3), 2.44 (dd, $^2J_{16eq,16ax}$ = 11.9 Hz, $^3J_{16eq,15ax}$ = 5.2 Hz, 1H, 16-H_{eq}), 2.65 (d, $^3J_{9\alpha,10\alpha}$ = 6.2 Hz, 1H, 9α-H), 2.78 (ddd, $^2J_{8\beta,8\alpha}$ = 12.6 Hz, $^3J_{8\beta,7\beta}$ = 11.3 Hz, $^4J_{8\beta,19syn}$ = 1.1 Hz, 1H, 8β-H), 3.10 (d, $^2J_{10\beta,10\alpha}$ = 18.3 Hz, 1H, 10β-H), 3.52 (s, 3H, 6-OCH_3), 4.42 (s, 1H, 5β-H), 5.05 (br s, 1H, 20-*OH*), 7.07 (br s, 1H, 3-*OH*), 6.53 (d, $J_{1,2}$ = 8.0 Hz, 1H, 1-H), 6.69 (d, $J_{2,1}$ = 8.0 Hz, 1H, 2-H); ^{13}C NMR ($CDCl_3$) δ = 17.4 (C-18), 21.9 (C-10), 24.8 (20CH_3), 29.7 (C-19), 29.8 (20CH_3), 32.3 (C-8), 35.4 (C-15), 36.0 (C-14); 43.4 (NCH_3), 45.1 (C-16), 46.5 (C-13), 47.7 (C-7), 52.6 (6OCH_3), 61.2 (C-9), 74.4 (C-20), 80.1 (C-6), 97.3 (C-5), 116.3 (C-2), 119.4 (C-1), 128.1 (C-11), 132.1 (C-12), 137.3 (C-3), 145.6 (C-4).; HRMS (TOF): Calcd. for $C_{23}H_{31}NO_4$ $[M+H]^+$: 386.2325; found: 386.2326.

4.1.2. General procedure for the preparation of 6-O-desmethyl-orvinol derivatives (2a, 2b, 2c, 2d)

Lithium-aluminum hydride (1.1 g, 28.9 mmol) was suspended in dry tetrahydrofuran (10 mL) under argon atmosphere. The suspension was cooled to 0 °C and dry carbon tetrachloride (0.74 mL, 1.18 g, 7.7 mmol) was carefully added dropwise under stirring. A solution of the corresponding orvinol derivative (**1a**, **1b**, **1c**, **1d**, 1.92 mmol) in dry tetrahydrofuran (10 mL) was added dropwise and the mixture was stirred under reflux for 36 h. The reaction mixture was cooled to 0 °C and diluted with tetrahydrofuran (20 mL). Water (5 mL) was dropped in under vigorous stirring and the suspension was filtered. The solid was washed with ethyl acetate (3 × 20 mL) and dichloromethane (2 × 15 mL). The combined organic phase was dried (Na_2SO_4) and the solvent was evaporated under reduced pressure. The residue was dried in vacuum (2 × 10^{-1} mbar, 16 h). The crude product was purified by column chromatography on silica gel (Kieselgel: 100 g, eluent system: 1. ethyl acetate − chloroform − 25% NH_3 solution 70:30:1 (v/v/v), 2. dichloromethane − methanol 9:1 (v/v). Analytical data and detailed NMR assignments for **2a**, **2b** and **2d** are presented in Supporting Information.

4.1.2.1. (5R,6R,7R,9R,13S,14S,20R)-(5α,7α)-4,5-Epoxy-18,19-dihydro-3,6-dihydroxy-α,17-dimethyl -α-propyl-6,14-ethenomorphinan-7-methanol (2c). Yield: 70%, mp. 127–128 °C; TLC: R_f [A] = 0.50, R_f [C] = 0.10, R_f [D] = 0.22; ^{1}H NMR ($CDCl_3$): δ = 0.62 (m, 1H, 19-H_{syn}), 0.89 (t, J = 7.0 Hz, 3H, 20-$CH_3CH_2CH_2$), 0.92 (m, 1H, 19-H_{anti}), 1.01 (dd, $^2J_{8\alpha,8\beta}$ = 13.0 Hz, $^3J_{8\alpha,7\beta}$ = 9.1 Hz, 1H, 8α-H), 1.06 (m, 1H, 18-H_{syn}), 1.36 (s, 3H, 20-CH_3), 1.37 (m, 1H, 15-H_{eq}), 1.38 (m, 2H, $CH_3CH_2CH_2$), 1.43 (m, 2H, $CH_3CH_2CH_2$), 1.67 (m, 1H, 15-H_{ax}), 1.83 (app t, $^3J_{7\beta,8\alpha}$ = 9.1 Hz, 1H, 7β-H), 1.87 (m, 1H, 18-H_{anti}), 2.14 (dd, $^2J_{10\alpha,10\beta}$ = 18.4 Hz, $^3J_{10\alpha,9\alpha}$ = 6.3 Hz, 1H, 10α-H), 2.04 (m, 1H, 16-H_{ax}), 2.25 (s, 3H, NCH_3), 2.31 (dd, $^2J_{16eq,16ax}$ = 11.5 Hz, $^3J_{16eq,15ax}$ = 4.9 Hz, 1H, 16-H_{eq}), 2.63 (ddd, $^2J_{8\beta,8\alpha}$ = 13.4 Hz, $^3J_{8\beta,7\beta}$ = 10.3 Hz, $^4J_{8\beta,19syn}$ = 3.0 Hz, 1H, 8β-H), 2.58 (d, $^3J_{9\alpha,10\alpha}$ = 6.3 Hz, 1H, 9α-H), 3.01 (d, $^2J_{10\beta,10\alpha}$ = 18.4 Hz, 1H, 10β-H), 4.00 (s, 1H, 5β-H), 5.46 (br s, 1H, 20-*OH*), 6.03 (br s, 1H, 6-*OH*), 6.47 (d, $^2J_{1,2}$ = 8.1 Hz, 1H, 1-H), 6.77 (d, $^2J_{2,1}$ = 8.1 Hz, 1H, 2-H), 8.27 (br s, 1H, 3-*OH*); ^{13}C NMR ($CDCl_3$): δ = 14.6 (20-$CH_3CH_2CH_2$), 15.6 ($CH_3CH_2CH_2$), 21.9 (C-10), 22.2 (C-18), 22.5 (20-CH_3), 30.0 (C-19), 31.5 (C-8), 36.3 (C-15), 34.5 (C-14), 43.6 ($CH_3CH_2CH_2$), 43.8 (NCH_3), 45.1 (C-13), 45.2 (C-16), 45.8 (C-7), 61.3 (C-9), 75.6 (C-20), 76.7 (C-6), 96.2 (C-5), 116.8 (C-2), 119.4 (C-1), 127.9 (C-11), 132.4 (C-12), 137.1 (C-3), 145.8 (C-4); MS (ESI) *m/z*: 400 $[M+1]^+$; HRMS (TOF): Calcd. for $C_{24}H_{33}NO_4$ $[M+H]^+$: 400.2482; found: 400.2480.

Analytical data and detailed NMR assignments for **2d**, **4**, **5**, **7** and **8** are presented in Supporting Information.

4.2. In vitro experiments

4.2.1. Chemicals

$MgCl_2$ x $6H_2O$, EGTA, Tris-HCl, NaCl, GDP, the GTP analogue GTPγS, were purchased from Sigma-Aldrich (Budapest, Hungary). The highly selective MOR agonist enkephalin analogue DAMGO was obtained from *Bachem Holding AG* (Bubendorf, Switzerland). The highly selective KOR agonist diphenethylamine derivative, HS665 [45] were kindly offered by *Dr. Helmut Schmidhammer* (University of Innsbruck, Austria). The morphine analogues were provided by *ABX* GmbH (Radeberg, Germany). The highly selective DOR agonist Ile^{5,6}-deltorphin II was synthesized in the Laboratory of Chemical Biology group of the *Biological Research Centre* (Szeged, Hungary). DAMGO, [Ile^{5,6}]-deltorphin II and HS665 were dissolved in water, morphine analogues were dissolved in ethanol and were stored in 1 mM stock solution at −20 °C. The radiolabeled GTP analogue, [^{35}S] GTPγS (specific activity: 3.7 × 10^{13} Bq/mmol; 1000 Ci/mmol) was purchased from Hartmann Analytic (Braunschweig, Germany). [^{3}H] DAMGO [46] (specific activity: 38.8 Ci/mmol), [^{3}H]Ile^{5,6}-deltorphin II (specific activity: 19.6 Ci/mmol) and [^{3}H]HS665 [47] (specific activity: 13.1 Ci/mmol) were radiolabelled by the *Laboratory of Chemical Biology* group in BRC (Szeged, Hungary). The

UltimaGold™ MV aqueous scintillation cocktail was purchased from PerkinElmer (Boston, USA).

4.2.2. Animals

For membrane homogenate preparations male and female Wistar rats and guinea pigs were used. Animals were housed in the local animal house of BRC (Szeged, Hungary). All the animals were kept in a temperature controlled room (21–24 °C) under a 12:12 h light/dark cycle and allowed free access to food and water. All housing and experiments were conducted according to the European Communities Council Directives (86/606/ECC) and the Hungarian Act for the Protection of Animals in Research (XXVIII.tv. 32.x). The total number of animals as well as their suffering was minimized.

4.2.3. Preparation

A crude membrane fraction of Wistar rat and guinea pig brains were prepared for ligand binding experiments according to Ref. [48] with changes. After decapitation, brains were rapidly removed and homogenised in 30 vol of ice-cold 50 mM Tris–HCl (pH 7.4) buffer with a teflon-glass homogeniser. After centrifugation at 40000*g* for 20 min at 4 °C, the resulting pellet were suspended in 30 vol of the same buffer and incubated for 30 min at 37 °C to remove endogenous opioids. Centrifugation was then repeated as described above. The final pellet were suspended in 5 vol of 50 mM Tris–HCl (pH 7.4) buffer and stored at −80 °C. Membranes were thawed, diluted with buffer and the resulting pellet were taken up in appropriate fresh buffer and immediately used. For the [^{35}S]GTPγS binding experiments the final pellet of rat and guinea pig brain membrane homogenates were suspended in 5 vol of ice-cold TEM (Tris-HCl, EGTA, $MgCl_2$) and stored at −80 °C for further use.

4.2.4. Receptor binding experiments

4.2.4.1. Competition binding experiments. In homologue displacements using [^{3}H]DAMGO, [^{3}H]Ile^{5,6}-deltorphin II or [^{3}H]HS665 the level of nonspecific binding was determined in the presence of 10 μM unlabeled naloxone (MOR and KOR) and HS665 (KOR), while total binding was determined in the absence of cold ligand. The incubation was followed by rapid filtration under vacuum (Brandel M24R Cell Harvester; Brandel Harvesters), and washed three times with 5 mL ice-cold 50 mM Tris-HCl. The filtration was accomplished through Whatman GF/C glass fibres (respectively). The radioactivity of the filters was measured in UltimaGold MV aqueous scintillation cocktail (Perkin Elmer, Waltham, MA) with Packard Tricarb 2300 TR liquid scintillation counter (Perkin Elmer, Waltham, MA). The competition binding assays were performed in duplicates and repeated at least three times.

4.2.4.2. Functional [^{35}S]GTPγS binding experiments. Rat and guinea pig brain membranes (~10 μg of protein/tube) were incubated at 30 °C for 60 min in Tris–EGTA buffer (50 mM Tris–HCl buffer, 3 mM $MgCl_2$, 1 mM EGTA, 100 mM NaCl, pH 7.4) containing 0.05 nM [^{35}S]GTPγS with increasing concentrations (10^{-10}-10^{-5} M) of opioid ligands tested in the presence of 30 μM GDP in a final volume of 1 mL as previously described [49]. Total binding was measured in the absence of test compounds, non-specific binding was determined in the presence of 10 μM unlabeled GTPγS and subtracted from total binding. The difference between total and non-specific binding values represents basal activity. The reaction was terminated by rapid filtration under vacuum (Brandel M24R Cell Harvester), and Whatman GF/B glass fiber filters were washed three times with 5 mL ice-cold 50 mM Tris-HCl (pH 7.4) buffer. The radioactivity of the dried filters was detected in Ultima GoldTM MV aqueous scintillation cocktail with Packard TriCarb 2300 TR liquid scintillation counter. [^{35}S]GTPγS binding experiments were performed in triplicates and repeated three times.

4.2.5. Data analysis

Experimental data were presented as means ± S.E.M. Points were fitted with the professional curve fitting program, GraphPad Prism 5.0 (GraphPad Prism Software Inc., San Diego, CA), using nonlinear regression analysis. In the [^{35}S]GTPγS binding assays the 'Sigmoid dose-response' fitting was used to establish the maximal efficacy (E_{max}) of the receptors' G-protein and the ligand potency (EC_{50}). Stimulation was given as percent of the specific [^{35}S]GTPγS binding observed over the basal activity, which was settled as 100%.

In the competition binding assays the 'One site competition' fitting was used to establish the equilibrium binding affinity (K_i value). Inhibition was given as percent of the specific binding observed.

4.3. In vivo experiments

After institutional ethical approval had been obtained (Institutional Animal Care Committee of the Faculty of Medicine at the University of Szeged), male Wistar rats (Charles River strain, Bioplan, Budapest, Hungary; 378 ± 5.1 g; n = 6–8/group) were used in the experiments. The animals were group-housed (4 animals/cage) with free access to food and water, and with a 12:12 h light/dark cycle. Animal suffering and the number of animals per group were kept at a minimum; therefore, the drugs were administered in cumulative doses in 30-min intervals (at 0th, 30th and 60th min), and injections were repeated 7 days apart for the same animal, as in our previous study [50].

The following drugs were applied for the *in vivo* nociceptive studies: etorphine-hydrochloride (**9**) [25,51] eight 6,14-ethenomorphinan derivatives synthesized as described earlier [16–22,24], **2a** and **1e**, **1f**, **2b**, **2d**, **4**, **5**, **7** as well as the new compound **2c**. The drugs were freshly diluted (0.01–10 μM) with distilled water from the stock solutions and administered subcutaneously (s.c.) in a volume of 2 mL/kg.

Osteoarthritis was induced by injecting MIA (Sigma-Aldrich Ltd. Budapest, Hungary; 1 mg/30 μL) into the tibiotarsal joint of the right hind leg on two consecutive days. MIA treatments were given to gently restrained conscious animals, using a 27-gauge needle, without anesthesia so as to exclude any drug interaction. These injections did not elicit signs of major distress. Within 14 days MIA had consistently been shown to cause severe end-stage cartilage destruction resulting in osteoarthritis-like joint pain accompanied with moderate edema [50,52,53]. The observer was blind to the drug treatment administered.

4.3.1. Behavioral nociceptive testing

The threshold for withdrawal from mechanical stimulation to the plantar aspect of the hindpaws was assessed using a dynamic plantar aesthesiometer (Ugo Basile, Comerio, Italy), which consists of an elevated wire mesh platform to allow access to the ventral surface of the hindpaws. Prior to baseline testing, each rat was habituated to a testing box for at least 20 min. Measurements were done with a straight metal needle (diameter 0.5 mm) that exerts an increasing upward force at a constant rate (6.25 g/s) with a maximum cut-off force of 50 g over an 8 s period. The measurement was stopped when the paw was withdrawn, and the results were expressed as paw withdrawal thresholds in grams.

4.3.2. Experimental paradigm

After MIA injections, baseline pain thresholds (2 times with 15 min interval) were determined 14 days later and their means provided the baseline value.

Cumulative-dosing procedure was applied (Table 4). The control group received distilled water. In the positive control group, animals were treated with **9** (0.1, 0.3, and 1.0 nmol/kg). The higher

doses of **9** were also applied in a preliminary experiment (1.0 and 3.0 nmol/kg) but 3.0 nmol/kg dose induced catatonia and respiratory depression in 100% of the animals, thus we determined the maximum dose as 1 nmol/kg. Response latencies were measured at 15 min intervals and the increasing doses of the drugs (three doses) were administered following two recordings. After the highest dose injection the pain threshold was assessed in every 15 min for 1 h, then hourly at the second and third hour to determine the time course of drug effects. Although, the motor behavior and general status of the animals were not investigated and quantified systematically, altered behavior (excitation, flaccidity or motor weakness) or any signs of opioid overdose (catatonia or respiratory depression) were not observed.

4.3.3. Statistical analysis

Data are presented as means ± SEM. Data sets were examined by repeated measures of ANOVA. Post hoc comparisons were carried out with the Fisher LSD test. A p value lower than 0.05 was considered significant. The mean paw withdrawal thresholds obtained 15 and 30 min after the injections (calculated after the individual drug injections) were used for linear regression analysis to determine the effective dose 30 (ED_{30}) values with 95% confidence intervals. Mean of 50 g would mean the complete relief of hyperalgesia, while mean of control value (29 g) means the zero effects, thus the difference (21 g) is the possible maximal effect. ED_{30} is equivalent to the dose that yielded 30% difference (7 g) in the paw withdrawal threshold compared to the baseline (pretreatment) values. Data analyses were performed with the STATISTICA (Statistica Inc., Tulsa, Oklahoma, USA) and GraphPad Prism 4.0 (GraphPad Softwre Inc. La Jolla, CA, US) softwares.

4.4. In silico studies

4.4.1. Molecular docking

The ligands were flexibly docked to the experimentally solved active and inactive states of MOR (http://www.rcsb.org, pdb codes 5c1m and 4dkl for the active and inactive receptor states, respectively). The receptor structures were kept rigid. Due to the known limitation of the docking algorithm *i.e.* the rings are kept rigid during the calculation, 10 different conformations were generated by molecular dynamics to emulate the conformational flexibility for aliphatic rings in accordance with experimental findings [54]. The 10 conformations and the initial energy minimized conformer were provided for docking for each ligand. Docking calculations were performed by the program PSOVINA [55], a variant of the formerly released VINA [56]. Coordinate files were converted to pdbqt format by AutoDock Tools [57] or PSOVINA. Docking box center was set to the geometric center of the ligands in the crystals. Due to the impact of the size of the docking box on the docking pose, namely on the set of interacting receptor atoms, the box size was specifically determined for each ligand [58] using the radius of giration (R_g) of the minimum energy conformer calculated by Open Babel. PSOVINA was used with default parameters, albeit docking was repeated 5 times instead of increased exhaustiveness parameter [59] and the lowest energy docking poses was kept for each ligand.

4.4.2. Analysis of docking results

The selected poses were analysed by the program BINANA [43] to extract the interacting ligand-receptor atom pairs, the docking energies and the energy contributions belonging to the specific atom pairs. Stabilizing or destabilizing assignments for the ligand-receptor contacts based on the method Soboljev et al. [44]. Analysis of the docking energies and the interacting receptor atoms were performed by principal component analysis (PCA) and multiple correspondence analysis (MCA), respectively, using program packages of the R programming environment v. 3.5.1 [60]. Calculations were performed by the PCA and MCA moduls of the R package "FactoMineR" [61]. Results were visualized using package "factoextra" [62]. For 3D visualization packages "rgl" and "pca3d" were used [63,64]. Docking calculations were performed on a Linux cluster running Rocks 6.2 cluster management program and CentOS 6.6 operation system and on the PRACE/NIIF cluster, and the analyses in Linux Mint 18.1 using in house bash and R scripts.

4.4.3. Generation of the ligand conformations

Open Babel v. 2.4.1 program package [65] was used in a two-step manner: 1. conformers were generated with the "–score energy" option to avoid high energy structures, 2. conformers were further transformed with "–rings" option to allow ring flexibility using MMFF94s force field.

Declaration of competing interest

The authors declare no conflict/competing financial of interest.

Acknowledgment

This research was supported by the following grants: OTKA-108518 (Dr. Sándor Benyhe), supported by the National Research, Development and Innovation Office (NKFIH), Budapest, Hungary. We acknowledge NIIF for awarding us access to resource based in Hungary at Szeged.

Abbreviations

βPh	beta-phenylethyl group, beta-phenethyl group, CH_2CH_2Ph
CPM	cyclopropylmethyl group
DAMGO	Tyr-D-Ala-Gly-(NMe)Phe-Gly-ol
DOR	δ-opioid receptor
EGTA	ethyleneglycol-tetraacetate
GDP	guanosine diphosphate
GTP	guanosine triphosphate
KOR	κ-opioid receptor
MIA	monosodium iodoacetate
MOR	μ-opioid receptor
S.E.M.	standard error of means
tris-HCl	tris-(hydroxymethyl)-aminomethane hydrochloride.

Appendix A. Supplementary data

Supplementary data to this article can be found online at https://doi.org/10.1016/j.ejmech.2020.112145.

References

[1] B.M. Cox, M.J. Christie, L. Devi, L. Toll, J.R. Traynor, Challenges for opioid receptor nomenclature: IUPHAR Review 9, Br. J. Pharmacol. 172 (2015) 317–323.
[2] Y. Feng, X. He, Y. Yang, D. Chao, X.Y. Lazarus Lh, Current research on opioid receptor function, Curr. Drug Targets 13 (2012) 230–246.
[3] B.L. Kieffer, C.J. Evans, Opioid receptors: from binding sites to visible molecules in vivo, Neuropharmacology 56 (2009) 205–212.
[4] C.W. Stewens, Bioinformatics and evolution of vertebrate nociceptin and opioid receptors, in: G. Litwack (Ed.), Vitamins and Hormones, Elsevier, 2015, pp. 57–94.
[5] G.L. Thompson, E. Kelly, A. Christopoulos, M. Canals, Novel GPCR paradigms at the μ-opioid receptor, Br. J. Pharmacol. 172 (2015) 287–296.
[6] S. Benyhe, F. Zádor, F. Ötvös, Biochemistry of opioid (morphine) receptors: binding, structure and molecular modelling, Acta Biol. Szeged. 59 (2015) 17–37.
[7] N.T. Burford, D. Wang, W. Sadée, G-protein coupling of mu-opioid receptors (OP3): elevated basal signalling activity, Biochem. J. 348 (2000) 531–537.
[8] J. Hughes, T.W. Smith, H.W. Kosterlitz, L.A. Fothergill, B.A. Morgan, H.R. Morris,

Identification of two related pentapeptides from the brain with potent opiate agonist activity, Nature 258 (1975) 577–579.
[9] C.H. Li, D. Chung, Isolation and structure of an untriakontapeptide with opiate activity from camel pituitary glands, Proc. Natl. Acad. Sci. U. S. A. 73 (1976) 1145–1148.
[10] A. Goldstein, W. Fischli, L.I. Lowney, M. Hunkapiller, L. Hood, Porcine pituitary dynorphin: complete amino acid sequence of the biologically active heptadecapeptide, Proc. Natl. Acad. Sci. U. S. A. 78 (1981) 7219–7223.
[11] J.E. Zadina, L. Hackler, L.J. Ge, A.J. Kastin, A potent and selective endogenous agonist for the mu-opiate receptor, Nature 386 (1997) 499–502.
[12] A.A. Pradhan, M.L. Smith, B.L. Kieffer, C.J. Evans, Ligand-directed signalling within the opioid receptor family, Br. J. Pharmacol. 167 (2012) 960–969.
[13] C.F. Semenkovich, A.S. Jaffe, Adverse effects due to morphine sulfate. Challenge to previous clinical doctrine, Am. J. Med. 79 (1985) 325–330.
[14] J.L. Whistler, H. Chuang, P. Chu, L.Y. Jan, M. Zastrow, Functional dissociation of mu opioid receptor signaling and endocytosis: implications for the Biology of opiate tolerance and addiction, Neuron 23 (1999) 737–746.
[15] S. Hosztafi, Chemistry-Biochemistry of Poppy 1. Chemical structures of alkaloids, in: J. Bernáth (Ed.), Poppy, the Genus Papaver, Harwood Academic Publishers, Amsterdam, 1998, pp. 105–158.
[16] J.R. Lever, R.F. Dannals, A.A. Wilson, H.T. Ravert, H.N. Wagner Jr., Synthesis of carbon-11 labeled diprenorphine: a radioligand for positron emission tomographic studies of opiate receptors, Tetrahedron Lett. 28 (1987) 4015–4018.
[17] J.R. Lever, S.M. Mazza, R.F. Dannals, H.T. Ravert, A.A. Wilson, J. Wagner, H. N, Facile synthesis of [^{11}C]buprenorphine for positron emission tomographic studies of opioid receptors, Int. J. Radiat. Appl. Instrum. Appl. Radiat. Isot. 41 (1990) 745–752.
[18] S.K. Luthra, F. Brady, D.R. Turton, D.J. Brown, K. Dowsett, S.L. Waters, A.K.P. Jones, R.W. Matthews, J.C. Crowder, Automated radiosyntheses of [6-*O*-methyl-^{11}C]diprenorphine and [6-*O*-methyl-^{11}C]buprenorphine from 3-*O*-trityl protected precursors, Appl. Radiat. Isot. 45 (1994) 857–873.
[19] J. Marton, B.W. Schoultz, T. Hjørnevik, A. Drzezga, B.H. Yousefi, H.-J. Wester, F. Willoch, G. Henriksen, Synthesis and evaluation of a full-agonist orvinol for **4**-Imaging of opioid receptors: [^{11}C]PEO, J. Med. Chem. 52 (2009) 5586–5589.
[20] J. Marton, G. Henriksen, Design and synthesis of an ^{18}F-labeled version of phenethyl orvinol ([^{18}F]FE-PEO) for **4**-imaging of opioid receptors, Molecules 17 (2012) 11554–11569.
[21] K.W. Bentley, D.G. Hardy, B. Meek, Novel analgesics and molecular rearrangements in the morphine-thebaine group II. Alcohols derived from 6,14-*endo*-etheno- and 6,14-*endo*-ethanotetrahydrothebaine, J. Am. Chem. Soc. 89 (1967) 3273–3280.
[22] K.W. Bentley, D.G. Hardy, Novel analgesics and molecular rearrangements in the morphine-thebaine group III. Alcohols of the 6,14-*endo*-ethanotetrahydrooripavine series and derived analogs of *N*-allylnormorphine and –norcodeine, J. Am. Chem. Soc. 89 (1967) 3281–3292.
[23] A. Coop, J.W. Janetka, J.W. Lewis, K.C. Rice, L-Selectride as a general reagent for the *O*-demethylation and *N*-decarbomethoxylation of opium alkaloids and derivatives, J. Org. Chem. 63 (1998) 4392–4396.
[24] J.W. Lewis, M.J. Readhead, Novel analgetics and molecular rearrangements in the morphine-thebaine group. XVIII. 3-Deoxy-6,14-*endo*-etheno-6,7,8,14-tetrahydrooripavines, J. Med. Chem. 13 (1970) 525–527.
[25] D. Biyashev, S. Garadnay, J. Marton, S. Makleit, A. Borsodi, S. Benyhe, Biochemical characterisation of newly developed beta-etorphine and beta-dihydroetorphine derivatives, Eur. J. Pharmacol. 442 (2002) 23–27.
[26] J.W. Lewis, S.M. Husbands, The orvinols and related opioids - high affinity ligands with diverse efficacy profiles, Curr. Pharmaceut. Des. 10 (2004) 717–732.
[27] S.M. Husbands, Buprenorphine and related orvinols, in: Research and Development of Opioid-Related Ligands, ACS Symposium series Washington DC, 2013, pp. 127–144.
[28] A. Coop, I. Berzetei-Gurske, J. Burnside, L. Toll, J.R. Traynor, S.M. Husbands, J.W. Lewis, Structural determinants of opioid activity in the orvinols and related structures. Ethers of 7,8-cyclopenta-fused analogs of buprenorphine, Helv. Chim. Acta 83 (2000) 687–693.
[29] B.M. Greedy, F. Bradbury, M.P. Thomas, K. Grivas, G. Cami-Kobeci, A. Archambeau, K. Bosse, M.J. Clark, M. Aceto, J.W. Lewis, J.R. Traynor, S.M. Husbands, Orvinols with mixed kappa/mu opioid receptor agonist activity, J. Med. Chem. 56 (2013) 3207–3216.
[30] X. Cui, A. Yeliseev, R. Liu, Ligand interaction, binding site and G protein activation of the mu opioid receptor, Eur. J. Pharmacol. 702 (2013) 309–315.
[31] J. Marton, Z. Szabó, S. Hosztafi, Herstellung von 6,14 Ethenomorphinan-derivaten, Liebigs Ann. Chem. (1993) 915–919, 1993.
[32] J. Marton, S. Hosztafi, S. Berényi, C. Simon, S. Makleit, Herstellung von 6,14-Ethenomorphinan- derivaten, Monatsh. Chem. 125 (1994) 1229–1239.
[33] J. Marton, C. Simon, S. Hosztafi, Z. Szabó, Á. Márki, A. Borsodi, S. Makleit, New nepenthone and thevinone derivatives, Bioorg. Med. Chem. 5 (1997) 369–382.
[34] V. Kumar, I.E. Ridzwan, K. Grivas, J.W. Lewis, M.J. Clark, C. Meurice, C. Jimenez-Gomez, I. Pogozheva, H. Mosberg, J.R. Traynor, S.M. Husbands, Selectively promiscuous opioid ligands: discovery of high affinity/low efficacy opioid ligands with substantial nociceptin opioid peptide receptor affinity, J. Med. Chem. 57 (2014) 4049–4057.
[35] A.P. Feinberg, I. Creese, S.H. Snyder, The opiate receptor: a model explaining structure-activity relationships of opiate agonists and antagonists, Proc. Natl. Acad. Sci. 11 (1976) 4215–4219.
[36] J.W. Lewis, K.W. Bentley, A. Cowan, Narcotic analgesics and antagonists, Annu. Rev. Pharmacol. 11 (1971) 241–270.
[37] J.J. Kopcho, J.C. Schaeffer, Selective *O*-demethylation of 7.alpha.-(aminomethyl)-6,14-*endo*-ethenotetrahydrothebaine, J. Org. Chem. 51 (1986) 1620–1622.
[38] S.W. Breeden, A. Coop, S.M. Husbands, J.W. Lewis, 6-*O*-demethylation of the thevinols with lithium aluminum hydride: selective demethylation of a tertiary alkyl methyl ether in the presence of an aryl methyl ether, Helv. Chim. Acta 82 (1999) 1978–1980.
[39] J.R. Traynor, L. Guo, A. Coop, J.W. Lewis, J.H. Woods, Ring-constrained orvinols as analogs of buprenorphine: differences in opioid activity related to configuration of C20 hydroxyl group, J. Pharmacol. Exp. Therapeut. 291 (1999) 1093–1099.
[40] A.L. Hopkins, C.R. Groom, A. Alex, Ligand efficiency: a useful metric for lead selection, Drug Discov. Today 9 (2004) 430–431.
[41] S. Hwang, J.-C. Thill, Using fuzzy clustering methods for delineating urban housing submarkets, in: GIS: Proceedings of the ACM International Symposium on Advances in Geographic Information Systems, 2007.
[42] B. Worley, S. Halouska, R. Powers, Utilities for quantifying separation in PCA/PLS-DA scores plots, Anal. Biochem. 433 (2013) 102–104.
[43] J.D. Durrant, M.J. A, BINANA: a novel algorithm for ligand-binding characterization, J. Mol. Graph. Model. 29 (2011) 888–893.
[44] V. Sobolev, A. Sorokine, J. Prilusky, E.E. Abola, M. Edelman, Automated analysis of interatomic contacts in proteins, Bioinformatics 15 (1999) 327–332.
[45] M. Spetea, I.P. Berzetei-Gurske, E. Guerrieri, H. Schmidhammer, Discovery and pharmacological evaluation of a diphenethylamine derivative (HS665), a highly potent and selective κ opioid receptor agonist, J. Med. Chem. 55 (2012) 10302–10306.
[46] H.A. Oktem, J. Moitra, S. Benyhe, G. Tóth, A. Lajtha, A. Borsodi, Opioid receptor labeling with the chloromethyl ketone derivative of [^{3}H]Tyr-D-Ala-Gly-(Me) Phe-Gly-Ol (DAMGO) II: covalent labeling of Mu opioid binding site by ^{3}H-Tyr-D-Ala-Gly-(Me)Phe chloromethyl ketone, Life Sci. 48 (1991) 1763–1768.
[47] E. Guerrieri, J.R. Mallareddy, G. Tóth, H. Schmidhammer, M. Spetea, Synthesis and pharmacological evaluation of [^{3}H]HS665, a novel, highly selective radioligand for the kappa opioid receptor, ACS Chem. Neurosci. 6 (2015) 456–463.
[48] S. Benyhe, J. Farkas, G. Tóth, M. Wollemann, Met5-enkephalin-Arg6-Phe7, an endogenous neuropeptide, binds to multiple opioid and nonopioid sites in rat brain, J. Neurosci. Res. 48 (1997) 249–258.
[49] E. Szűcs, A. Büki, G. Kékesi, G. Horváth, S. Benyhe, Mu-Opioid (MOP) receptor mediated G-protein signaling is impaired in specific brain regions in a rat model of schizophrenia, Neurosci. Lett. 619 (2016) 29–33.
[50] G. Kovács, Z. Petrovszki, J. Mallareddy, G. Tóth, G. Benedek, G. Horváth, Characterization of antinociceptive potency of endomorphin-2 derivatives with unnatural amino acids in rats, Acta Physiol. Hung. 99 (2012) 353–363.
[51] J. Marton, Z. Szabó, S. Garadnay, S. Miklós, S. Makleit, Studies on the synthesis of beta-thevinone derivatives, Tetrahedron 54 (1998) 9143–9152.
[52] S.E. Bove, S.L. Calcaterra, R.M. Brooker, C.M. Huber, R.E. Guzman, P.L. Juneau, D.J. Schrier, K.S. Kilgore, Weight bearing as a measure of disease progression and efficacy of anti-inflammatory compounds in a model of monosodium iodoacetate-induced osteoarthritis, Osteoarthritis Cartilage 11 (2003) 821–830.
[53] D.A. Kalbhen, Chemical model of osteoarthritis - a pharmacological evaluation, J. Rheumatol. 14 (1987).
[54] E. Perola, P.S. Charifson, Conformational analysis of drug-like molecules bound to proteins: an extensive study of ligand reorganization upon binding, J. Med. Chem. 47 (2004) 2499–2510.
[55] M.C. Ng, S. Fong, S.W. Siu, PSOVina: the hybrid particle swarm optimization algorithm for protein-ligand docking, J. Bioinf. Comput. Biol. 13 (2015) 1541007.
[56] O. Trott, A.J. Olson, AutoDock Vina, Improving the speed and accuracy of docking with a new scoring function, efficient optimization and multithreading, J. Comput. Chem. 31 (2010) 455–461.
[57] M.F. Sanner, Python: a programming language for software integration and development, J. Mol. Graph. Model. 17 (1999) 57–61.
[58] W.P. Feinstein, M. Brylinski, Calculating an optimal box size for ligand docking and virtual screening against experimental and predicted binding pockets, J. Cheminf. 7 (2015).
[59] M.M. Jaghoori, B. Bleijlevens, S.D. Olabarriaga, 1001 Ways to run AutoDock Vina for virtual screening, J. Comput. Aided Mol. Des. 30 (2016), 273-249.
[60] R.C. Team, R: A Language and Environment for Statistical Computing, R Foundation for Statistical Computing, Vienna., 2018.
[61] S. Lê, J. Josse, F. Husson, FactoMineR: an R package for multivariate analysis, J. Stat. Software 25 (2008) 1–18.
[62] K. Alboukadel, F. Mundt, Factoextra: Extract and Visualize the Results of Multivariate Data Analyses. R. Package Version 1.0.5, 2017.
[63] D. Adler, D. Murdoch, Rgl: 3D Visualization Using OpenGL. R. Package Version 0.100.19, 2019, 2019.
[64] J. Weiner, Pca3d: Three Dimensional PCA Plots. R Package Version 0.10, 2017.
[65] N.M. O'Boyle, M. Banck, C.A. James, C. Morley, T. Vandermeersch, G.R. Hutchison, Open Babel: an open chemical toolbox, J. Cheminf. 3 (2011).

II.

Edina Szűcs, Azzurra Stefanucci, Marilisa Pia Dimmito, Ferenc Zádor, Stefano Pieretti, Gokhan Zengin, László Vécsei, Sándor Benyhe, Adriano Mollica (2020) **Discovery of Kynurenines containing oligopeptides as potent opioid receptor agonists.** BIOMOLECULES, 10:1-18.

biomolecules

MDPI

Article

Discovery of Kynurenines Containing Oligopeptides as Potent Opioid Receptor Agonists

Edina Szűcs [1,2], Azzurra Stefanucci [3,*], Marilisa Pia Dimmito [3], Ferenc Zádor [1], Stefano Pieretti [4], Gokhan Zengin [5], László Vécsei [6], Sándor Benyhe [1], Marianna Nalli [7] and Adriano Mollica [3]

1 Institute of Biochemistry, Biological Research Center, Hungarian Academy of Sciences, Temesvári krt. 62., H-6726 Szeged, Hungary; szucs.edina@brc.hu (E.S.); zador.ferenc@brc.hu (F.Z.); benyhe.sandor@brc.hu (S.B.)

2 Doctoral School of Theoretical Medicine, Faculty of Medicine, University of Szeged, Dómtér 10, H-6720 Szeged, Hungary

3 Department of Pharmacy, University of Chieti-Pescara "G. d'Annunzio", Via dei Vestini 31, 66100 Chieti, Italy; marilisa.dimmito@unich.it (M.P.D.); a.mollica@unich.it (A.M.)

4 National Center for Drug Research and Evaluation, Istituto Superiore di Sanità, Viale Regina Elena 299, 00161 Rome, Italy; stefano.pieretti@iss.it

5 Department of Biology, Science Faculty, Selcuk University, 42250 Konya, Turkey; gokhanzengin@selcuk.edu.tr

6 MTA-SZTE Neuroscience Research Group, Department of Neurology, Interdisciplinary Excellence Centre, Faculty of Medicine, University of Szeged, H-6725 Szeged, Hungary; vecsei.laszlo@med.u-szeged.hu

7 Laboratory affiliated with the Institute Pasteur Italy-Cenci Bolognetti Foundation, Department of Drug Chemistry and Technologies, Sapienza University of Rome, Piazzale Aldo Moro 5, I-00185 Roma, Italy; marianna.nalli@uniroma1.it

* Correspondence: a.stefanucci@unich.it

Received: 27 December 2019; Accepted: 6 February 2020; Published: 12 February 2020

Abstract: Kynurenine (kyn) and kynurenic acid (kyna) are well-defined metabolites of tryptophan catabolism collectively known as "kynurenines", which exert regulatory functions in host-microbiome signaling, immune cell response, and neuronal excitability. Kynurenine containing peptides endowed with opioid receptor activity have been isolated from natural organisms; thus, in this work, novel opioid peptide analogs incorporating L-kynurenine (L-kyn) and kynurenic acid (kyna) in place of native amino acids have been designed and synthesized with the aim to investigate the biological effect of these modifications. The kyna-containing peptide (**KA1**) binds selectively the μ-opioid receptor with a Ki = 1.08 ± 0.26 (selectivity ratio μ/δ/κ = 1:514:10000), while the L-kyn-containing peptide (**K6**) shows a mixed binding affinity for μ, δ, and κ-opioid receptors, with efficacy and potency (E_{max} = 209.7 + 3.4%; $LogEC_{50}$ = −5.984 + 0.054) higher than those of the reference compound DAMGO. This novel oligopeptide exhibits a strong antinociceptive effect after i.c.v. and s.c. administrations in in vivo tests, according to good stability in human plasma ($t_{1/2}$ = 47 min).

Keywords: peptides; kynurenines; binding affinity; μ-opioid receptor; pharmacophore; G-protein activation

1. Introduction

The kynurenine pathway (KP) is an essential part of the tryptophan metabolism in mammalian tissues, where it is responsible for the formation of two principal metabolites, namely, L-kynurenine (kyn) and kynurenic acid (kyna). Kyn can arise in peptides and proteins by post/translational modifications or direct oxidation of tryptophan. It is present in lens crystallins, human Cu^{2+}/Zn^{2+}

dismutase, milk proteins, actin oxidized in vivo, and several bioactive compounds produced by bacteria and marine organisms [1]. Daptomycin is a cyclic kyn-containing lipodepsipeptide approved by the Food and Drug Administration (FDA), isolated from *Streptomyces roseoporus* used in the treatment of Gram-positive pathogen skin infections [2]. Cyclomontanin B isolated from *Annona montana* exhibits promising anti-inflammatory activity [3]. The kyn-containing peptide FP-Kyn-L-NH_2 is the minor component of Australian red tree frog skin *Litoria rubella* collected in central Australia, endowed with opioid activity at 10^{-7} M (Figure 1) [4].

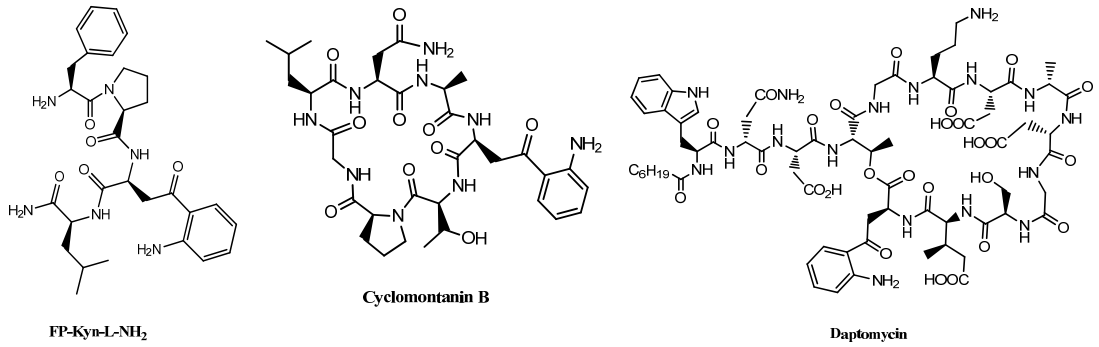

Figure 1. Natural bioactive compounds containing kyn residue.

The occurrence of kyn in natural products suggests a possible specificity towards their biological targets. The enzymes of the human kynurenine pathway are expressed in different tissues and cell types throughout the body [1]. In humans, the majority of kyn is excreted by urine; thus, its bioavailability increases according to the tryptophan flux downstream of the KP [5]. Kyn is able to penetrate the central nervous system (CNS) by transport across the blood–brain barrier (BBB), but it is also produced locally [6].

Kyna has been originally discovered in canine urine, but a huge amount has been measured in the gut, bile, human saliva, synovial and amniotic fluid; it has also been detected in food products such as broccoli, some potatoes, and honeybee products [1]. Kyna possesses an antagonistic effect on the N-methyl-D-aspartate (NMDA) receptor and other glutamate receptors such as AMPA and kainate receptors [7,8]. Kyna is also found to have an agonistic effect on the G protein coupled receptor GPR35 [9,10], which can be found in various tissues and organs such as gastrointestinal tract, liver, immune system, central nervous system, and cardiovascular system [11]. NMDA receptors are essential for the control of the glutamatergic work at the CNS; in contrast to the kainate and AMPA receptors, the NMDA mediates the influx of Ca^{2+} ions into neurons, playing an important role in synaptic plasticity, memory, and learning [7,8]. Overactivation of NMDA receptors can lead to excitotoxicity, severe cell damage, and apoptosis of neurons, which are strongly related to neurodegenerative and CNS disorders such as depression, stroke, ischemia, and neuropathic pain [10–12]. Different therapeutic approaches based on thekynurenine pathway have been postulated to circumvent this problem, such as the use of kynurenic acid prodrugs or analogs able to penetrate more readily than the parent compounds or the involvement of ascorbate conjugation to promote the interaction of kyna with SVCT2 transport protein [13–15]. Intracisternal kyna attenuates formalin-induced nociception in animals together with antagonist activity at the glycine binding site of NMDA, which is associated with analgesic properties in rats [16]. At the peripheral sites, kyna decreases the nociceptive behavior in the tail flick and hot plate tests [16]. Administration of L-kyn and probenecid together with kyna analogs inhibits NMDA receptors in animal models of trigeminal activation and sensitization [17]. Noteworthy, kyna and its analogs are able to act on second-order neurons, decreasing mechanical allodynia and pain sensitivity in different animal pain models [18]. Considering the presence of kyn residue in natural peptide sequences and the important role exerted by both kynurenines at the CNS [19–21], we plan to investigate the biological consequences of the insertion of these residues in opioid pharmacophoric sequences. Kyn could be used in place of

phenylalanine, considering its aromatic side chain, whereas kyna could be used as *C*-terminus to mimic an additional aromatic residue. In this preliminary work, we performed the synthesis and biological screening of six novel kynurenines containing peptides, aiming to investigate the modifications imposed by the presence of kyn and kyna on the biological properties of known endogenous and synthetic opioid peptides in vivo and in vitro. Peptide **KA1** retains the DAMGO primary sequence, but the OH terminal group is esterified by kynurenic acid. Peptides **K2** and **K3** are EM-2 analogs in which the Phe residues in positions 3 and 4 have been replaced with kyn and kyn *C*-terminal amides, respectively. Peptides **K4–K6** are enkephalin-like peptides containing kyn in position 5, bearing as *C*-terminal the methyl ester, acid, and amide group, respectively. The novel chemical entities were prepared following solution phase peptide synthesis and were obtained as TFA salts in good overall yields and excellent purities.

2. Materials and Methods

2.1. Chemistry

All reagents and solvents were acquired from Sigma-Aldrich (Milano, Italy). Solution phase peptide synthesis was applied to prepare the final products **KA1, K2–K6** as TFA salts, following the procedures reported below. Boc-protected intermediates were purified by silica gel column chromatography where necessary, or by trituration in Et_2O. Final products **KA1**, **K2–K6** were purified by RP–HPLC on a Waters XBridge BEH130 (C18 5.0 μm, 250 × 10 mm column; flow rate of 7 mL/min; Waters Binary pump 1525; eluent: linear gradient of H_2O/ACN 0.1% TFA, ranging from 5% to 95% ACN in 32 min). The purity of the N^{α}-Boc-protected products was confirmed by NMR analysis on a Varian Mercury 300 MHz. The purity of all final compounds was assessed by NMR analysis, ESI–LRMS, and by analytical RP–HPLC (C18-bonded 4.6 × 150 mm; flow rate of 1 mL/min; eluent: gradient of H_2O/ACN 0.1% TFA, ranging from 5% to 95% ACN in 26 min, recorded at 254, 275, and 213 nm and was found to be ≥95%). The mass spectrometry (MS) equipment was composed as follows: LCQ Thermo Finnigan ion trap mass spectrometer (San Jose, CA, USA) with an electrospray ionization (ESI) source; capillary temperature: 300 °C; spray voltage: 4.00 kV; nitrogen (N_2) as the sheath and auxiliary gas.

2.2. General Procedures

2.2.1. Formation of Ethanolamine-Kynurenic Acid Ester

Kynurenic acid (2 mmol, 1 equiv.) was dissolved in DMF (5 mL) stirring in agitation at 0 °C, then a mixture of Boc-*N*-aminoethanol (2 mmol, 1 equiv.) and DMAP (0.6 mmol, 0.3 equiv.) in DMF (3 mL) was transferred in the round bottom flask. After 10 min, EDC·HCl (2.2 mmol, 1.1 equiv.) was added to the reaction mixture in agitation at 0 °C for 10 min, then at r.t. overnight. The solvent was removed in a rotary evaporator and the oily residue was taken up with EtOAc and washed with 5% citric acid solution (3 times), $NaHCO_3$ s.s. (3 times), and NaCl s.s. (3 times). Organic phases were collected and dried on Na_2SO_4 anhydrous, filtered and dried in rotavapor and high vacuum to give a yellow oily product. The crude product was triturated with Et_2O (2 times), the aqueous layer filtered up, and the white solid product dried in a rotary evaporator and high vacuum.

2.2.2. Coupling Reaction

Boc-protected compound (1.1 equiv.) was dissolved in DMF (5 mL) in an iced-cooled bottom flask, then EDC·HCl (1.1 equiv.) and HOBt hydrate (1.1 equiv.) were added stirring for 10 min. A solution of *N*-terminal free intermediate (1 equiv.) and DIPEA (3.3 equiv.) in DMF (5 mL) was transferred in the ice-cooled bottom flask at 0 °C and allowed to react at r.t. overnight. The solvent was removed in a rotary evaporator; the oily residue was taken up with EtOAc and washed with 5% citric acid solution (3 times), $NaHCO_3$ s.s. (3 times), and NaCl s.s. (3 times). Organic phases were collected and dried on Na_2SO_4 anhydrous, filtered and dried in a rotavapor and high vacuum to give

a yellow oily product. The crude product was triturated with Et_2O (2 times), the aqueous layer filtered up and the white solid product dried in a rotary evaporator and high vacuum.

2.2.3. Amidation

The Boc-protected or free *N*-terminal compound (1 equiv.) was dissolved in THF (7 mL) stirring at −15 °C, then NMM (2.5 equiv.) and *i*BCF (2.1 equiv.) were added to the solution allowing to react for 30 min. Then NH_4OH aq. solution (0.21 mL) was added to the reaction mixture at −15 °C for 30 min. The reaction mixture was allowed to react at r.t. for 2 h. The solvent was removed in rotavapor and the solid residue was dissolved in EtOAc washing with 5% citric acid solution (3 times), $NaHCO_3$ s.s. (3 times), and NaCl s.s. (3 times). Organic phases were collected and dried on Na_2SO_4 anhydrous, filtered and dried in a rotavapor and high vacuum to give a yellow oily product. The crude product was triturated with Et_2O (2 times), the aqueous layer filtered up, and the product dried in a rotary evaporator and high vacuum to give a white solid product.

2.2.4. Saponification

Boc-protected compound (0.1 mmol, 1 equiv.) was dissolved in THF (5 mL) stirring at r.t. then NaOH 1M (4 equiv.) was added dropwise, allowing it to react for 3 h. The solvent was removed in a rotavapor; the oily residue was taken up with water and washed with Et_2O (2 times). The aqueous solution was acidified with HCl 1 M until complete precipitation of the solid residue, which was extracted with EtOAc 3 times. The organic layers were collected, dried on Na_2SO_4 anhydrous, filtered and dried in a rotavapor and high vacuum to give a white solid product.

2.3. Synthesis and Characterization

Description of the reaction procedures [22–24] and compounds characterization are reported in detail in the Supplementary Materials.

2.4. In Vitro Biological Assays

2.4.1. Chemicals

Tris-HCl, EGTA, NaCl, $MgCl_2 \cdot 6H_2O$, GDP, the GTP analog GTPγS, and the L-tryptophan metabolite kynurenic acid were from Sigma-Aldrich (Budapest, Hungary); Tyr-D-Ala-Gly-(NMe)Phe-Gly-ol (DAMGO) was purchased from Bachem Holding AG (Bubendorf, Switzerland); endomorphin-2 (EM-2) was kindly provided by MTA-ELTE Research Group of Peptide Chemistry (Budapest, Hungary); Ile^{5,6}-deltorphine II (Ile^{5,6}Delt II) was purchased from Isotope Laboratory of BRC (Szeged, Hungary); and the highly selective KOR agonist diphenethylamine derivative, HS665 [25], was offered by Dr. Helmut Schmidhammer (University of Innsbruck, Austria). Naloxone was provided by Endo Laboratories DuPont de Nemours (Wilmington, DE, USA). The non-competitive NMDA antagonist, (+)-MK 801 maleate (MK-801) and L-kynurenine (L-kyn) were obtained from Tocris Bioscience (Bristol, UK). A solution of each ligand in water was stored in 1 mM stock solution at –20 °C. The radiolabelled GTP analog, [^{35}S]GTPγS (specific activity: 1000 Ci/mmol), was acquired from Hartmann Analytic (Braunschweig, Germany). [^{3}H]DAMGO [26] (specific activity: 38.8 Ci/mmol), [^{3}H]Ile^{5,6}Delt II (specific activity: 19.6 Ci/mmol), and [^{3}H]HS665 [27] (specific activity: 13.1 Ci/mmol) were radiolabelled in the Isotope Laboratory of BRC (Szeged, Hungary). [^{3}H]MK-801 [28] (specific activity: 30 Ci/mmol) was purchased from PerkinElmer (Boston, MA, USA) and the UltimaGold™ MV aqueous scintillation cocktail was from PerkinElmer (Boston, MA, USA).

2.4.2. Animal

Male and female Wistar rats and guinea pigs were used for membrane preparations. The animals were guarded in a temperature-controlled room, ranging from 21 to 24 °C, under a 12:12 light and dark cycle with water and food ad libitum. All housing and experiments were conducted in accordance with the European Communities Council Directives (86/606/ECC) and the Hungarian Act

for the Protection of Animals in Research (XXVIII.tv. 32.§). The total number of animals, as well as their suffering, was minimized whenever possible.

2.4.3. Preparation of Brain Samples for Binding Assays

Rats and guinea pigs were decapitated, and their brains were quickly removed. The brains were used for membrane preparation following the procedure reported by Benyhe [29] for binding and [^{35}S]GTPγS binding experiments, in agreement with the protocol of Zádor et al. [30].

Homogenization of brains was performed in 30 volumes (*v*/*w*) of ice-cold 50 mM Tris-HCl pH 7.4 buffer with a Teflon-glass Braun homogenizer at 1500 rpm. The centrifuge was settled at 18000 rpm for 20 min at 4 °C, the resulting supernatant discarded, and the pellet taken up in the original volume of Tris-HCl buffer. Incubation of homogenate at 37 °C for 30 min was performed in a shaking water-bath. Five volumes of 50 mM Tris-HCl pH 7.4 buffer were used to suspend the final pellet at −80 °C. For the [^{35}S]GTPγS binding experiments, the brains were homogenized with a Dounce in 5 volumes (*v*/*w*) of ice-cold TEM (Tris-HCl, EGTA, $MgCl_2$) at −80 °C. The protein content of the membrane preparation was determined by the method of Bradford, BSA being used as a standard [31].

2.4.4. Receptor Binding Assays

Functional [^{35}S]GTPγS Binding Experiments

The functional [^{35}S]GTPγS binding experiments were performed as previously described [32,33]. Briefly the membrane homogenates were incubated at 30 °C for 60 min in Tris-EGTA buffer (pH 7.4) composed of 50 mM Tris-HCl, 1 mM EGTA, 3 mM $MgCl_2$, 100 mM NaCl, containing 20 MBq/0.05 cm^3 [^{35}S]GTPγS (0.05 nM) and increasing concentrations (10^{-10} to 10^{-5} M) of ligands. The experiments were performed in the presence of excess GDP (30 μM) in a final volume of 1 mL. Total binding was measured in the absence of test compounds, non-specific binding was determined in the presence of 10 μM unlabeled GTPγS. The reaction was terminated by rapid filtration under vacuum and washed three times with 5 mL ice-cold 50 mM Tris-HCl (pH 7.4) buffer through Whatman GF/B glass fibers. The radioactivity of the filters was detected in an UltimaGold™ MV aqueous scintillation cocktail with a Packard Tricarb 2300TR liquid scintillation counter.

Binding Experiments

In MOR, DOR, and KOR displacement, aliquots of frozen rat and guinea pig brain membrane homogenates were thawed and suspended in 50 mM Tris-HCl buffer (pH 7.4); in NMDA displacement, the Tris-HCl buffer (pH 7.4) contained 100 μM glycine and 100 μM L-glutamic acid. Samples were incubated in the presence of the unlabeled ligands in increasing concentrations (10^{-10} to 10^{-5} M) for at 35 °C for 45 min with [^{3}H]DAMGO, for at 35 °C for 45 min with [^{3}H]Ile^{5,6}Delt II, at 25 °C for 30 min with [^{3}H]HS665, and at 25 °C for 120 min with [^{3}H]MK-801. The non-specific and total binding was determined in the presence and absence of 10 μM unlabelled naloxone (MOR and DOR), HS665 (KOR), and MK-801 (NMDA). Radioactivity of the filter disks was measured, as written above.

Data Analysis

Experimental data are presented as means ± S.E.M. Sigmoid dose-response curves were fitted with GraphPad Prism 5.0 (GraphPad Prism Software Inc., San Diego, CA, USA). An unpaired *t*-test with two-tailed *p* value was performed to determine the significance level. In the competition binding assays, the 'One site competition' fitting was used to establish the equilibrium binding affinity (K_i value).

2.5. In Vivo Tests

2.5.1. Animals

In our experiments, we used CD-1 male mice (Harlan, Italy, 25–30 g) maintained in colony, housed in cages (7 mice per cage) under standard light/dark cycle (from 7:00 a.m. to 7:00 p.m.), temperature (21 ± 1 °C) and relative humidity (60% ± 10%) for at least 1 week. Food and water were available ad libitum. The Service for Biotechnology and Animal Welfare of the Istituto Superiore di Sanità and the Italian Ministry of Health authorized the experimental protocol according to Legislative Decree 26/14.

2.5.2. Treatment Procedure

DMSO was purchased from Merck (Rome, Italy). Peptides solutions were freshly prepared using saline containing 0.9% NaCl and DMSO in the ratio DMSO/saline 1:5 *v*/*v* every experimental day. These solutions were injected at a volume of 10 μL/mouse for intracerebroventricular (i.c.v.) administrations or at a volume of 20 μL/mouse for subcutaneous administrations.

2.5.3. Surgery for i.c.v. Injections

For i.c.v. injections, mice were lightly anesthetized with isoflurane, and an incision was made in the scalp, and the bregma was located. Injections were performed using a 10 μL Hamilton microsyringe equipped with a 26-gauge needle, 2 mm caudal and 2 mm lateral from the bregma at a depth of 3 mm.

2.5.4. Tail Flick Test

The tail flick latency was obtained using a commercial unit (Ugo Basile, Gemonio, Italy), consisting of an infrared radiant light source (100 W, 15 V bulb) focused onto a photocell utilizing an aluminum parabolic mirror. During the trials, the mice were gently hand-restrained using leather gloves. Radiant heat was focused 3–4 cm from the tip of the tail, and the latency (s) of the tail withdrawal to the thermal stimulus was recorded. The measurement was interrupted if the latency exceeded the cut off time (15 s at 15 V). The baseline latency was calculated as mean of three readings recorded before testing at intervals of 15 min and the time course of latency determined at 15, 30, 45, 60, 90, and 120 min after treatment. Data were expressed as time course of the maximum percentage effect (%MPE) = (post-drug latency − baseline latency)/(cut-off time − baseline latency) × 100.

2.5.5. Formalin Test

In the formalin test, the injection of a dilute solution of formalin (1%, 20 μL/paw) into the dorsal surface of the mouse hind paw evoked biphasic nociceptive behavioral responses, such as licking, biting the injected paw, or both, occurring from 0 to 10 min after formalin injection (the early phase) and a prolonged phase, occurring from 15 to 40 min (the late phase). Before the test, mice were individually placed in a Plexiglas observation cage (30 × 14 × 12 cm) for one hour, to acclimatize to the testing environment. The total time the animal spent licking or biting its paw during the early and late phase of formalin-induced nociception was recorded.

2.5.6. Data Analysis and Statistics

Experimental data were expressed as mean ± s.e.m. In the tail flick test, significant differences among the groups were evaluated with two-way ANOVA followed by Sidak's multiple comparisons test. Formalin test data were analyzed by using one-way ANOVA, followed by Holm–Sidak's multiple comparisons test. GraphPad Prism 6.03 software was used for all the analyses. Statistical significance was set at $p < 0.05$. The data and statistical analysis comply with the recommendations on experimental design and analysis in pharmacology.

2.6. Stability in Human Plasma Sample Preparation

Five microliters of **K6** (500 μg in 250 μL of water) were added to 45 μL of fresh human plasma, then incubated at 37 ± 1° C. Prepared samples were removed at several designated time points and

incubation was stopped by adding an equal volume of the sequencing mixture (5% aqueous $ZnSO_4$ solution, MeOH, and ACN; 5:3:2), which precipitated proteins, to achieve a final concentration of 100 μg/mL. The mixture was vortexed and centrifuged at 12000× *g* for 5 min, then 20 μL of clear supernatant was directly injected into the HPLC system (Waters model 600 solvent pump and 2996 photodiode array detector, with XBridge BEH 130 C18, 4.6 × 250 mm, 5 μm). The samples were tested in three independents experiments (n = 3) and reported values represent the mean ± standard error (SEM). Data were analysed using simple regression analysis (significant deviation from zero: $F_{1,13}$ = 171.9, $p < 0.0001$; Y = −0.9705 × X + 95.98).

3. Results and Discussion

3.1. Chemistry

Simple modifications of kyna scaffold through the insertion of aromatic substituents [34], *C*-terminal derivatization as methyl ester [35], or amide bearing a water-soluble side chain [36] have been abundantly documented in the literature, rather than the insertion of kyna into a peptide sequence. On the contrary, different papers highlight the scarce propensity of the kyn carboxylic group to react with *N*-terminus free amino acids involved in the coupling reaction, which renders this unusual amino acid difficult to manage as a building block for peptide synthesis [22,23].

Taking this in mind, we focused our attention on the functionalization of kyna via a variant of Steglich esterification with the previously prepared Boc-protected 2-aminoethanol [23] so as to obtain intermediate **2** in 60% yield after purification by column chromatography (see General Procedure) [24]. Compound **2** was deprotected with a mixture of TFA:DCM = 1:1 at r.t. for 1 h and the so obtained intermediate was coupled with Boc-*N*(Me)Phe-OH, following the standard procedure for coupling reaction [36].

Peptide elongation/deprotection steps were repeated to reach the complete Boc-protected peptide **6** in 66% yield, starting from intermediate compound **5,** after silica gel column chromatography (Scheme 1). The final peptide **KA1** has been obtained in 71% yield after RP–HPLC purification. The purity of the sample was assessed by analytical RP–HPLC recorded at 254 nm and was found to be ≥95%.

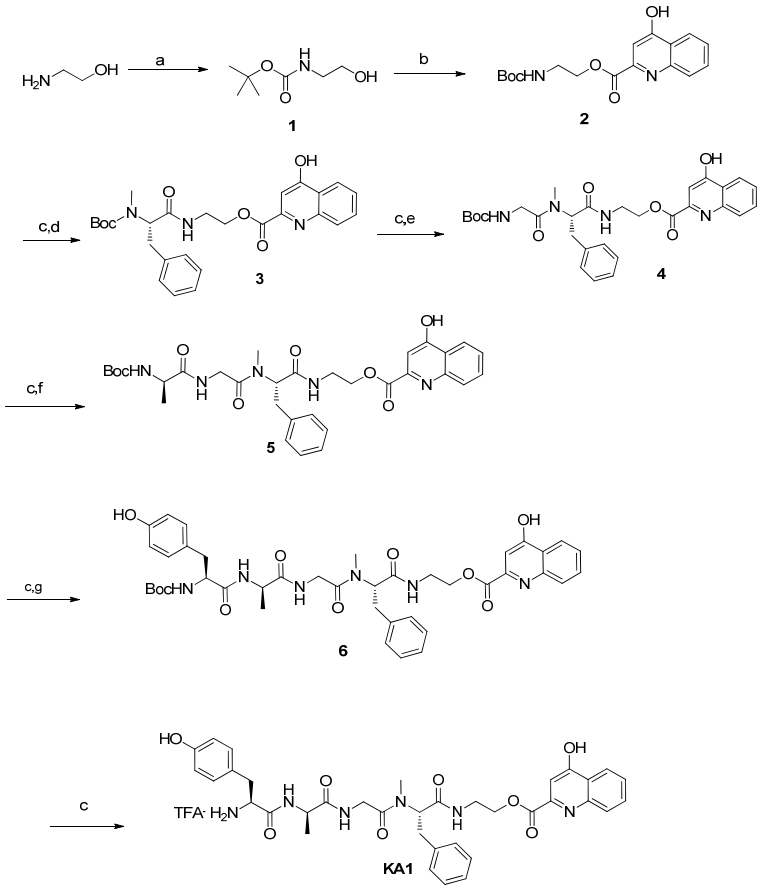

Scheme 1. Synthesis of peptide **KA1**. Reagents and conditions: (**a**) Boc_2O, NaOH 1 M, THF, 10 min at 0 °C, then 16 h at r.t. quantitative; (**b**) kynurenic acid, EDC·HCl, DMAP, DMF, 10 min at 0 °C, then 36 h at r.t., 60% yield after silica gel column chromatography; (**c**) TFA/DCM 1:1 1 h at r.t. quantitative; (**d**) Boc-*N*-Me-Phe-OH, EDC·HCl, HOBt, DIPEA, DMF, 10 min at 0 °C, then 16 h at r.t., 75% yield after reaction work-up; (**e**) Boc-Gly-OH, EDC·HCl, HOBt, DIPEA, DMF, 10 min at 0 °C, then 16 h at r.t., 70% yield after reaction work-up; (**f**) Boc-DAla-OH, EDC·HCl, HOBt, DIPEA, DMF, 10 min at 0 °C, then 16 h at r.t., 80% yield after silica gel column chromatography; (**g**) Boc-Tyr-OH, EDC·HCl, HOBt, DIPEA, DMF, 10 min at 0 °C, then 16 h at r.t., 66% yield from **5**, after silica gel column chromatography.

Then L-kyn was converted in its Boc-derivative **7** following the procedure reported by Tsentalovich et al. [23] to prepare the EM-2 analogs **K2** and **K3** (Scheme 2). Firstly intermediate **7** was coupled with H-Phe-NH_2, previously prepared following the general procedure of amidation, to obtain intermediate **8** in 61% yield. The Boc-protecting group was removed from compound **8**, and the so obtained TFA salt was coupled with Boc-Pro-OH to give intermediate **9** in good yield (81%). Repeated steps of coupling/purification/deprotection afforded the final compound **K2** in 72% yield from **10**, and excellent purity after RP–HPLC purification of the crude product. Conversely, Boc-Kynurenine **7** was transformed in the amide Boc-derivative **11** in a 71% yield. Then it was deprotected with a mixture of TFA:DCM = 1:1 at r.t. for 1 h and the so obtained TFA salt was coupled with BocPhe-OH to afford intermediate **12** quantitatively. Then repeated steps of coupling/purification/deprotection were performed to reach peptide **K3** in high yield (83% from **14**) and excellent purity after RP–HPLC purification of the crude compound.

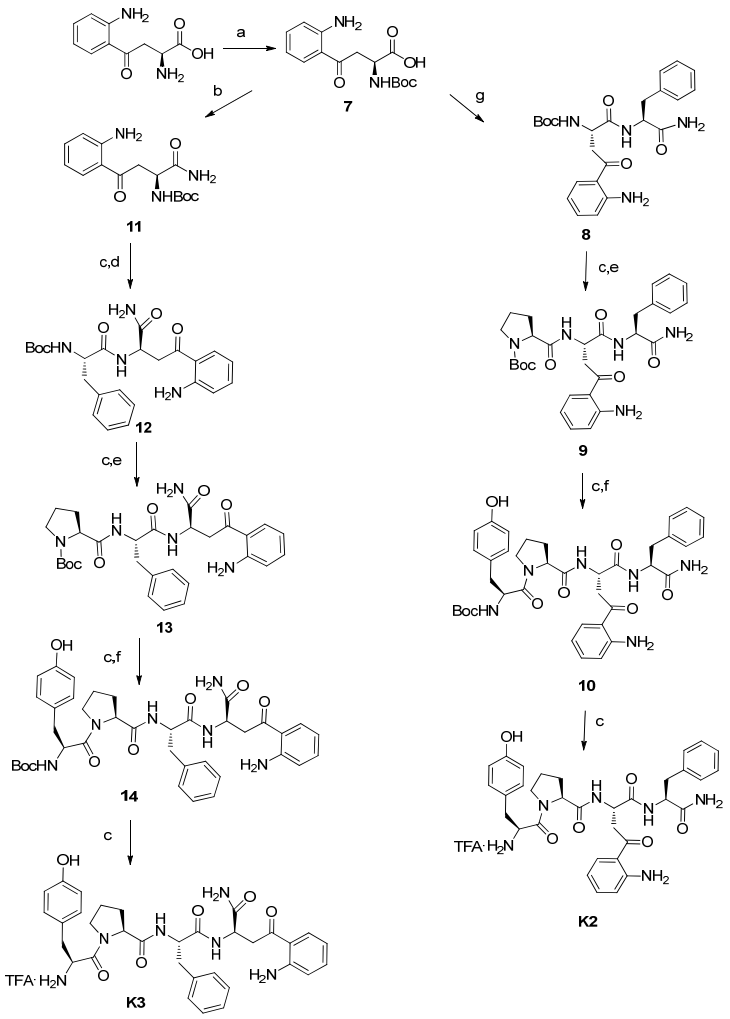

Scheme 2. Synthesis of peptides **K2, K3**. Reagents and conditions: (**a**) Boc_2O, $NaHCO_3$, NaOH 1 M, dioxane/H_2O (2:1), 10 min at 0 °C, then 30 min at r.t. quantitative; (**b**) *i*BCF, NMM, NH_4OH, THF, 30 min at −10°C, then 16 h at r.t., 71% yield after trituration; (**c**) TFA/DCM 1:1, 1 h at r.t. quantitative; (**d**) Boc-Phe-OH, EDC·HCl, HOBt, DIPEA, DMF, 10 min at 0 °C, then 16 h at r.t.-quantitative; (**e**) Boc-Pro-OH, EDC·HCl, HOBt, DIPEA, DMF, 10 min at 0 °C, 16 h at r.t., 72% yield for **13** after trituration, 81% yield for **9**; (**f**) Boc-Tyr-OH, EDC·HCl, HOBt, DIPEA, DMF, 10 min at 0 °C, 16 h at r.t., 95% yield for **14** after trituration, 73% yield for **10**; (**g**) H-Phe-NH_2, EDC·HCl, HOBt, DIPEA, DMF, 10 min at 0 °C, then 16 h at r.t., 61% yield from **7** after trituration.

Finally, linear peptides **K4–K6** have been synthesized as methyl ester, acid, and amide derivatives, respectively, starting from L-kyn methyl ester **15** (Scheme 3), prepared following the procedure described in the literature [24,36]. Repeated steps of deprotection/coupling reaction were performed to reach intermediate **19** in high yield after trituration in Et_2O. Boc group removal of intermediate **19** gave **K4** in good yield and excellent purity after RP–HPLC purification. Saponification of intermediate compound **19** afforded **20,** following the general procedure; the conversion of the latter in the amide **21** was performed as previously described by Stefanucci et al. [24]. Boc group removal of the linear peptides **20** and **21** afforded products **K5** and **K6** in good yields (72% and 52%, respectively), and excellent purity after RP–HPLC purification (98% and 96%, respectively).

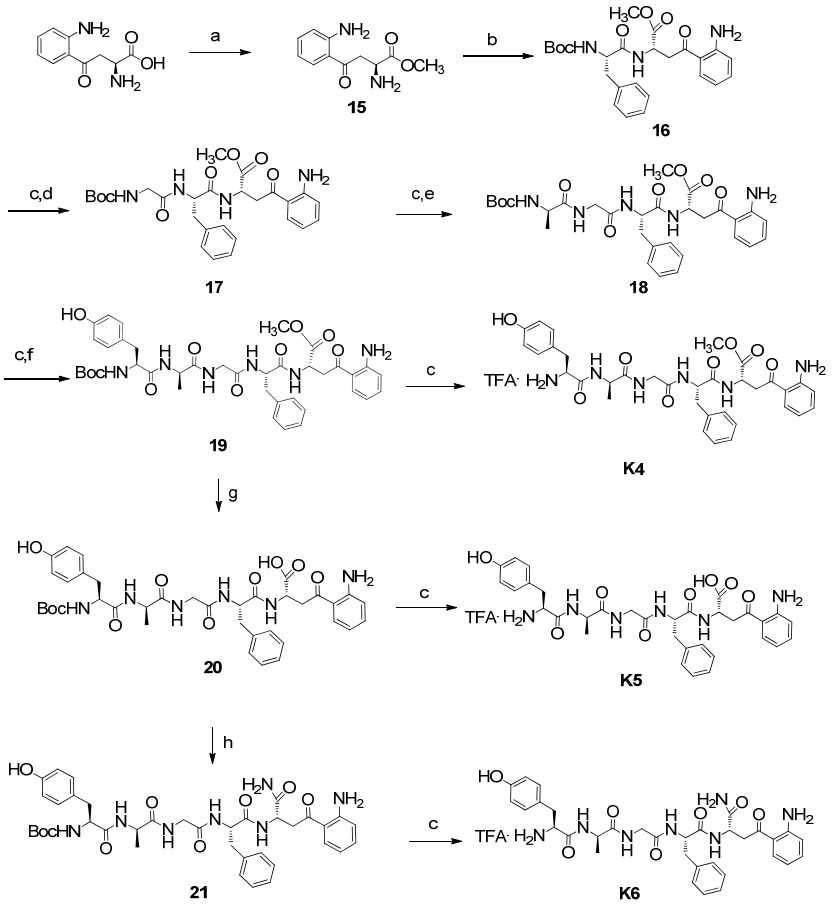

Scheme 3. Synthesis of linear peptides **K4–K6**. Reagents and conditions: (**a**) $SOCl_2$, MeOH, 30 min at 0 °C, 16 h at r.t., quantitative; (**b**) Boc-Phe-OH, EDC·HCl, HOBt, DIPEA, DMF, 10 min at 0 °C, then 16 h at r.t., 60% after silica gel column chromatography; (**c**) TFA/DCM 1:1, 1 h at r.t. quantitative; (**d**) Boc-Gly-OH, EDC·HCl, HOBt, DIPEA, DMF, 10 min at 0 °C, 16 h at r.t., quantitative; (**e**) Boc-DAla-OH, EDC·HCl, HOBt, DIPEA, DMF, 10 min at 0 °C, 16 h at r.t., 84% yield after silica gel column chromatography; (**f**) Boc-Tyr-OH, EDC·HCl, HOBt, DIPEA, DMF, 10 min at 0 °C, 16 h at r.t., 72% yield after trituration; (**g**) NaOH 1 M, THF, 3 h at r.t., quantitative; (**h**) *i*BCF, NMM, NH_4OH (aq), THF, 30 min at −15 °C, 2 h at r.t., 52% yield after trituration.

3.2. In Vitro Studies

3.2.1. Binding Assays

Kyna and its analog (KYNA1) previously reported by Zádor et al. did not directly bind μ, δ, κ-receptors in vitro [37]. However, after chronic and acute administration, they altered opioid receptor function in vivo and in vitro through the NMDA receptor co-localized in the cortex and striatum of mice and rats, though the interaction of opioid receptors and NMDA have been deeply discussed in the literature [37,38]. Kyna is able to bind to the NMDA receptor at micromolar affinity [38]. To test if our novel peptides are able to target both of these systems, they were examined in a receptor binding radioassay using highly specific tritium-labelled primary ligands for opioid and NMDA receptor binding sites. [^{3}H]DAMGO, [^{3}H]Ile^{5,6}Delt II, and [^{3}H]MK-801 equilibrium competition (displacement) studies were conducted in rat brain homogenates, while κ-opioid receptor tests were performed with [^{3}H]HS665 in guinea pig brain homogenates. The novel ligands showed similar equilibrium inhibitory affinities (K_i value) in the μ-opioid system as DAMGO except **K3** (Table 1, Figure S1A). In the δ-opioid system, the ligands showed lower binding affinity (higher Ki) compared to the selective δ-opioid receptor selective agonist Ile^{5,6}Delt II (Figure S1B). In the κ-opioid receptor system, the

compounds showed higher Ki values than that of the selective κ-opioid agonist HS665 (Figure S1C). In the NMDA receptor binding assays, the peptides did not produce any competing activity (Figure S1D). Peptide **KA1** possesses the best binding affinity, with a Ki value very close to that of the reference compound DAMGO (1.08 ± 0.26 nM vs. 0.90 ± 0.28 nM), suggesting that the insertion of kyna into the DAMGO sequence does not impair its binding potency at the μ-opioid receptor. The peptide **K6,** presenting the enkephalin-like structure linked to L-kyn *C*-terminal amide, is able to bind all three opioid receptors with significant affinity, showing a moderate preference for the μ-opioid receptor (affinity ratio 1:18:70 for μ, δ, k, respectively), whereas compounds **K4** and **K5** are able to bind only μ- and δ-opioid receptors. It is reasonable to believe that the *C*-terminal amide derivatization in peptide **K6** confers the ability to bind to the κ-opioid receptor. Concerning the endomorphin-2 (EM-2) analogs **K2** and **K3**, the replacement of Phe^3 with L-kyn improves the binding affinity and selectivity of **K2** for μ-opioid receptors with respect to the standard compound EM-2, with a weak affinity for κ-opioid receptors, while the incorporation of L-Kyn amide in position 4 causes the loss of selectivity for MOR in favor of a modest binding affinity for μ- and δ-opioid receptors. Peptide **K2** shows a Ki value two-folds lower than that of EM-2 on the μ-opioid receptor, which let us suppose the positive influence of L-Kyn in position 3 on **K2** binding ability.

Table 1. Displacement of [^{3}H]DAMGO, [^{3}H]Ile^{5,6}Delt II, [^{3}H]HS665, and [^{3}H]MK-801 by DAMGO, Ile^{5,6}Delt II, HS665, MK-801, and oligopeptides in membranes of rat and guinea pig brains. The IC_{50} values for the MOR, DOR, KOR, and NMDA, according to the competition binding curves (see Figure S1), were converted into equilibrium inhibitory constant (K_i) values using the Cheng–Prusoff [39] equation.

Ligand	K_i + S.E.M. (nM) Opioid System			NMDA System
	DAMGO [a]	Ile^{5,6}Delt II [a]	HS665 [b]	MK-801 [a]
DAMGO	0.90 ± 0.28	n.d. [c]	n.d. [c]	n.d. [c]
Ile^{5,6}Delt II	n.d. [c]	8.85 ± 0.77	n.d. [c]	n.d. [c]
HS665	n.d. [c]	n.d. [c]	2.38 ± 0.25	n.d. [c]
MK-801	n.d. [c]	n.d. [c]	n.d. [c]	11.45 ± 1.04
EM-2	3.16 ± 0.3	n.d. [c]	n.d.[c]	n.d. [c]
KYNA	n.d. [c]	n.d. [c]	n.d. [c]	>10000
L-kyn	n.d. [c]	n.d. [c]	n.d. [c]	>10000
KA1	1.08 ± 0.26	554.7 ± 0.8	>10000	>10000
K2	1.39 ± 0.30	>10000	1043 ± 0.3	>10000
K3	197.3 ± 0.36	158.8 ± 1.6	>10000	>10000
K4	2.29 ± 0.28	31.2 ± 0.7	>10000	>10000
K5	9.11 ± 0.32	94.4 ± 0.8	>10000	>10000
K6	1.84 ± 0.27	32.5 ± 0.8	127.7 ± 0.3	>10000

[a] rat brain membrane, [b] guinea pig brain membrane, [c] not determined.

3.2.2. Binding-Protein Activation Assays

The effect of kyn or kyna combined peptides on G-protein activation was investigated in functional [^{35}S]GTPγS binding assays in rat and guinea pig brain membranes. All ligands produced dose-dependent stimulations described by sigmoid curves (Figures S2). **K6** showed higher efficacy (E_{max}) than DAMGO (Table 2). Moreover, 10 μM cyprodime and 10 μM naltrindole, which are selective MOR and DOR antagonists, respectively [40,41], significantly reversed the agonist effects of the ligands in rat brain membrane homogenates (Figure S3A). In guinea pig brain membrane homogenates, the ligands did not activate G-protein except **K4** and **K6** (Figure S3B). Additionally, 10 μM norbinaltorphine decreased significantly the agonist effect of **K4** but did not change the effect of **K6** (Table 3). Altogether, these data reveal that peptide **KA1** acts as a selective μ-opioid agonist, being able to decrease the GTPγS binding percentage under the basal level in the presence of 10 μM cyprodime. Peptides **K2** and **K3** possess a mixed μ/δ agonist activity profile, while peptides **K4–K6** show a modest mixed μ/δ-opioid receptor agonism. Probably peptide **K6** is the strongest mixed μ/δ/κ

opioid agonist due to its ability to bind protein G with an efficacy value over the basal level in presence of each selective opioid antagonist at 10 μM.

Table 2. G-protein activation DAMGO, and novel oligopeptides in [^{35}S]GTPγS binding assays using rat brain membrane homogenates. The values were calculated according to dose-response binding curves.

Ligand	Maximal Stimulation (Efficacy)	Potency
	E_{max} ± S.E.M. (%)	Log EC_{50} ± S.E.M.
DAMGO	172.0 ± 3.5	−6.384 ± 0.101
KA1	140.9 ± 1.4	−6.504 ± 0.076
K2	121.6 ± 2.5	−7.535 ± 0.354
K3	114.0 ± 2.1	−6.993 ± 0.422
K4	155.5 ± 4.8	−6.073 ± 0.172
K5	149.2 ± 3.5	−5.990 ± 0.111
K6	209.7 ± 3.4	−5.984 ± 0.054

Table 3. The maximal G-protein efficacy (E_{max}) of novel oligopeptides in the absence or presence of the selective MOR antagonist cyprodime and the selective DOR antagonist naltrindole in rat brain membrane homogenates and in the absence or presence of the selective KOR antagonist norbinaltorphine in guinea pig brain membrane homogenates in [^{35}S]GTPγS binding assays. The values were calculated according to bar graphs in Figure S3.

		MOR	DOR		KOR
	Ligand	Ligand + Cyp	Ligand + NTI	Ligand	Ligand + Nor-BNI
		E_{max} ± S.E.M. (%)			
KA1	139.6 ± 8.2	94.7 ± 3.7 **	102.5 ± 1.3 *	111.7 ± 1.1	100.7 ± 6.2 ^{ns}
K2	129.9 ± 8.2	88.0 ± 3.3 **	88.8 ± 1.9 **	92.8 ± 2.0	100.7 ± 6.0 ^{ns}
K3	118.9 ± 3.0	98.5 ± 1.2 **	97.8 ± 1.7 **	95.2 ± 2.2	106.0 ± 6.3 ^{ns}
K4	160.6 ± 5.7	101.6 ± 2.6 ***	103.6 ± 3.2 ***	125.2 ± 2.0	104.9 ± 9.5 *
K5	153.1 ± 5.9	108.8 ± 1.6 **	103.8 ± 1.9 ***	106.9 ± 0.3	110.5 ± 5.0 ^{ns}
K6	211.7 ± 3.1	108.5 ± 2.4 ***	113.3 ± 2.9 ***	139.8 ± 2.3	142.1 ± 7.1 ^{ns}

Experimental data were processed by GraphPad Prism 5.0 using bar graphs. ns: not significant; * $p < 0.05$; ** $p < 0.01$; *** $p < 0.001$ based on unpaired *t*-tests.

3.3. In Vivo Studies

Data obtained from binding experiments indicate **K6** as the best of the series; thus, tail flick and formalin tests were performed in order to evaluate the effects of this novel peptide in two different pain animal models. The tail flick test measures the time in which the animal withdraws the tail from a thermal nociceptive stimulus; this time is increased by analgesics. Compounds were centrally injected, and the response measured from 15 to 120 min after the administration. Compounds **K6** and DAMGO greatly increase the time of response to thermal nociceptive stimuli and both effects were in the same order to magnitude (Figure 2).

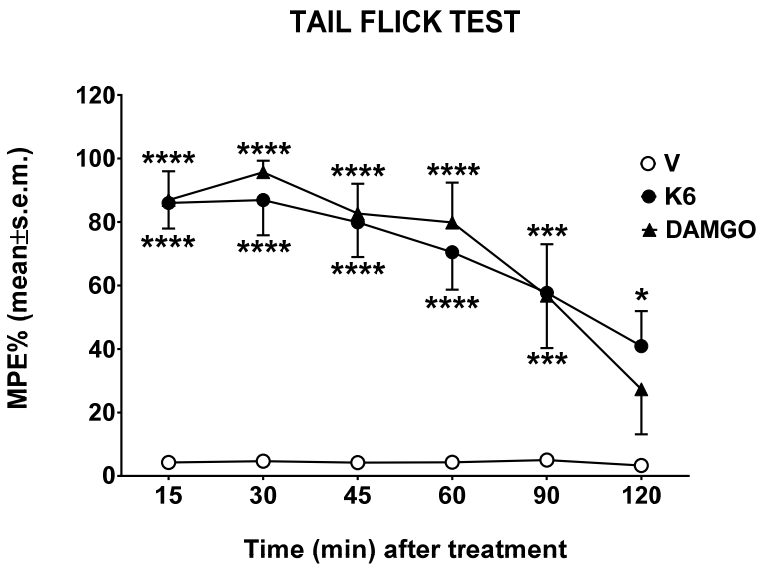

Figure 2. The effect of **K6** and DAMGO in the tail flick test. Compounds were administered in the left cerebral ventricle at the dose of 10 μg/10 μL, and the time to respond to thermal stimuli measured from 15 to 120 min. V is for vehicle-treated animals. Statistical analysis: two-way ANOVA followed by Sidak's multiple comparisons test. * is for $p < 0.05$, *** is for $p < 0.001$, and **** is for $p < 0.0001$ vs. V. n = 7.

Since it was reported that some opioid peptides such as DAMGO are also peripheral acting [42], we performed a formalin test administering **K6** and DAMGO subcutaneously in mice paws. The formalin test measures the behavioral response to chemical nociceptive stimuli evoked by a formalin diluted solution injected in the mice paw. From 0 to 10 min after the injection, an early phase response occurs with direct stimulation of peripheral nociceptors, while a response to inflammatory pain appears from 15 to 40 min as a late prolonged phase. Compound **K6** was able to reduce the nociceptive response to formalin in the early phase, whereas a light but not significant reduction was induced in the late phase of the formalin test (Figure 3). After the DAMGO injection, we observed a reduction of the nociceptive behavior both early and late in the formalin test (Figure 3). The formalin early phase, which depends upon the direct excitement of sensory neurons through TRPA1 cation channel activation [43] of MORs at the peripheral endings of nociceptors, is responsible for meaningful analgesia [44], and it is not surprising that **K6** and DAMGO reduced formalin-induced nociception in the early phase of the test. The differences observed in the late phase are probably due to a different metabolic fate of **K6** and DAMGO after subcutaneous administration, depending upon the protease activity that might act in different ways on **K6** and DAMGO chemical structures.

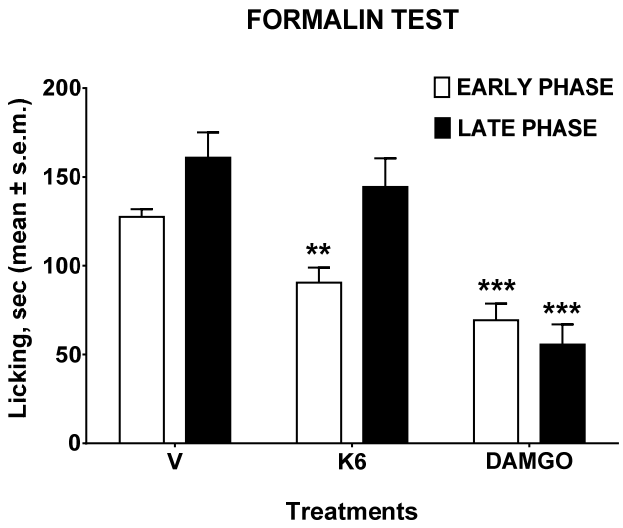

Figure 3. The effect of **K6** and DAMGO in the formalin test. Compounds were administered subcutaneously (s.c.) in the dorsal hind paw of mice at the dose of 100 μg/20 μL, 15 min before a s.c. injection of dilute formalin solution (1% in saline, 20 μL/paw). Early phase represents the formalin-induced nociceptive behavior recorded from 0 to 10 min after formalin injection; late phase is for the formalin-induced nociceptive behavior recorded from 15 to 40 min after formalin injection. V is for vehicle-treated animals. Statistical analysis: one-way ANOVA followed by Holm–Sidak's multiple comparisons test. ** is for $p < 0.01$ and *** is for $p < 0.001$ vs. V. n = 7.

3.4. Plasma Stability Results

The plasma stability of compound **K6** was tested by incubation in human plasma at 37 °C. The degradation curve (Figure 4) was built by plotting the total amount of remaining peptide (expressed as μg/mL) vs. time (minutes). Concentration data were obtained in triplicate and analyzed as simple linear regression using GraphPad 8.3.1. The novel compound exhibits good stability in human plasma, showing a $t_{1/2}$ = 47 min, according to the results obtained from the tail flick test after i.c.v. administration.

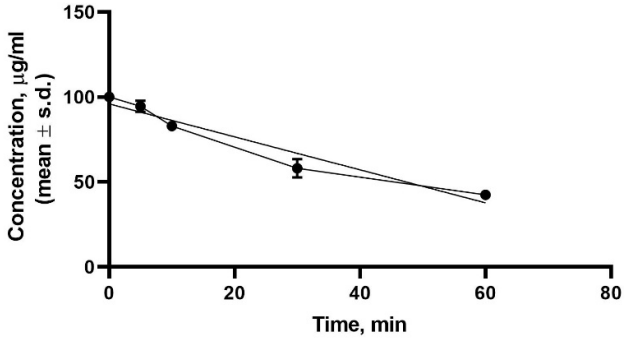

Figure 4. Stability of compound **K6** in human plasma. Concentration of K6 in μg/mL measured from 0 to 60 min in triplicate.

4. Conclusions

Chemical modification of endogenous opioid peptides promotes the development of novel analogs with increased potency and improved pharmacokinetic properties, e.g., the synthetic bivalent peptide biphalin enhanced stroke immunohistochemical and behavioral neuroprotection in comparison to DPDPE and DAMGO, reducing glutamate toxicity and oxidative stress [45–48].

Metabolites of the KP, especially kyna and L-kyn, play crucial roles in maintaining the normal brain function, preventing the over-activation of excitatory amino acid receptors, thus offering novel therapeutical opportunities for brain neuroprotection. In this work, we have synthesized six novel opioid analogs incorporating the L-kyn and kyna residues at different positions of several opioid peptide scaffolds. They were characterized by in vitro and in vivo assays to evaluate their ability to bind the NMDA/opioid receptors and to induce analgesic effects after i.c.v. and s.c. administration. These novel peptides do not bind to the NMDA receptors, and some of them showed good/high affinity for opioid receptors with different selectivity profiles. In particular, **KA1** exhibits the binding constant (Ki = 1.08) very close to that of DAMGO for the μ-opioid receptor and a pronounced selectivity but medium-low efficacy (E_{max} = 139%); thus the esterification of the ethanolamine portion with kyna does not add any particular advantage to the parent peptide DAMGO. On the other hand, the presence of L-kyn residue in place of native Phe in position 3 (**K2**) leads a potent and selective opioid fragment toward MOR (selectivity ration μ/δ/κ = 1:10000:750), whereas the substitution in position 4 (**K3**) leads to a weak and unselective agonist at MOR and DOR. In the analogs **K4–K6**, the kyna residue was inserted in the fifth position of the YaGP peptide, with different *C*-terminus, respectively, methyl ester, free carboxylic acid, and amide. **K4** and **K5** show a similar mixed binding affinity for MOR and DOR, with a preference for MOR and none or weak affinity for KOR.

On the contrary, peptide **K6** shows an interesting behavior since it is able to bind all three opioid receptors with binding affinity ranging from high to modest (Ki^{μ} = 1.84 nM, Ki^{δ} = 32.5 nM, Ki^{κ} = 127.7 nM), with a potency ($logEC_{50}$ = −5.598) and efficacy at MOR (E_{max} = 211%) higher than that of DAMGO (E_{max} = 172%). Its activity on the GTPγS binding assay on rat brain membrane and guinea pig ileum is well antagonized by the co-administration of the selective antagonists for MOR and DOR at 10 μM concentration, prompting us to deeply investigate its anti-nociceptive effect in vivo. The formalin test, which is a model of inflammatory pain, revealed that the antinociceptive effect exerted by **K6** after subcutaneous administration is significant only in the early phase, whereas DAMGO is also active in the late phase. In the tail flick test, the **K6** analgesic profile after i.c.v. administration is superimposable to that of DAMGO, according to a good stability profile in human plasma. These data are encouraging to further develop opioid peptides containing kynurenine moieties since the insertion of kyna and kyn in our opioid model improved, in some cases, the binding affinity and was able to modulate the selectivity. Also, the possible role played by the metabolism of these peptides and their possible implication in different neuropathic and chronic pain models is unknown and worth further investigation.

Supplementary Materials: The following are available online at www.mdpi.com/xxx/s1, Figure S1: MOR (A), DOR (B), KOR (C) and NMDA (D) binding affinity of the novel oligopeptides, Figure S2: The effect of oligopeptides on G-protein activity compared to DAMGO in [^{35}S]GTPγS binding assay in rat brain membrane homogenates, Figure S3: The effect of novel oligopeptides on G-protein activity in [^{35}S]GTPγS binding assays in the absence or presence of the selective MOR antagonist cyprodime (Cyp) and the selective DOR antagonist naltrindole (NTI) in rat brain membrane homogenates (Figure A) and the selective KOR antagonist norbinaltorphine (nor-BNI) in guinea pig brain membrane homogenates (Figure B).

Author Contributions: Conceptualization, A.S. and S.B.; Data curation, E.S., F.Z., S.P. and G.Z.; Formal analysis, F.Z. and L.V.; Investigation, A.S., M.N. and S.P.; Methodology, E.S. and M.P.D.; Validation, S.B.; Writing – original draft, A.S.; Writing – review & editing, L.V. and S.B. All authors have read and agreed to the published version of the manuscript.

Funding: This research was supported by the project GINOP 2.3.2-15-2016-00034, provided by National Research, Development and Innovation Office (NKFI), Budapest, Hungary, and the Ministry of Human Capacities, Hungary grant 20391-3/2018/FEKUSTRAT.

Conflicts of Interest: The authors declare no conflict of interest.

Abbreviations: KP, kynurenine pathway; kyn, kynurenine; kyna, kynurenic acid; FDA, Food and Drug Administration; CNS, central nervous system; BBB, blood brain barrier; GPR35, G protein-coupled receptor 35; SVCT2, Sodium-dependent vitamin C transporter 2; MOR, μ-opioid receptor; DOR, δ-opioid receptor; KOR, k-opioid receptor; GPCRs, G protein coupled receptors; NMR, Nuclear magnetic resonance; TFA, trifloroacetic acid; ACN, acetonitrile; RP-HPLC, Reverse Phase High performance liquid chromatography; TMS,

trimethylsilane; ESI, Electrospray ionization; LRMS, Low Resolution Mass Spectroscopy; HOBt, 1-hydroxybenzotriazole; DMAP, 4-Dimethylaminopyridine; EDC·HCl, 1-Ethyl-3-(3-dimethylaminopropyl)carbodiimide hydrochloride; EtOAc, ethyl acetate; THF, tetrahydrofurane; NMM, N-methylmorpholine; iBCF, isobuthylchloroformiate; DMSO, dimethylsulfoxide; Boc, tert-butyloxycarbonyl; Ar, aryl; EM-2; endomorphine-2; BSA, Bovine serum albumin; i.c.v., intracerebroventricular; Cyp, cyprodime; NTI, naltrindole; Nor-BNI, norbinaltorphine; DPDPE, [D-Pen,D-Pen5]Enkephalin; DIPEA, N,N-Diisopropylethylamine; DMF, dimethylformamide; DCM, dichloromethane; MeOH, methanol; TIPS, triisopropylsilane; EGTA, ethylene glycol-bis(2-aminoethylether)-N,N,N′,N′-tetraacetic acid; GDP, guanosine 5'-diphosphate; GTP, guanosine-5'-triphosphate; DMSO, dimethylsulfoxide; DAMGO, [D-Ala^2, N-MePhe^4, Gly-ol]-enkephalin; IleDelt II, Ile^{5,6}-deltorphin II; [^{35}S]GTPγS guanosine-5′-[^{35}S]thiophosphate; NMDA, N-methyl-D-aspartate receptor; Tris-HCl, tris-(hydroxymethyl)-aminomethane hydrochloride.

References

1. Cervenka, I.; Agudelo, L.Z.; Ruas, J.L. Kynurenines: Tryptophan's metabolites in exercise, inflammation, and mental health. *Science* **2017**, *357*, 9794, doi:10.1126/science.aaf9794.
2. Ye, Y.; Xia, Z.; Zhang, D.; Sheng, Z.; Zhang, P.; Zhu, H.; Xu, N.; Liang, S. Multifunctional pharmaceutical effects of the antibiotic daptomycin. *BioMed Res. Int.* **2019**, 8609218, doi:10.1155/2019/8609218.
3. Chuang, P.-H.; Hsieh, P.-W.; Yang, Y.-L.; Hua, K.-F.; Chang, F.-R.; Shiea, J.; Wu, S.-H.; Wu, Y.-C. Cyclopeptides with Anti-inflammatory Activity from Seeds of Annona Montana. *J. Nat. Prod.* **2008**, *71*, 1365–1370.
4. Ellis-Steinborner, S.T.; Scanlon, D.; Musgrave, I.F.; Nha Tran, T.T.; Hack, S.; Wang, T.; Abell, A.D.; Tyler, M.J.; Bowie, J.H. An unusual kynurenine-containig opioid tetrapeptide from the skin gland secretion of the Australian red tree frog Litoria rubella. Sequence determination by electrospray mass spectrometry. *Rapid Commun. Mass Spectrom.* **2011**, *25*, 1735–1740.
5. Guillemin, G.J.; Kerr, S.J.; Smythe, G.A.; Smith, D.G.; Kapoor, V.; Armati, P.J.; Croitoru, J.; Brew, B.J. Kynurenine pathway metabolism in human astrocytes: A paradox for neuronal protection. *J. Neurochem.* **2001**, *78*, 842–853.
6. Schwarcz, R.; Bruno, J.P.; Muchowski, P.J.; Wu, H.-Q. Kynurenines in the mammalian brain: When physiology meets pathology. *Nat. Rev. Neurosci.* **2012**, *13*, 465–477.
7. Vécsei, L.; Szalárdy, L.; Fülöp, F.; Toldi, J. Kynurenines in the CNS: Recent advances and new questions. *Nat. Rev. Drug. Discov.* **2013**, *12*, 64–82.
8. Yeganeh Salehpour, M.; Mollica, A.; Momtaz, S.; Sanadgol, N.; Farzaei, M.H. Melatonin and multiple sclerosis: From plausible neuropharmacological mechanisms of action to experimental and clinical evidence. *Clin. Drug Investig.* **2019**, *39*, 607–624.
9. Birch, P.J.; Grossman, C.J.; Hayes, A.G. Kynurenate and FG9041 have both competitive and non-competitive antagonist actions at excitatory amino acid receptors. *Eur. J. Pharmacol.* **1988**, *151*, 313–315.
10. Perkins, M.N.; Stone, T.W. Actions of kynurenic acid and quinolinic acid in the rat hippocampus *in vivo*. *Exp. Neurol.* **1985**, *88*, 570–579.
11. Wang, J.; Simonavicius, N.; Wu, X.; Swaminath, G.; Reagan, J.; Tian, H.; Ling, L. Kynurenic acid as a Ligand for Orphan G Protein-coupled Receptor GPR35. *J. Biol. Chem.* **2006**, *281*, 22021–22028.
12. Shore, D.M.; Reggio, P.H. The therapeutic potential of orphan GPCRs, GPR35 and GPR55. *Front. Pharmacol.* **2015**, *6*, 69, doi:10.3389/fphar.2015.00069.
13. Bonina, F.P.; Arenare, L.; Ippolito, R.; Boatto, G.; Battaglia, G.; Bruno, V.; de Caprariis, P. Synthesis, pharmacokinetics and anticonvulsant activity of 7-chlorokynurenic acid prodrugs. *Int. J. Pharm.* **2000**, *202*, 79–88.
14. Luhavaya, H.; Sigrist, R.; Chekan, J.R.; McKinnie, S.M.K.; Moore, B.S. Biosynthesis of l-4-Chlorokynurenine, an antidepressant prodrug and a non-proteinogenic amino acid found in lipopeptide. *Antibiotics* **2019**, *58*, 8394–8399.
15. Manfredini, S.; Vertuani, S.; Pavan, B.; Vitali, F.; Scaglianti, M.; Bortolotti, F.; Biondi, C.; Scatturin, A.; Prasad, P.; Dalpiaz, A. Design, synthesis and activity of ascorbic acid prodrugs of nipecotic, kynurenic and diclophenamic acids, liable to increase neurotropic activity. *J. Med. Chem.* **2002**, *45*, 559–562.
16. Vamos, E.; Pardutz, A.; Klivenyi, P.; Toldi, J.; Vecsei, L. The role of kynurenines in disorders of the central nervous system: Possibilities for neuroprotection. *J. Neurol. Sci.* **2009**, *283*, 21–27.
17. Knyihár-Csillik, E.; Toldi, J.; Mihály, J.A.; Krisztin-Péva, B.; Chadaide, Z.; Németh, H.; Vécsei, L. Kynurenine in combination with probenecid mitigates the stimulation-induced increase of c-fos

immunoreactivity of the rat caudal trigeminal nucleus in an experimental migraine model. *J. Neural. Transm.* **2007**, *114*, 417–421.

18. Gábor, N.-G.; Dvorácskó, S.; Bohár, Z.; Benyhe, S.; Tömböly, C.; Párdutz, A.; Vécsei, L. Interactions between the kynurenine and the endocannabinoid system with special emphasis on migraine. *Int. J. Mol. Sci.* **2017**, *18*, 1617. doi:10.3390/ijms180816116.
19. Stone, T.W.; Caroline, M.; Forrest, M.; Darlington, L.G. Kynurenine pathway inhibition as a therapeutic strategy for neuroprotection. *FEBS J.* **2012**, *279*, 1386–1397.
20. Deora, G.S.; Kantham, S.; Chan, S.; Dighe, S.N.; Veliyath, S.K.; McColl, G.; Parat, M.O.; McGeary, R.P.; Ross, B.P. Multifunctional analogs of kynurenic acid for the treatment of Alzheimer's disease: Synthesis, pharmacology, and molecular modeling studies. *ACS Chem. Neurosci.* **2017**, *8*, 2667–2675.
21. Zádori, D.; Nyiri, G.; Szonyi, A.; Szatmári, I.; Fülöp, F.; Toldi, J.; Freund, T.F.; Vécsei, L.; Klivényi, P. Neuroprotective effects of a novel kynurenic acid analogue in a transgenic mouse model of Huntington's disease. *J. Neurol. Transm.* **2011**, *18*, 865–875.
22. Ghilardi, A.; Pezzoli, D.; Bellucci, M.C.; Malloggi, C.; Negri, A.; Sganappa, A.; Tedeschi, G.; Candiani, G.; Volonterio, A. Synthesis of multifunctional PAMAM-Aminoglycoside conjugates with enhanced transfection efficiency. *Bioconjug Chem.* **2013**, *24*, 1928–1936.
23. Tsentalovich, Y.P.; Yanshole, V.V.; Polienko, Y.F.; Morozov, S.V.; Grigor'ev, I.A. Deactivation of excited states of kynurenine covalently linked to nitroxides. *Photochem. Photobiol.* **2011**, *87*, 22–31.
24. Stefanucci, A.; Novellino, E.; Mirzaie, S.; Macedonio, G.; Pieretti, S.; Minosi, P.; Szűcs, E.; Erdei, A.I.; Zádor, F.; Benyhe, S.; et al. Opioid receptor activity and analgesic potency of DPDPE peptide analogues containing a xylene bridge. *ACS Med. Chem. Lett.* **2017**, *8*, 449–454.
25. Spetea, M.; Berzetei-Gurske, I.P., Guerrieri, E.; Schmidhammer, H. Discovery and pharmacological evaluation of a diphenethylamine derivative (HS665), a highly potent and selective k-opioid receptor agonist. *J. Med. Chem.* **2012**, *55*, 10302–10306.
26. Oktem, H.A.; Moitra, J.; Benyhe, S.; Tóth, G.; Lajtha, A.; Borsodi, A. Opioid receptor labeling with the chloromethyl ketone derivative of [3H]Tyr-D-Ala-Gly-(Me)Phe-Gly-ol (DAMGO) II: Covalent labeling of mu opioid binding site by 3H-Tyr-D-Ala-Gly-(Me)Phe chloromethyl ketone. *Life Sci.* **1991**, *48*, 1763–1768.
27. Guerrieri, E.; Mallareddy, J.R.; Tóth, G.; Schmidhammer, H.; Spetea, M. Synthesis and pharmacological evaluation of [(3)H]HS665, a novel, highly selective radioligand for the kappa opioid receptor. *ACS Chem. Neurosci.* **2015**, *6*, 456–463.
28. Basu, N.; Scheuhammer, A.M.; Rouvinen-Watt, K.; Grochowina, N.; Evans, R.D.; O'Brien, M.; Chan, H.M. Decreased N-methyl-d-aspartic acid (NMDA) receptor levels are associated with mercury exposure in wild and captive mink. *Neurotoxicology* **2007**, *28*, 587–593.
29. Benyhe, S.; Farkas, J.; Tóth, G.; Wollemann, M. Met5-enkephalin-Arg6-Phe7, an endogenous neuropeptide, binds to multiple opioid and nonopioid sites in rat brain. *J. Neurosci. Res*. **1997**, *48*, 249–258.
30. Zádor, F.; Kocsis, D.; Borsodi, A.; Benyhe, S. Micromolar concentrations of rimonabant directly inhibits delta opioid receptor specific ligand binding and agonist-induced G-protein activity. *Neurochem. Int.* **2014**, *67*, 14–22.
31. Bradford, M.M. A rapid and sensitive method for the quantitation of microgram quantities of protein utilizing the principle of protein-dye binding. *Anal. Biochem.* **1976**, *72*, 248–254.
32. Sim, L.J.; Selley, D.E.; Childers, S.R. In vitro autoradiography of receptor-activated G proteins in rat brain by agonist-stimulated guanylyl 5'-[gamma-[35S]thio]-triphosphate binding. *Proc. Natl. Acad. Sci. USA* **1995**, *92*, 7242–7246.
33. Traynor, J.R.; Nahorski, S.R. Modulation by mu-opioid agonists of guanosine-5'-O-(3-[35S]thio)triphosphate binding to membranes from human neuroblastoma SH-SY5Y cells. *Mol. Pharmacol.* **1995**, *47*, 848–854.
34. Neises, B.; Steglich, W. Simple Method for the Esterification of Carboxylic Acids. *Angew. Chem. Int. Ed. Engl.* **1978**, *17*, 522–524.
35. Mollica, A.; Costante, R.; Stefanucci, A.; Pinnen, F.; Luisi, G.; Pieretti, S.; Borsodi, A.; Bojinik, E.; Benyhe, S. Hybrid peptides endomorphin-2/DAMGO: Design, synthesis and biological evaluation. *Eur. J. Med. Chem.* **2013**, *68*, 167–177.
36. Stefanucci, A.; Lei, W.; Hruby, V.J.; Macedonio, G.; Luisi, G.; Carradori, S.; Streicher, J.M.; Mollica, A. Fluorescent-labeled bioconjugates of the opioid peptides biphalin and DPDPE incorporating fluorescein-maleimide linkers. *Future Med. Chem.* **2017**, *9*, 859–869.

37. Zádor, F.; Samavati, R.; Szlavicz, E.; Tuka, B.; Bojnik, E.; Fulop, F.; Toldi, J.; Vecsei, L.; Borsodi, A. Inhibition of opioid receptor mediated G-Protein activity after chronic administration of kynurenic acid and its derivative without direct binding to opioid receptors. *CNS Neurol. Disord. Drug Targets* **2014**, *13*, 1520–1529.
38. Kemp, J.A.; Grimwood, S.; Foster, A.C. Characterization of the antagonism of excitatory amino acid receptors in rat cortex by kynurenic acid. *Br. J. Pharmacol.* **1987**, *91*, 314P.
39. Cheng, Y.-C.; Prusoff, W.H. Relationship between the inhibition constant (K1) and the concentration of inhibitor which causes 50 per cent inhibition (I50) of an enzymatic reaction. *Biochem. Pharmacol.* **1973**, *22*, 3099–3108.
40. Márki, A.; Monory, K.; Otvos, F.; Tóth, G.; Krassnig, R.; Schmidhammer, H.; Traynor, J.R.; Roques, B.P.; Maldonado, R.; Borsodi, A. Mu-opioid receptor specific antagonist cyprodime: Characterization by in vitro radioligand and [^{35}S]GTPγS binding assays. *Eur. J. Pharmacol.* **1999**, *383*, 209–214.
41. Portoghese, P.S.; Sultana, M.; Takemori, A.E. Naltrindole, a highly selective and potent non-peptide delta opioid receptor antagonist. *Eur. J. Pharmacol.* **1988**, *146*, 185–186.
42. Smith, H.S. Peripherally-acting opioids. *Pain Physician* **2008**, *11*, 121–132.
43. McNamara, C.R.; Mandel-Brehm, J.; Bautista, D.M.; Siemens, J.; Deranian, K.L.; Zhao, M.; Hayward, N.J.; Chong, J.A.; Julius, D.; Moran, M.M.; et al. TRPA1 mediates formalin-induced pain. *Proc Natl Acad Sci USA* **2007**, *104*, 13525–13530.
44. Stein, C. Opioid receptors. *Annu. Rev. Med.* **2016**, *67*, 433–451.
45. Yang, L.; Wang, H.; Shah, K.; Karamyan, V.T.; Abbruscato, T.J. Opioid receptor agonists reduce brain edema in stroke. *Brain Res.* **2011**, *1383*, 307–316.
46. Yang, L.; Shah, K.; Wang, H.; Karamyan, V.T.; Abbruscato, T.J. Characterization of neuroprotective effects of biphalin, an opioid receptor agonist, in a model of focal brain ischemia. *J. Pharmacol. Exp. Ther*. **2011**, *339*, 499–508.
47. Yang, L.; Islam, M.R.; Karamyan, V.T.; Abbruscato, T.J. In vitro and in vivo efficacy of a potent opioid receptor agonist, biphalin, compared to subtype-selective opioid receptor agonists for stroke treatment. *Brain Res.* **2015**, *1609*, 1–11.
48. Davis, T.P.; Abbruscato, T.J.; Egleton, R.D. Peptides at the blood brain barrier: Knowing me knowing you. *Peptides* **2015**, *72*, 50–56.